THE THERMOCLINE AND CURRENT STRUCTURE
IN SUBTROPICAL/SUBPOLAR BASINS

by
Rui Xin Huang

B.Sc. University of Science and Technology, China
(1965)

SUBMITTED IN PARTIAL FULFILLMENT OF THE
REQUIREMENTS FOR THE DEGREE OF
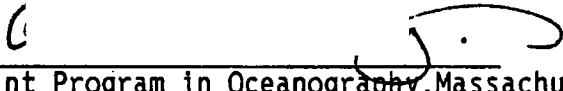DOCTOR OF PHILOSOPHY

at the

MASSACHUSETTS INSTITUTE OF TECHNOLOGY

and the

WOODS HOLE OCEANOGRAPHIC INSTITUTION

May, 1984

Signature of Author _____
Joint Program in Oceanography,Massachusetts
Institute of Technology – Woods Hole
Oceanographic Institution

Certified by _____
Thesis Supervisor

Accepted by _____
Chairman, Joint Committee for Physical
Oceanography, Massachusetts
Institute of Technology – Woods Hole
Oceanographic Institution.

THE THERMOCLINE AND CURRENT STRUCTURE

IN SUBTROPICAL/SUBPOLAR BASINS

by

Rui Xin Huang

Submitted to the Joint Committee for Physical Oceanography,

Massachusetts Institute of Technology and Woods Hole

Oceanographic Institution, on May 15, 1984, in partial fulfillment

of the requirements for the degree of Doctor of Philosophy.

ABSTRACT

Part one of this thesis discusses the structure of the thermocline and the
current pattern within a two-layer model. The corresponding flow field is
explored as the amount of water in the upper layer is gradually reduced (or as
the wind stress is gradually increased).

In the model, when the amount of water in the upper layer is less than a
first critical value, the lower layer outcrops near the middle of the western
boundary. A dynamically consistent picture includes a whole loop of boundary
currents, which surround the outcropping zone completely and have quite
different structures. In addition to the boundary currents found in previous
models, there is an isolated western boundary current (i.e. bounded on one
side by the wall and on the other by a streamline along which the upper layer
thickness vanishes), an internal boundary current and possibly isolated
northern/southern boundary currents. Within the limitations of the two-layer
model, the isolated western boundary current appears to represent the Labrador

Current while the internal boundary current may represent the North Atlantic Current. A first baroclinic mode of water mass exchange occurs across the ZWCL (zero-wind-curl-line).

When the amount of water in the upper layer is less than a second critical value, the upper layer separates from the eastern wall and becomes a warm water pool in the south-west corner of the basin. Under this warm water pool is the ventilated lower layer.

The sea surface density distribution is not specified; it is determined from a consistent dynamical and mass balance. Implicit in this model is the assumption that advection dominates in the mixed layer.

The subtropical gyre and the subpolar gyre combine asymmetrically with respect to the ZWCL.

Chapter I discusses the case when the lower layer depth is infinite. Chapter II discusses the case when the lower layer depth is finite. In the Addendum the climatological meaning of this two-layer model is discussed.

Part two of this thesis concerns the use of a continuously stratified model to represent the thermocline and current structures in subtropical/subpolar basins. The ideal fluid thermocline equation system is a nonlinear, non-strict hyperbolic system. In an Addendum to Chapter III the mathematical properties of this equation system are studied and a proper way of formulating boundary value problems is discussed. Although the equations are not of standard type, so that no firm conclusions about the existence and uniqueness of solutions have been drawn, some possible approaches to properly posed boundary value problem are suggested. Chapter III presents some simple numerical solutions of the ideal fluid thermocline equation for a subtropical

gyre and a subtropical/subpolar basin using one of these approaches. Our model predicts the continuous three dimensional thermocline and current structures in a continuously stratified wind-driven ocean. The upper surface density and Ekman pumping velocity are specified as input data; in addition, the functional form of the potential vorticity is specified.

The present model emphasizes the idea that the ideal fluid thermocline model is incomplete. The potential vorticity distribution can not be determined within this idealized model. This suggests that the diffusion and upwelling/downwelling within the western boundary current and the outcropping zone in the north-west corner are important parts of the entire circulation system.

Acknowledgments

Table of Contents

Chapter I

A Two-layer Model for the Thermocline and Current Structure

in Subtropical/Subpolar Basins

I. Lower Layer with Infinite Depth

Abstract

A study is made of the thermocline and current structures of a subpolar gyre and a double gyre basin. A simple two-layer model is used, and its behavior is explored as the amount of water in the upper layer is gradually reduced (or as the wind stress is gradually increased). When the amount of water in the upper layer is less than (or the wind stress is larger than) a critical value, the lower layer outcrops near the middle of the western boundary. A dynamically consistent picture includes a strong, "isolated" western boundary current (i.e. bounded on one side by the wall and on the other by a streamline along which the upper layer thickness vanishes) flowing southward and an "internal" boundary current (i.e. a current that flows in the interior of the ocean and separates these two layers) flowing northward. The isolated western boundary current may represent the Labrador Current, and the internal boundary current may represent the North Atlantic Current. For a typical case there is some water mass exchange across the ZWCL (zero-wind-curl-line).

The analysis in this chapter follows Parsons's (1969) idea; i.e., we assume that the lower layer has an infinite depth, so that the flow pattern can be found with relatively simple algebra.

1. Introduction

A fairly narrow vertical zone of large temperature and salinity gradients exists in all of the world's oceans. The thermocline theory is concerned with the structure of this region of rapid vertical variation. The ocean is driven from above by wind-stress and differential heating. There is strong coupling between density and velocity fields, which makes the thermocline problem highly non-linear; moreover, the complicated boundary conditions of the ocean basins make the problem even more difficult.

During the early stages of the development of thermocline theory, much effort was devoted to trying to find similarity solutions. The similarity solution approach is based on special balances of terms in the nonlinear partial differential equation. Though some similarity solutions give a good qualitative description for the ocean thermocline, there is no reason why these special term balances should hold. In addition, a very serious difficulty with similarity solutions is that they cannot satisfy the full boundary conditions required for a three-dimensional basin.

Recently, there has been some renewal of interest in finding non-similarity solutions for the thermocline problem. Rhines and Young (1982) propose an unventilated model with the potential vorticity being homogenized below the directly wind-driven top layer. Their model rather successfully describes the bowl-shaped subtropical gyre with its homogeneous potential vorticity pool. Though they include weak dissipation for the interior flow, their model cannot deal with the strong dissipation within the western boundary current.

2

Luyten, Pedlosky and Stommel (1983, LPS hereafter), following the classical thermocline theory more closely, use a ventilated model of the ocean. By specifying the density distribution at the base of the mixed layer within the downwelling region, their multi-layer model describes the large departures of isopycnal depths on planetary scales. Their model gives a global picture of the outcropping, ventilation and unventilated zones. However, it has the same disadvantage as other models based on the ideal fluid thermocline theory; it does not include a western boundary current or any kind of dissipation. As a result, it cannot satisfy the western boundary condition and it is not clear whether or how the fluxes of various water masses can be balanced. There is another shortcoming: the surface density distribution within the subtropical gyre is imposed a-priori from data averaging. Actually, the density distribution on the base of the Ekman layer should be determined by the interaction between the local, more or less one-dimensional mixed layer dynamics, and the large-scale geostrophic flow underneath. In their model the ZWCL is a constant density line and is treated as a real boundary between two gyres. This assumption might be intuitive or simply convenient. However, although the Sverdrup transport is zero on this line, there is no reason, a-priori, why this line should be a real boundary between these two gyres. In fact, a first baroclinic mode of water mass exchange across this line is found in this paper; this baroclinic mode combines these two gyres into a united body.

The ventilated thermocline model requires the density distribution on the base of the mixed layer as a given upper boundary condition. Actually, the thermal structure of the mixed layer depends on both the local air-sea

3

interaction and the advection. Suppose the surface heat flux due to air-sea interaction is a simple linear Rayleigh type law $Q = \sigma(T^A - T^o)$; where $1/\sigma$ is the time scale for the water mass in the whole upper layer to be warmed up. If T_c is the advection time scale, then $K = 1/T_c\sigma$ is the ratio of these two time scales. For the shallow Ekman layer $K \ll 1$, meaning that the local air-sea interaction dominates the temperature distribution, while as for a whole layer with depth of an order of a kilometer, $K \gg 1$ meaning that the advection dominates the temperature distribution. The ventilated thermocline model discusses the case $K \ll 1$ for the Ekman layer. The other extreme case $K \gg 1$ represents another classic approach to the thermocline theory: the purely wind-driven layer model with a finite amount of water in the upper layer.

Parsons (1969) first used this latter approach to discuss the Gulf Stream separation mechanism in a subtropical basin. Based on the assumption of a finite amount of warm upper layer water, Parsons concludes that reducing the volume of warm upper layer water below a critical value causes the lower layer to surface near the northwest corner of the basin. The western boundary current of the upper layer leaves the western wall and becomes an internal jet stream which separates the warm upper layer from the cold lower layer. For simplicity Parsons assumes the lower layer is infinitely deep, so it is motionless. By this assumption, the algebra has been made much easier. However, this assumption needs modification. No matter how deep is the lower layer and how small is the lower layer velocity, the vertically integrated mass flux is a non-zero finite number. Thus Parsons's model has to be improved. This problem will be discussed in Chapter II.

Veronis (1973) uses a similar approach for the world ocean circulation. Instead of using a purely wind-driven circulation model, he specifies the upper-layer thickness on the eastern wall from observational data. Thus his model in a sense partly includes the heating effect. For the interior ocean, Veronis extends Parsons's model to the two-gyre case. To balance the mass flux within the whole basin, Veronis proposes isolated northern and western boundary currents, but he gives no dynamical analysis for these boundary currents. In his solution the proposed northern boundary currents are against the local wind (westerly). However, having a northern boundary current going against the local wind seems inconsistent with the lowest order dynamics.

Since the work of Stommel (1948), the subtropical gyre and its western boundary current have become a classic problem. Although some difficult questions for the subtropical gyre remain to be answered, this gyre and its western boundary current are topics which have been studied extensively by oceanographers; there are a lot of observational data and many theories which work out nicely for them. However, there is no good model for the subpolar gyre. Though there have been many observational papers, corresponding dynamical modelling efforts are rare (see, for example, Veronis, 1973; Pedlosky and Young, 1983). In most numerical models for a two-gyre basin the subpolar gyre is treated simply as a mirror image of the subtropical gyre. Of course, this is true only for quasi-geostrophic models. Physically, the subpolar and subtropical gyres have quite different structures. The latter is anticyclonic, so that all isopycnal depths increase westward, making the gyre bowl-shaped. The subpolar gyre is cyclonic, so that the upper layer thickness

decreases westward. In a typical subpolar basin isopycnals outcrop, making an open dome-shaped structure.

The analysis in this chapter considers the limited-volume upper-layer cases in connection with two-layer models of a subpolar gyre and a two-gyre basin. Many factors of the solutions presented here are similar to those of Veronis; the major differences are inclusion of the dynamics of the boundary layers and discussion of evolution of the flow pattern as the external parameters change. In our model a non-dimensional number $\lambda = TL/g'\rho_0 d^2$ determines the basic flow pattern.

When λ is small (weak wind forcing or a large amount of upper layer water) there is the subcritical state. The upper layer covers the whole basin resulting in the classical picture: an anticyclonic subtropical gyre with its western boundary current flowing northward and a cyclonic subpolar gyre with its western boundary current flowing southward.

When λ is moderate (normal wind forcing and normal amount of upper layer water) there is the supercritical state (I). Starting from the subcritical state, the wind-driven circulation evolves as parameter λ increases. Physically, as the amount of light water in the upper layer is gradually reduced (or as the wind stress is increased), at some critical point the upper-layer thickness in the middle of the western boundary becomes zero. What does the flow pattern look like if the amount of light water is reduced (or if the wind forcing is increased) further? The only logical solution we find is a peculiar loop of boundary currents near the middle of the western boundary of the subpolar basin. Within this loop the lower layer surfaces. On the western wall, there is an isolated western boundary current which moves southward to balance the northward Sverdrup transport within the interior ocean.

6

For a two-gyre basin the outcropping first appears in the subpolar gyre; when the amount of light water is small (or if the wind stress is large) the outcropping zone expands into the southern half of the basin. In a sense, Parsons's model forms a part of our model, cut off along the ZWCL. In our model the surfacing line is $\Psi = \Psi_m < 0$, but in Parsons's model the surfacing line corresponds to $\Psi = 0$, a condition which, as will be shown, is not necessarily met in a two-gyre basin.

For a two-gyre basin, a typical flow pattern has an outcropping zone occupying a large part of the subpolar basin and extending into the subtropical gyre. There is a whole loop of strong boundary currents around the outcropping zone: an internal jet flowing northeastward transporting warm water into the subpolar basin, an isolated northern boundary current flowing westward and an isolated western boundary current flowing southward transporting all the upper-layer water around to make a balanced pattern. Southward of the ZWCL the Gulf Stream separates from the coast and joins with the Labrador Current (the isolated western boundary current) to form a strong, warm internal jet. The mass flux of the Gulf Stream after its separation is the sum of the interior Sverdrup transports in both the subtropical and the subpolar basins. The water mass exchange across the ZWCL might be an important part of the poleward heat flux mechanism.

One notices, however, that the Sverdrup relation is not satisfied in the middle of the ZWCL where the internal jet crosses the ZWCL. This problem will be discussed in the following analysis.

When λ is big (very strong wind forcing or small amount of upper layer water), the upper layer water becomes a warm water pool near the southwest corner of the basin.

7

2. Basic Equations

In this section we consider the steady wind-driven circulation within a square subpolar basin. The origin of a Cartesian coordinate system is at the southwest corner of the basin with the x-axis directed eastward and the y-axis northward. The continuous stratification in the real ocean is modelled here as two immiscible layers, the upper layer and the lower layer with uniform density ρ_0 and ρ_1, respectively. In order to make the model more realistic, the interface is placed at about the depth of the thermocline, so that the upper layer is essentially the light water above the thermocline and the lower layer is the water beneath the thermocline.

For simplicity we assume that:

1) The pressure is hydrostatic.

2) The lower layer has infinite depth.

3) The effect of friction is an interfacial drag proportional to the velocity .

4) The flow can be represented by the vertically integrated average velocity.

The momentum and continuity equations for the upper layer can be written as

$$D(uu_x + vu_y) - fDv = -g'DD_x + \tau^x/\rho_0 - ku \tag{2.1}$$

$$D(uv_x + vv_y) + fDu = -g'DD_y + \tau^y/\rho_0 - kv \tag{2.2}$$

$$(Du)_x + (Dv)_y = 0 \tag{2.3}$$

where (u, v) is the horizontal velocity vector, (τ^x, τ^y) is the wind-stress vector, f = the Coriolis parameter of the earth, $g' = g(1 - \rho_0/\rho_1)$ is the reduced gravity, D is the upper layer thickness, and k is the drag coefficient.

8

Within the β-plane approximation we write

$$f = f_0 + \beta y$$

Note that the β-plane approximation is not really valid for a planetary scale. Veronis uses a spherical coordinates in his study. Nevertheless, the β-plane approximation gives a qualitatively correct picture even for a planetary scale. Thus the β-plane approximation is used in our simple model.

To obtain the non-dimensional equations, we introduce non-dimensional quantities by the following relations:

$$(x,y) = L(x',y')$$

$$\vec{\tau} = T\vec{\tau}'$$

$$D = dD' \tag{2.4}$$

$$(u,v) = g'd/L^2\beta(u',v')$$

$$f = L\beta f'$$

where

$$f' = f_0 + y' - 0.5 \tag{2.5}$$

$$f_0 = (R/L)\tan\theta_0 \tag{2.6}$$

T is the wind stress scale

d is the mean depth of the upper layer

If the total volume of the upper layer water is V, then the following relation holds

$$V = dL^2 \tag{2.7}$$

Dropping the primes for dimensionless variables, the momentum equations and continuity equation become

$$R_0 D(uu_x + vu_y) - fDv = -DD_x + \lambda\tau^x - \varepsilon u \qquad (2.8)$$

$$R_0 D(uv_x + vv_y) + fDu = -DD_y + \lambda\tau^y - \varepsilon v \qquad (2.9)$$

$$(Du)_x + (Dv)_y = 0 \qquad (2.10)$$

where the three non-dimensional parameters are

$$R_0 = g'd/L^4\beta^2, \qquad \varepsilon = k/\beta Ld, \qquad \lambda = TL/g'\rho_0 d^2 \qquad (2.11)$$

For typical cases, both R_0 and ε are very small and the nonlinear advection terms are neglected in the following discussion in order to derive simple analytical solutions. The fact that ε is a small number is used to follow a standard boundary layer perturbation approach to the basic equations.

Introduce a streamfunction

$$Du = -\Psi_y \quad , \quad Dv = \Psi_x \qquad (2.12)$$

Then the basic equations become

$$-f\Psi_x = -DD_x + \varepsilon/D \cdot \Psi_y + \lambda\tau^x \qquad (2.13)$$

$$-f\Psi_y = -DD_y - \varepsilon/D \cdot \Psi_x + \lambda\tau^y \qquad (2.14)$$

$$\Psi = 0 \text{ at } x = 0, 1 \text{ and } y = 0, 1 \qquad (2.15)$$

The solutions are subjected to the following constraint:

$$\int_0^1 \int_0^1 D dx dy = 1 \qquad (2.16)$$

which comes from equation (2.7).

For simplicity in the following discussion the wind stress is assumed to be in x-direction only, $\vec{\tau} = (\tau, 0)$. We begin with a subpolar basin model and explore the evolution of the flow pattern as λ increases gradually.

3. The Subcritical State

When there is a large amount of upper-layer water (or if the wind forcing is very weak) the upper layer covers the whole subpolar basin, and the solution is the classical subpolar cyclonic gyre with a strong western boundary current flowing southward. The structure of this boundary current is discussed in the following section. In the interior, there is the interior Sverdrup solution

$$\Psi_{in} = \lambda(1-x)\tau_y \tag{3.1}$$

$$D_{in}^2 = D_e^2 + 2\lambda(1-x)(f\tau_y-\tau) \tag{3.2}$$

where D_e is the upper-layer thickness along the eastern boundary. For the assumed pure zonal wind stress, D_e is a constant. In a subpolar gyre τ_y is always negative, and simple differentiation shows that D_{in} attains its minimum value at $(0, y_0)$ where $\tau_{yy} = 0$, and Ψ_{in} also attains its minimum value at the same point. As the volume of the light water in the upper layer is gradually reduced (or if the wind stress is gradually increased), λ increases and D_e increases almost linearly with λ (Fig. 1-1). This relation can be calculated by (2.16) and (3.2)

$$\int_0^1\int_0^1(D_e^2+2\lambda(1-x)(f\tau_y-\tau))^{1/2}dxdy = 1 \tag{3.3}$$

At a critical value λ_c, the upper-layer thickness becomes zero at point $(0, y_0)$. For a wind stress pattern $\tau = \cos\pi y$, $\lambda_c = 0.123$, $D_{ec} = 1.244$, and $D_{in} = 0$ appears at point $(0, 0.5)$. Above the critical value λ_c, there is no solution possible in which the upper layer covers the whole subpolar basin. This is the supercritical state which will be discussed next and the corresponding $\lambda - D_e$ relation is calculated by (4.5) in the next section.

11
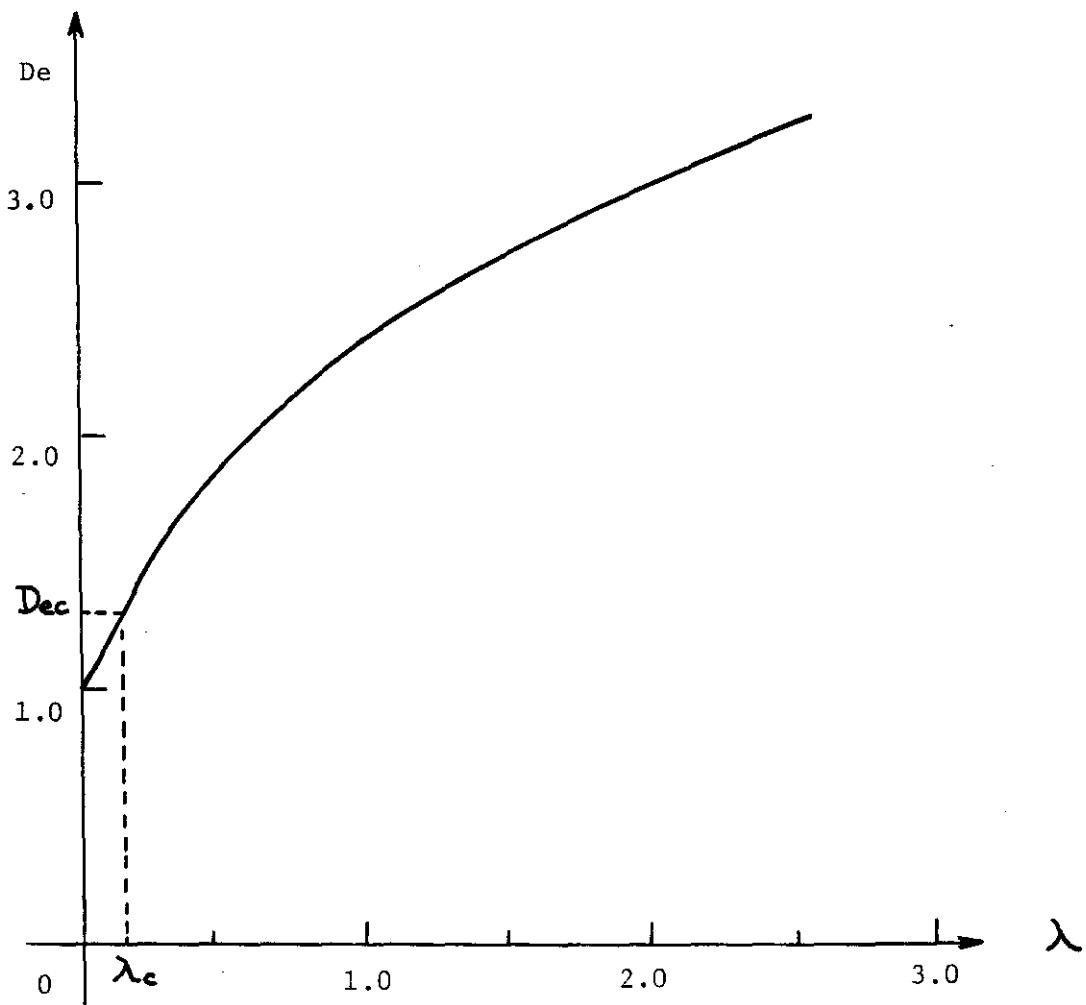
Fig. 1-1. The relation between λ and De (the layer thickness on the eastern wall) for a subpolar basin. $\lambda_c = 0.123$, Dec=1.244.

11-a

4. The Supercritical State (I)

Suppose the lower layer surfaces within a small area around point $(0, y_0)$. From equation (3.2), the line $D_{in} = 0$ is

$$(1-x)(f\tau_y - \tau) = -D_e^2/2\lambda \qquad (4.1)$$

along which the streamfunction of the interior Sverdrup solution is

$$\Psi_s = -D_e^2\tau_y/2(f\tau_y - \tau) \qquad (4.2)$$

By simple differentiation, one finds the total derivative

$$d\Psi_s/dy = D_e^2\tau\tau_{yy}/2(f\tau_y - \tau)^2 \qquad (4.3)$$

thus $y = y_0$ is a stationary point. Away from $y = y_0$, $d\Psi_s/dy$ is non-zero; therefore, Ψ_s is not constant along the $D_{in} = 0$ line. However, the surfacing line should be a streamline $\Psi = \Psi_m$. Since the line $D_{in} = 0$ does not satisfy this dynamic requirement, the current should move around and search out a position where the consistent dynamical balance holds. Here we are only interested in the steady circulation case, so that we do not discuss this adjustment process. The shape of this outcropping line, $X = X(y)$, will be discussed in the next section. At the same time, to transport the northward interior Sverdrup mass flux back southward, there should be an isolated western boundary current. (For our purely zonal wind forcing case, an eastern boundary current is dynamically impossible. Unlike the traditional boundary currents in layer models, here we are dealing with boundary currents that are separated from the interior domain of the upper layer by the outcropped lower layer. Thus they are isolated from the main body of the upper layer.) On northern/southern parts of the western boundary, if the upper layer is not separated from the wall, there are classic western boundary currents

(See Section 6, Fig. 1-4a). The internal free surfacing line is a "western" boundary for the upper layer flow, so there is an intense internal boundary current along this surfacing line. When the surfacing line meets the northern/southern boundaries, there are isolated northern/southern boundary currents as well. All these boundary currents will be discussed in the next section.

In the supercritical cases the integration condition (2.16) should be written as

$$\iint_\Omega D \, d\Omega = 1 \tag{4.4}$$

where Ω is the area that the upper layer fluid actually occupies and D is the upper layer thickness. Because the boundary layers are very narrow, their contributions to the integral (4.4) are order ε. Furthermore, the contribution of the interior boundary current is a small negative correction term to the integration; the contributions from the isolated western boundary current or the isolated northern/southern boundary currents are small positive terms. Thus these terms tend to compensate each other. Within the lowest order approximation one thus can simply use the region on the right-hand-side of the outcropping line as Ω and D_{in} as D in calculation. For the case we are discussing, $\vec{\tau} = (\tau, 0)$ and τ is independent of x, the double integration in (4.4) can be changed into a simple 1-D integration

$$\int_0^1 \frac{\{1+2\lambda/D_e^2 \cdot [1-X(y)](f\tau_y-\tau)\}^{3/2}-1}{3\lambda/D_e^2 \cdot (f\tau_y-\tau)} dy = \frac{1}{D_e} \tag{4.5}$$

After finding out the surfacing line $X = X(y)$, this integration condition gives the relationship between λ and D_e as the right part of the curve in Fig. 1-1.

13

5. Boundary Layer Structures

1) Semi-geostrophy condition

For an arbitrary boundary current it is convenient to use a new coordinate system (r, s) with the outcropping lower layer water occupying the region r < 0 (Fig. 1-2). Assume that the boundary layer thickness is much smaller than the curvature radius of the surfacing line, we can neglect the curvature terms in the momentum equations and treat the (r, s) coordinates as local Cartesian coordinates. After introducing the stretched boundary layer coordinate

$$\eta = r/\varepsilon \tag{5.1}$$

(2.13) and (2.14) become

$$-f\Psi_\eta = -DD_\eta + \varepsilon^2 \Psi_s/D + \varepsilon\lambda\tau^r \tag{5.2}$$

$$-f\Psi_s = -DD_s - \Psi_\eta/D + \lambda\tau^s \tag{5.3}$$

To the lowest order, (5.2) represents the semi-geostrophy condition across the narrow boundary layer; meanwhile (5.3) is the ageostrophic downstream balance which is typical of all kinds of boundary currents.

Integrating (5.2) across the boundary current gives the semi-geostrophy condition

$$\Psi - D^2/2f = g(s) + O(\varepsilon) \tag{5.4}$$

where g(s) can be determined for specific boundary currents from the corresponding boundary conditions.

By cross-differentiating and subtracting (5.2) and (5.3), we obtain the potential vorticity equation

$$\partial/\partial\eta \cdot (D^{-1}\partial\Psi/\partial\eta) + f_s\partial\Psi/\partial\eta = -\varepsilon[\lambda(\nabla\times\tau)_z + f_r\Psi_s] - \varepsilon^2\partial/\partial s \cdot (D^{-1}\partial\Psi/\partial s) \tag{5.5}$$

14
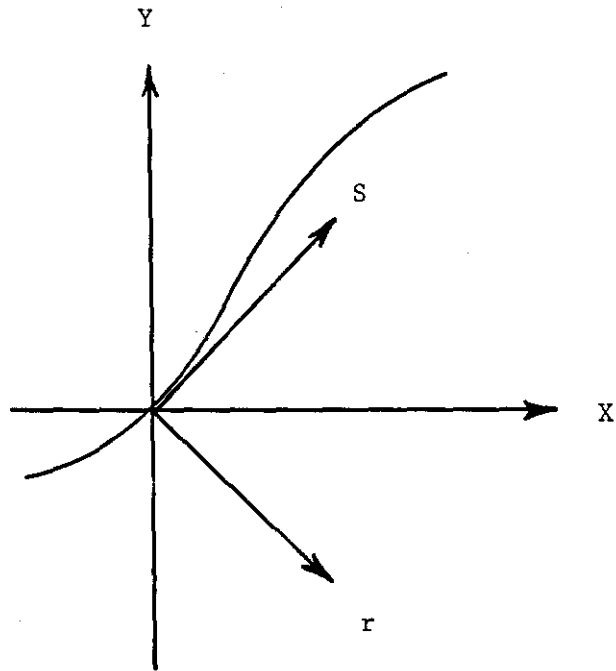
Fig. 1-2. The local coordinate system (r,s).

where

$$f_s = df/ds, \qquad f_r = df/dr.$$

To the lowest order this equation is simply

$$(\Psi_\eta/D)_\eta + f_s \, \Psi_\eta = 0 \tag{5.6}$$

which we can integrate to get

$$\Psi_\eta/D + f_s \, \Psi = h(s) \tag{5.7}$$

Using semi-geostrophy, this equation becomes

$$D_\eta + f_s \, D^2/2 = h_1 \, (s) \tag{5.8}$$

However, for most cases it is more direct to put the semi-geostrophy condition into the ageostrophic momentum equation and find the boundary layer solutions.

In the following analysis we will use this semi-geostrophy condition to find the shape of the outcropping line. Then we will discuss the interior boundary current, the classical western boundary current, the isolated western boundary current, the isolated northern boundary current, and the isolated southern boundary current.

2) The Outcropping Line

Applying the boundary condition for the unknown free boundary

$$\Psi = \Psi_m \, , \, D = 0 \qquad \text{at } \eta = 0 \tag{5.9}$$

the semi-geostrophy condition becomes

$$\Psi - D^2/2f = \Psi_m \tag{5.10}$$

where $\Psi_m < 0$ is an unknown constant. Note that (5.10) applies to the entire width of the boundary layer. By using (3.1) and (3.2) the above condition can be written as

$$\Psi_m = -D_e^2/2f + \lambda(1-x)\tau/f \tag{5.11}$$

15

To determine the surfacing line for a given λ, we need two more conditions. Assume that the surfacing line meets the western wall at $y = y_c$ so that

$$\Psi_m = - D_e^2/2f_c + \lambda\tau_c/f_c \tag{5.12}$$

where

$$f_c = f_0 + y_c - 0.5 \tag{5.13}$$

$$\tau_c = \tau(y_c)$$

Then the equation for surfacing line can be written as

$$1-X = [D_e^2(f_c-f)/2+\lambda f\tau_c]/\lambda\tau f_c \tag{5.14}$$

Since the surfacing line is allowed to cross the zero-wind-line, the numerator on the right-hand side of equation (5.14) should be zero at $y = y_t$ where $\tau(y_t) = 0$, giving

$$D_e^2 = 2\lambda\tau_c f_t/(f_t-f_c) \tag{5.15}$$

The final form for the surfacing line is therefore

$$X(y)= 1 - \tau_c/\tau\cdot(y_t-y)/(y_t-y_c) \tag{5.16}$$

As $y \to y_t$, the limit is finite

$$X_t= 1 + \tau_c/(y_t-y_c)\tau_y(y_t) \tag{5.17}$$

Now putting equations (5.15) and (5.16) into (3.2) gives an equation for the upper layer thickness along this surfacing line:

$$D_{in}^2 = 2\lambda\tau_c f[1+(f_t-f)\tau_y/\tau]/(y_t-y_c) \tag{5.18}$$

It is obvious that $D_{in} \to 0$ as $y \to y_t$. To guarantee that $D_{in}^2 \geqslant 0$ everywhere along the surfacing line, the following condition should be satisfied

$$(y_t-y)\tau_y/\tau \geqslant -1 \tag{5.19}$$

which means

$\tau \geq (y_t - y)|\tau_y|$ when $\tau > 0$, $y < y_t$

$\tau \leq -(y - y_t)|\tau_y|$ when $\tau < 0$, $y > y_t$ (5.20)

or, if τ_{yy} exists,

$\tau_{yy} \geq 0$ for $y > y_t$

$\tau_{yy} \leq 0$ $y < y_t$ (5.21)

If τ_{yy} is continuous at y_t, the condition (5.21) means

$\tau_{yy} = 0$ at $y = y_t$ where $\tau = 0$ (5.22)

This condition guarantees that as λ passes over λ_c the lower layer outcrops near $(0, y_0)$ where $\tau = 0$, thus assurming a continuous transition between the subcritical case and the supercritical case. (If this condition is not satisfied, the surfacing line meets the eastern wall below the zero-wind-stress line. For the wind stress being used an eastern boundary current is not possible and the procedure above cannot be used to find the steady solution to satisfy all the necessary boundary conditions. As yet, we have not been able to find a solution for more general wind stress patterns.)

This constraint can be explained from the basic force balance. Putting the semi-geostrophy condition (5.10) into (5.3), we get

$f_s(\Psi - \Psi_m) = -\Psi_\eta / D + \lambda \tau^s$ (5.23)

Because $\Psi \sim \Psi_m$ near the outcropping line, it follows that

$-\Psi_\eta / D + \lambda \tau^s = 0$ (5.24)

which means, under our assumption (neglecting the nonlinear advection term and the pressure gradients in the lower layer), that the basic downstream momentum balance is between the friction force and the local wind. Therefore

$dX/dy \cdot \tau > 0$ (5.25)

and

dX/dy=0 only if $\tau = 0$ (5.26)

However, from (4.1) by differentiation and noting that generally $f\tau_y - \tau$

is nonzero where τ_{yy} is zero, we have

dX/dy=0 appears where $\tau_{yy}=0$ · (5.27)

This relation can be explained from the Sverdrup mass transport relation (3.1)

because the streamfuction attains its extreme value at the stationary point

where $\tau_{yy} = 0$. Combining (5.26) and (5.27), we find the same constraint

(5.22).

Veronis uses a relation similar to (5.14) to determine the outcropping

line. Because D_e and τ are specified from data and there is no easterly

near the northern boundary in his model, there is no singular latitude and

(5.14) works well in his model. To build up a mass balance he proposes the

existence of the isolated northern and western boundary currents. However, as

is shown in Appendix A, the only possible momentum balance (within the

dynamics being used here) for an isolated northern boundary current is a

balance between the local wind stress and the friction force. To have a

continuous mass transport within the whole basin, the northern boundary

current should flow westward. However, the friction force would then be

eastward. Thus it is still not clear how a westward isolated northern boundary

current is formed within a westerly zone.

One can see from the analysis above that including the nonlinear advection

terms or the pressure gradients in the lower layer might release this

constraint on the wind profile. This is left for further numerical

investigation.

18

As the volume of light water is further reduced (or if the wind stress is further increased), the surfacing line may not meet the western wall. Instead, it may meet the southern wall at $x = x_s$. By arguments like those above the surfacing line equation is

$$X(y) = 1- 2(1-x_s)(y_t-y)/\tau(y) \tag{5.28}$$

Fig. 1-3 shows the typical surfacing lines.

3) The Structure of the Interior Boundary Current

We apply the following boundary conditions

$$D = 0 \qquad \text{at } \eta = 0 \tag{5.29}$$

$$D = D_{in}, \ D_\eta = 0 \quad \text{at } \eta = \infty \tag{5.30}$$

to equation (5.8). The result is a simple first-order ordinary differential equation

$$dD/d\eta + f_s(D^2-D_{in}^2) = 0 \tag{5.31}$$

$$D(0) = 0 \tag{5.32}$$

whose solution is

$$D = D_{in}(1-\exp(-f_s D_{in}\eta))/(1+\exp(-f_s D_{in}\eta)) \tag{5.33}$$

where D_{in} is the layer thickness for the interior solution at the outcropping line. The corresponding streamfunction Ψ can be calculated from the semi-geostrophy condition (5.10). From this equation the boundary layer thickness is inversely proportional to df/ds so that in the southern end of the interior boundary, the boundary current becomes more and more spread out. Obviously, the boundary layer strength is zero at point (x_t,y_t) where the interior solution satisfies the outcropping line condition exactly.
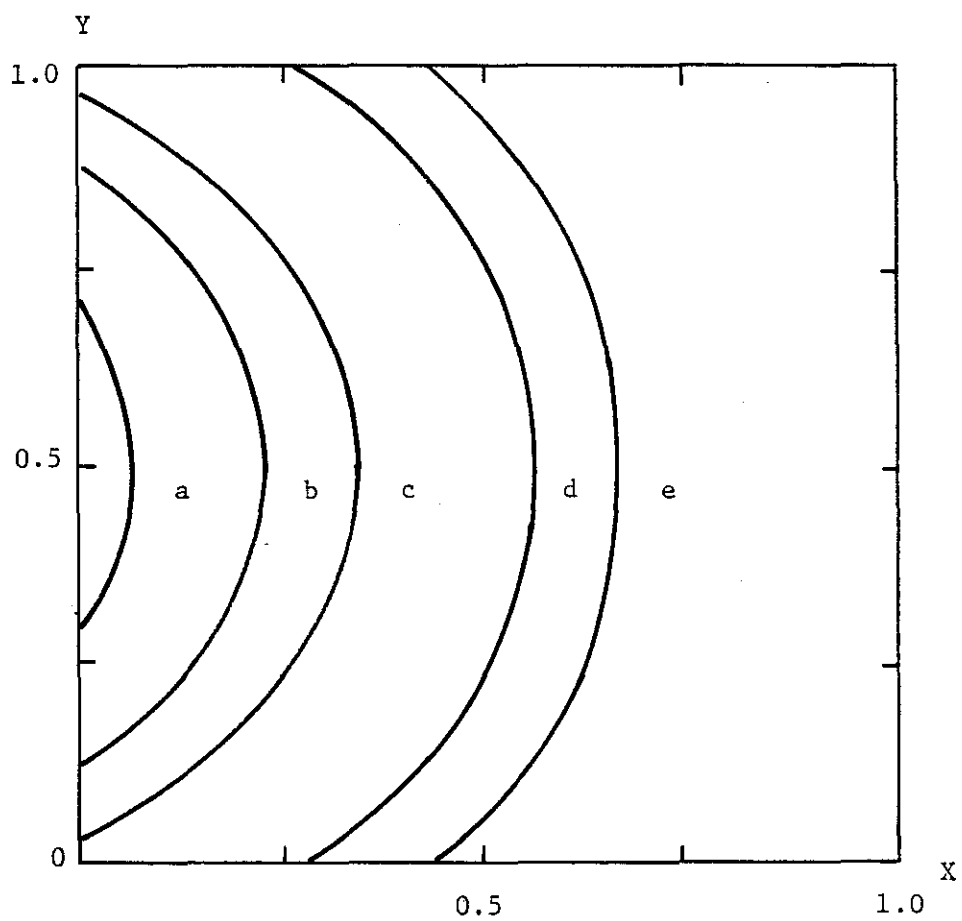
Fig. 1-3. Typical outcropping lines for a subpolar basin model.
lambda= 0.1385 (a); 0.2027 (b); 0.3927 (c); 0.841 (d); 1.642 (e).

19—a

4) The Structure of the Classical Western Boundary Current

Using boundary layer coordinates

$$\eta = -x/\varepsilon, \quad s = -y$$

the corresponding boundary layer domain is

$$\eta = (\eta_\infty, 0], \quad \eta_\infty < 0 .$$

The corresponding equations (5.4) and (5.8) become

$$\Psi - D^2/2f = -D_w^2/2f \qquad (5.34)$$

$$D_\eta + D^2/2 = D_{in}^2 /2 \qquad (5.35)$$

with the following boundary condition

$$D^2(0) = D_w^2 = D_{in}^2 - 2f\Psi_{in} \qquad (5.36)$$

Integrating equation (5.35) with the boundary condition (5.36), the solution is

$$D = D_{in}(1-B\exp(D_{in}\eta))/(1+B\exp(D_{in}\eta)) \qquad (5.37)$$

where

$$B = (D_{in}-D_w)/(D_{in}+D_w) \qquad (5.38)$$

The corresponding streamfunction Ψ can be calculated from (5.34).

5) The Structure of the Isolated Western Boundary Current

Using the same boundary layer coordinates as above, the semi-geostrophy gives one equation

$$\Psi - D^2/2f = - D_w^2 /2f \qquad (5.39)$$

D_w can be determined by

$$D_w^2 = -2f\Psi_m \qquad (5.40)$$

where Ψ_m comes from the interior boundary layer solution. The other equation can be derived either from

$$\Psi_\eta(2f\Psi+D_w^2)^{-1/2} + \Psi = \Psi_m \qquad (5.41)$$

with the boundary condition

$$\Psi(0) = \Psi_m \tag{5.42}$$

or from the equation

$$dD/d\eta + D^2/2 = 0 \tag{5.43}$$

with the boundary condition

$$D(0) = D_w \tag{5.44}$$

The solution is

$$\Psi = D_w^2[(1-D_w\eta/2)^{-2} - 1] \tag{5.45}$$

$$D = (1/D_w - \eta/2)^{-1} \tag{5.46}$$

One peculiarity is that this isolated western boundary current is rather wide; its thickness tends to zero only at $\eta = x/\varepsilon \rightarrow -\infty$. It is easy to prove that the total volume of this isolated western boundary current is order ε.

Actually, η need not go to $-\infty$. This is so because our upper layer includes the mixed layer so that when the layer thickness is less than the mixed layer thickness, the solution is no longer valid. On the other hand, even within Parsons's model other terms in the equations should be considered when D is less than ε. Physically, we expect that the boundary layer has a slightly different structure near the outcropping edge.

6) The Structure of the Northern Boundary Current

A classical scaling for the northern boundary current is $\delta \sim \varepsilon^{1/2}$. However, for an isolated northern/southern boundary current, the appropriate scaling is $\delta \sim \varepsilon$ (see Appendix A for details). For the northern boundary current here the proper boundary layer coordinates are

$$\eta = (y-y_n)/\varepsilon, \quad s = -x$$

21

where $y = y_n$ is the outcropping line. We have the same semi-geostrophy condition as for the isolated western boundary current.

$$\Psi - D^2/2f = \Psi_m \qquad (5.47)$$

However, now $df/ds = 0$, so that the potential vorticity equation is

$$(\Psi_\eta/D)_\eta = O(\varepsilon) \qquad (5.48)$$

or

$$\Psi_\eta/D = fD_\eta = g(s) \qquad (5.49)$$

This means that the layer thickness is a linear function of η. To determine the two unknown constants we have to include at least the $O(\varepsilon)$ term. Using semi-geostrophy, the equation for the across-stream velocity (the s-momentum equation) becomes

$$D_\eta + \lambda f\tau = 0 \qquad \text{at} \quad y = 1 \qquad (5.50)$$

As discussed in relation to (5.24), this equation means that the downstream momentum balance is between the local wind and the friction force. Because $\tau(1) = -1$, the solution for (5.50) is

$$D = \lambda f_{nb}\eta \qquad (5.51)$$

$$\Psi = \Psi_m + \lambda^2 f_{nb}\eta^2/2 \qquad (5.52)$$

and the northern boundary layer width is

$$\eta_{on} = D_w/\lambda f_{nb} \qquad (5.53)$$

where

$$f_{nb} = f_0 + 0.5 \qquad (5.54)$$

$$D_w = (-2f_{nb}\Psi_m)^{1/2} \qquad (5.55)$$

are, respectively, the Coriolis parameter and the layer thickness along the northern wall required for transporting the mass of water Ψ_m (compare (5.40) and (5.60)).

22

7) The Structure of the Southern Boundary Current

Following the same argument as before, the corresponding boundary layer solution is

$$D = \lambda f_{sb} \eta \qquad (5.56)$$

$$\Psi = \Psi_m + \lambda^2 f_{sb} \eta^2 / 2 \qquad (5.57)$$

and the southern boundary layer width is

$$\eta_{os} = D_w / \lambda f_{sb} \qquad (5.58)$$

where

$$f_{sb} = f_0 - 0.5 \qquad (5.59)$$

$$D_w = (-2 f_{sb} \Psi_m)^{1/2} \qquad (5.60)$$

are the Coriolis parameter and the layer thickness on the southern wall.

REMARK. When a boundary current joins with another boundary current or the interior flow, the flow pattern is much more complicated. Here we do not discuss the details of these matching flows. All figures in the following discussion are plotted by a computer subroutine that smooths out the matching region automatically.

6. Flow Patterns in a Subpolar Basin

Because the wind stress has been assumed to be

$$\tau = \cos\pi y \qquad 0 \leq y \leq 1 \tag{6.1}$$

it follows that

$$\tau_{yy} = \tau = 0 \qquad \text{at } y_t = 0.5 \tag{6.2}$$

This wind stress pattern satisfies (5.22). Using the condition

$$D = 0 \qquad \text{at } (x_t, y_t = 0.5) \tag{6.3}$$

and equations (3.2) and (5.7), we find the following relation

$$\lambda/D_e^2 = (0.5-y_c)/2f_0\tau_c \tag{6.4}$$

Putting relations (6.4) and (5.16) into integration relation (4.5) gives us an equation between y_c and D_e, or λ and D_e. Fig. 1-1 shows the numerical result for the above wind stress pattern. When the upper layer contains large amount of light water, λ is almost zero and $D_e \simeq 1$. As the amount of light water decreases, λ increases and D_e increases almost linearly with λ. After λ becomes bigger than λ_c, the lower layer outcrops and a loop of boundary currents appears.

Fig. 1-4 shows the typical flow patterns for a subpolar basin. An isolated western boundary current flows southward returning the northward interior Sverdrup mass flux. An internal boundary current separates the light water of the upper layer from the heavy water of the lower layer. At $y = 0.5$ this boundary current has a zero width and zero mass flux because the interior solution itself satisfies the surfacing line condition exactly. Northward or southward from this point, more and more streamlines join the internal boundary current, making it a stronger and stronger internal jet.

24

contour. -.3516 to -.0391, int. .0391   contour. -.4729 to .0525, int. .0525

(a)

L -.3907

(b)

L -.525

contour. -1.135 to 0.00, int. 0.126

(c)

L -1.26
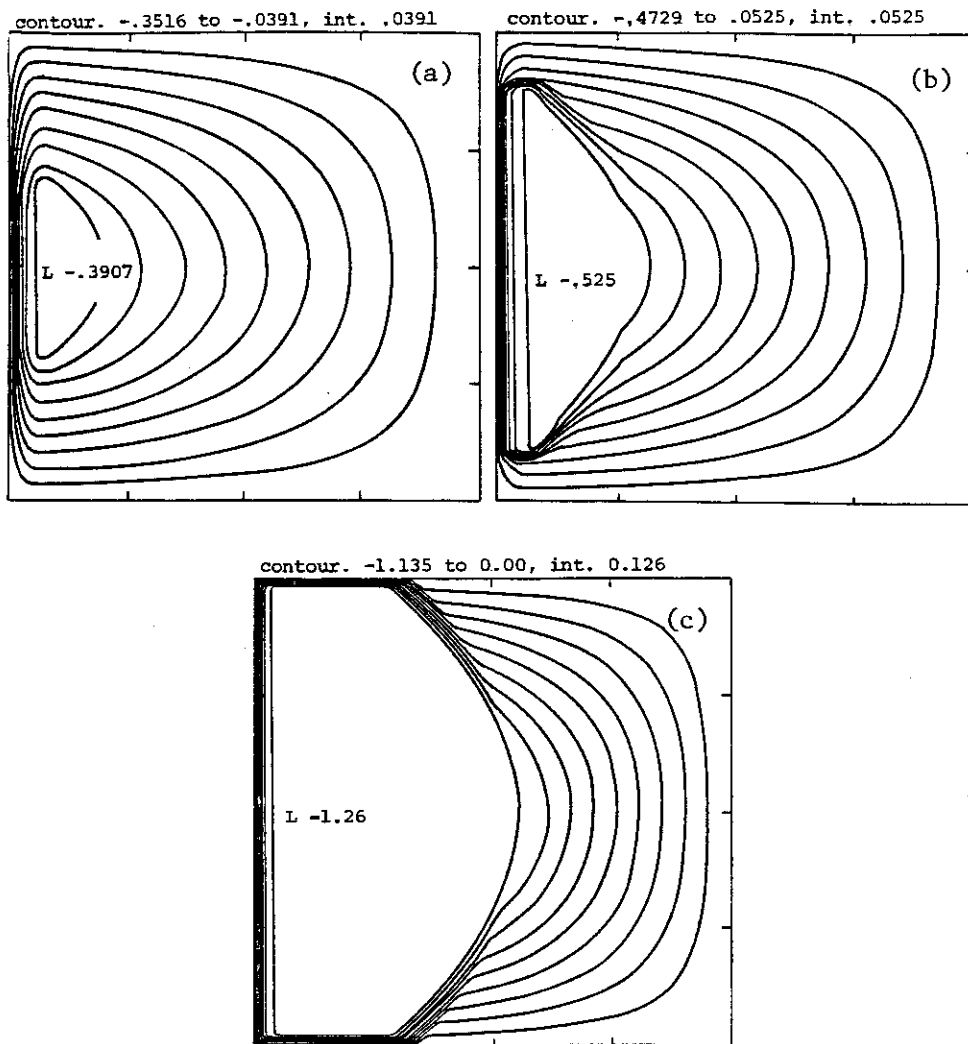
Fig. 1-4. Flow patterns for a subpolar basin.
lambda= 0.138 (a); 0.220 (b); 0.840 (c).
De = 1.28 (a); 1.45 (b); 2.24 (c).
Yc = 0.3 (a); 0.1 (b); Xc=.25(c).

In Parsons's model for the subtropical basin, the outcropping appears on the northwest corner at first and there are no isolated western or northern boundary currents. In a subpolar basin, an isolated western boundary current is necessary for a dynamically consistent model. This boundary current is strong and narrow and contains relatively warm water. In the North Atlantic Ocean, the Labrador Current is one example of this kind of isolated boundary current.

7. Flow Patterns in a Subtropical/Subpolar Basin

It is easy to apply the argument for a subpolar basin to a subtropical-subpolar basin. All the formulae are basically the same, except $0 \le y \le 1$ means the whole basin, and $0 \le y \le 0.5$ is the subtropical part of the basin, while $0.5 \le y \le 1$ is the corresponding subpolar part of the basin. Choosing a typical wind-stress pattern

$$\tau = -\cos 2\pi y \qquad\qquad 0 \le y \le 1, \qquad\qquad (7.1)$$

we can use almost the same formulae as before, with some minor changes ($y_t \rightarrow 0.75$, $f_0 \rightarrow f'_0$ et.).

Fig. 1-5 shows the relations between λ and D_e, λ and $-\psi_m$ for a two-gyre basin. It is easy to see that as λ increases, starting from $\lambda = 0$, D_e increases almost linearly with λ. Above $\lambda = \lambda_c$ is the supercritical state (I) with the internal boundary current forming within the subpolar basin. As λ increases further, D_e increases, the outcropping area enlarges, and the surfacing line moves outward into the interior of the basin. Finally, when $\lambda > \lambda_d$ the outcropping area extends across the ZWCL. The isolated western boundary current moves into the subtropical basin and joins the northward western boundary current there, forming the strong internal jet which flows northeastward. As the internal jet moves into the interior of the basin, its intensity decreases gradually as it loses its mass to the interior Sverdrup flow. However, there is a finite amount of water, $-\psi_m$, in this internal jet as it crosses the ZWCL. The value of this mass flux is exactly the value needed to balance the maximum internal Sverdrup mass flux in the middle of the subpolar gyre.
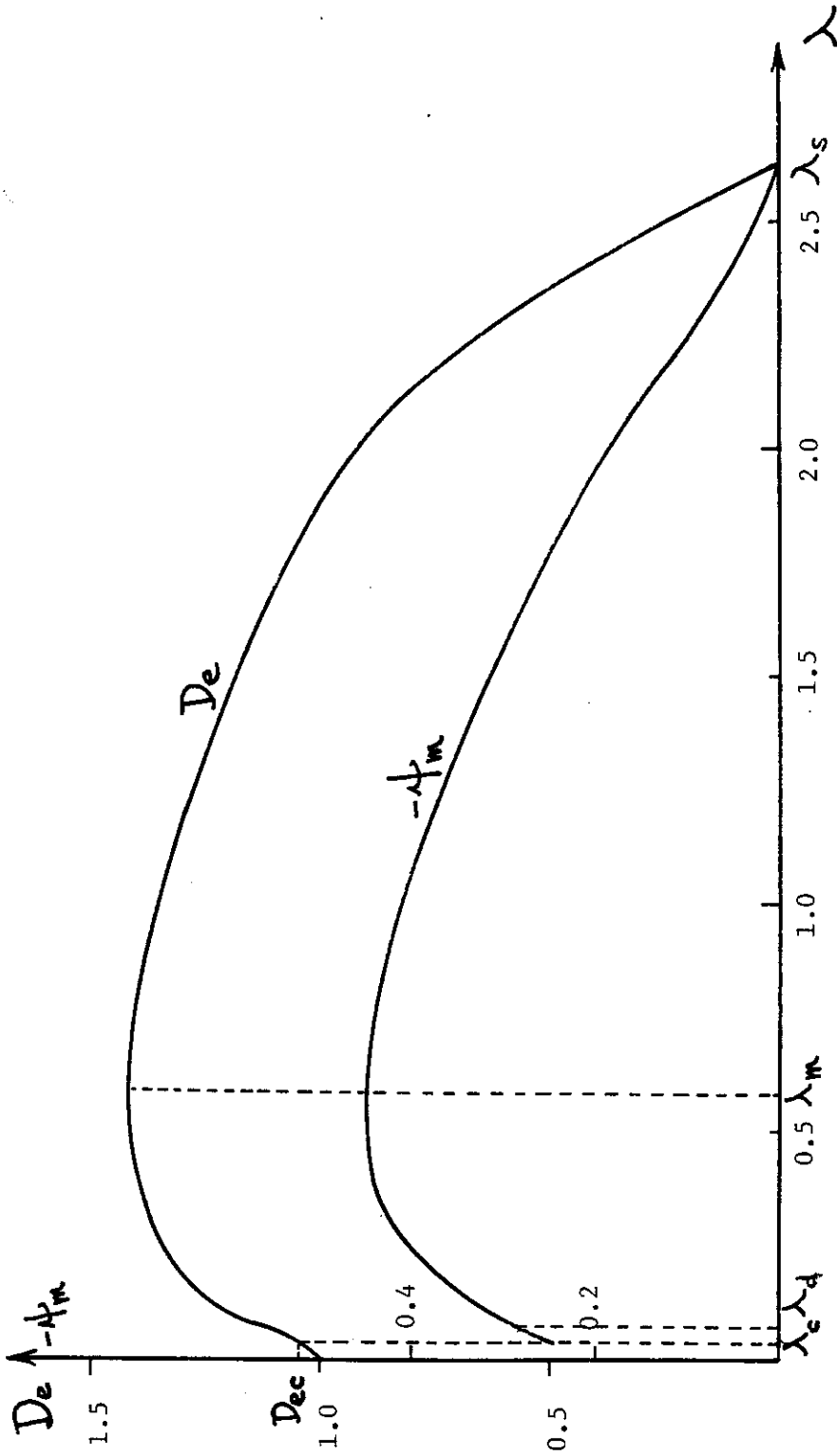
Fig. 1-5. Relations between λ and $\mathcal{D}_e$; λ and $-\psi_m$ for a subtropical-subpolar basin. The first critical value is $\lambda_c = 0.0384$; the second critical value is $\lambda_s = 2.627$. Dec= 1.0422, $\lambda_d = 0.0713$, $\lambda_m = 0.590$ (see text for explanation).

26-a

In Fig. 1-5 the curve for $-\psi_m$ starts from $\lambda = \lambda_c$ because $-\psi_m$ is meaningless for the subcritical state. For the first supercritical state $-\psi_m$ is the total mass flux of the upper layer in the subpolar basin. As shown in Fig. 1-5, both D_e and $-\psi_m$ increase with λ when $\lambda < \lambda_m$. At $\lambda = \lambda_m$ both D_e and $-\psi_m$ attain their maximum value ($D_{em} = 1.422$, $-\psi_{mm} = 0.449$). As λ increases further, both D_e and $-\psi_m$ decrease till $\lambda = \lambda_s$ when both D_e and $-\psi_m$ become zero. This figure shows an important feature of the generalized Parsons's model that both the layer thickness on the eastern wall and the cross-ZWCL mass transport increase with λ first, and decrease with λ after attaining local maximum. This feature might have important meaning for climate modelling (see Addendum).

Fig. 1-6 shows typical outcropping lines for a two-gyre basin; three curves with $\lambda = 0.11$, 0.246, 1.09 correspond to the first supercritical state. (Cases for $\lambda = 7.12$ and 19.5 belong to the second supercritical state which will be discussed in the next section).

One notices that the Sverdrup relation is not satisfied on part of the ZWCL. When the internal jet crosses the ZWCL, there is a strong interfacial friction. Thus if we consider the upper layer alone, the mass flux is non-zero on the ZWCL. Both Veronis's model and the present model have the same shortcoming. Actually, the interfacial friction drives water in the lower layer. No matter how deep the lower layer is, there is a finite amount of water mass transport within it. In the case of a deep lower layer, the bottom friction is much smaller than the interfacial friction. Thus the total mass flux of these two layers should satisfy the Sverdrup relation wherever the bottom friction is not strong. (The western boundary current region is a place
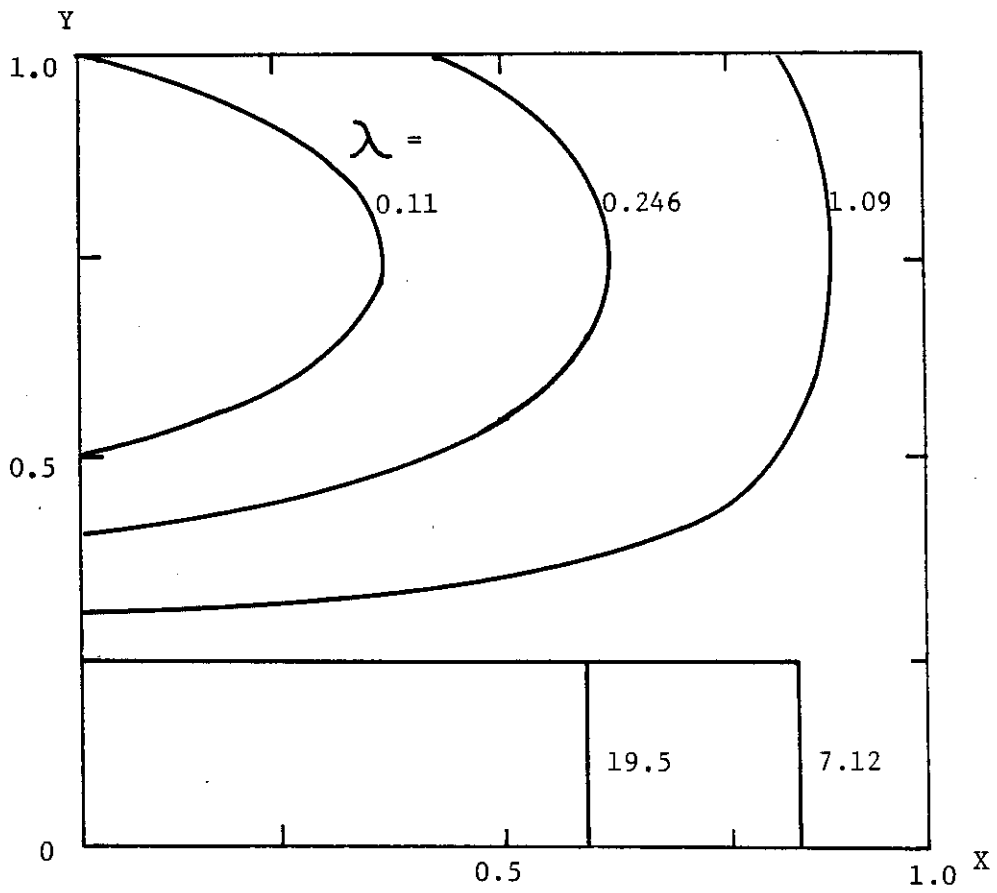
Fig. 1-6. Typical outcropping lines for a subtropical-subpolar
basin, for both the first supercritical state and the
second supercritical state.

where this relation breaks down.) In the second chapter we will solve this problem by using a model with a finitely deep lower layer.

Fig. 1-7 shows some examples of the two-gyre basin flow pattern. These examples show that as the surfacing line moves into the subtropical basin, it gradually acquires a west-east orientation. The boundary layer becomes wider along this part of the surfacing line and the streamlines spread over a fairly wide region.

Compared with the commonly accepted quasi-geostrophic model, the present model gives a quite different picture of the flow in a subtropical-subpolar basin. Traditional quasi-geostrophic models retain the nonlinear advection term, but by assuming quasi-geostrophy these models ignore the nonlinear interaction between the wind-driven circulation and the basic density stratification. Typical flow patterns for a two-gyre basin are always symmetric with the ZWCL. Our model ignores the nonlinear advection term but retains the nonlinearity connected with the change in layer thickness. By allowing the layer thickness to go to zero, our model includes a very strong nonlinearity. Now that the flow pattern is asymmetric with the ZWCL, the two gyres combine into a united body through the strong interior jet and the water mass exchange across the ZWCL.

It is easy to see that putting $\Psi_m = 0$ into formula (5.11) gives the surfacing line for Parsons's model. As we can see from the argument in Section 5, setting $\Psi_m = 0$ does not work for the subpolar basin. (The surfacing line would meet the eastern wall below $y = y_t$, making a consistent solution impossible.) Using the solution for a two-gyre basin, it is easy to prove that the outcropping line intrudes into the subtropical basin before the interior

contour. -.1985 to .2191, int. .0522   contour. -.2798 to .3366, int. .0685

contour. -.36 to .8577, int. .1353   contour. -.449 to 2.881, int. .370
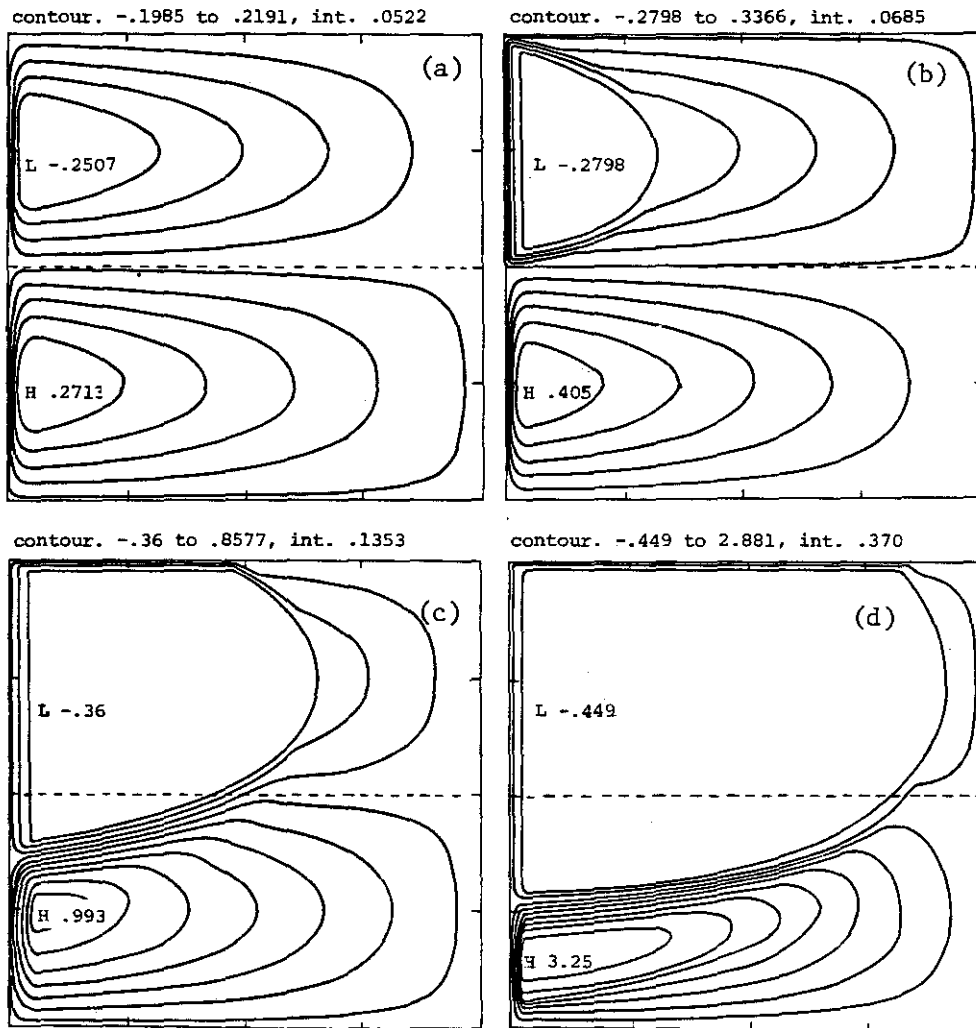
Fig. 1-7. Flow patterns for a subtropical-subpolar basin.
epsilon= 0.02,
lambda = 0.047 (a); 0.070 (b); 0.153 (c); 0.610 (d),
De = 1.065 (a); 1.130 (b); 1.270 (c); 1.420 (d),
Yc = 0.6   (a); 0.5   (b); 0.403 (c); 0.303 (d).

solution has a zero layer thickness there. In this sense, Parsons's model is a degenerate case only for a single subtropical basin.

Fig. 1-8 shows the north-south and east-west sections of a two-gyre basin thermocline structure. Our two-layer model gives a simplified picture for the bowl-shaped subtropical gyre and the dome-shaped subpolar gyre.

Z

isolated w.b.c.   interior b.c.

1.

0
W
                                                          E

X

(a)

interior b.c.   isolated n.b.c.

Z   ZWCL

1.0

0
S   N

Y

(b)

upper layer
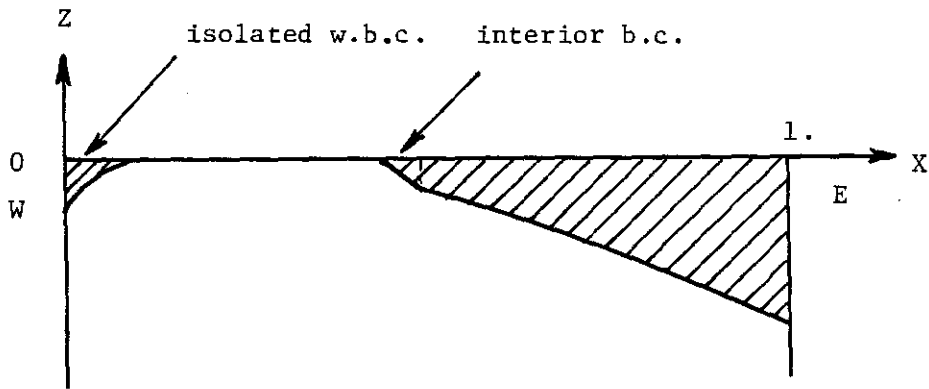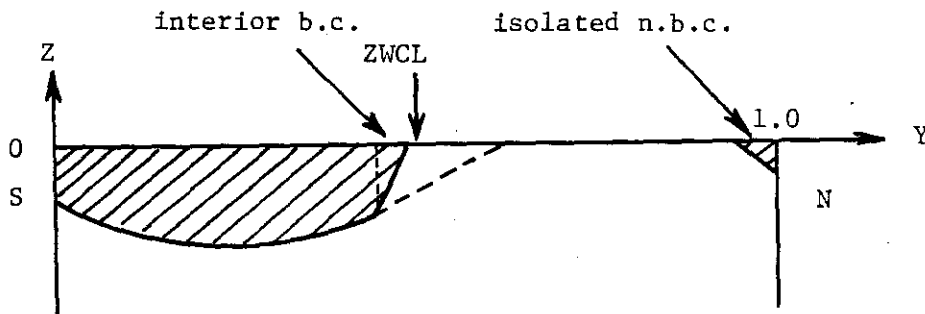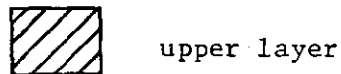
Fig. 1-8. Schematic diagrams for the thermocline structure in
a subtropical-subpolar basin. (a) A longitudinal section
in the subpolar basin; (b) a meridional section. There are
the bowl-shaped thermocline in the subtropical gyre and
the dome-shaped thermocline with outcropping in the subpolar
gyre.

8. Supercritical State (II)

From Fig. 1-6 one can see that as λ increases, the surfacing line approaches the eastern wall and the line $y = .25$. Finally, when $\lambda = \lambda_s$ (= 2.627 for the wind stress pattern we used), the second critical value, the layer thickness along the eastern wall is zero and the surfacing line is $y = .25$ where $\tau = 0$. If λ increases further, the warm upper layer separates from the eastern wall and the lower layer outcrops in the southeast corner of the basin. Here the line between the upper layer and the lower layer is a free eastern boundary for the upper layer. In the following discussion an analysis of this free eastern boundary is presented and the whole upper-layer flow pattern is discussed.

1) The free eastern boundary condition

Because this surfacing line is an "eastern boundary" for the upper layer, there is no boundary current connected with it. It is a free boundary. To determine the shape of this free boundary, one has to use additional dynamical relations. It turns out that the dynamical structure of the upper mixed layer is important for determining this free boundary.

For more general purposes, the following discussion includes the case when the lower layer is in motion. After introducing the vertically integrated streamfunctions Ψ_0 and Ψ_1, the momentum equations for a two-layer model can be written as

$$-f\nabla\Psi_0 = -g\nabla\eta + (\vec{\tau} + \vec{\tau_b})/D \tag{8.1}$$

$$-f\nabla\Psi_1 = g\nabla(\delta\rho D/\rho_0 - \eta) + (\vec{\tau_b} - \vec{\tau_0})/h, \tag{8.2}$$

where

  η is the free surface elevation

  $\vec{\tau}$ is the sea-surface wind stress

  $\vec{\tau_D}$ is the interfacial friction

  $\vec{\tau_b}$ is the bottom friction (neglected in the following analysis).

Eliminating η from (8.1) and (8.2) yields

$$-f\nabla\Psi_0 = -f\nabla\Psi_1 - g'\nabla D + \vec{\tau_D}/h + (\vec{\tau}+\vec{\tau_D})/D \qquad (8.3)$$

By definition

$$U_0 = -\Psi_{0y}, \quad V_0 = \Psi_{0x} \qquad (8.4)$$

$$U_1 = -\Psi_{1y}, \quad V_1 = \Psi_{1x}$$

Using the fact that this surfacing line is a streamline for the upper layer,

one introduces

  $\gamma = V_0/U_0$ as the slope for the surfacing line.

By assuming that (8.3) is valid on this surfacing line, (8.3) can be written as

$$\gamma = \frac{fV_1 + g'D_x - \tau^x/D - \tau_{Dx}(1/D+1/h)}{fU_1 - g'D_y + \tau^y/D + \tau_{Dy}(1/D+1/h)} \qquad (8.5)$$

Note that

$$D_y = -D_x/(\partial y/\partial x)_{D=const.} = -D_x/\gamma \qquad (8.6)$$

Thus (8.5) can be simplified

$$\gamma = -\frac{\tau^x - fDV_1 + \tau_{Dx}(1+D/h)}{\tau^y + fDU_1 + \tau_{Dy}(1+D/h)} \qquad (8.7)$$

From (8.7) it is obvious that to determine the free boundary one needs to know the specific friction force terms and the lower layer velocity field. The latter can be easily calculated from simple Sverdrup dynamics, integrating from the eastern wall.

The simplest mixed layer model is a slab model. According to the assumption of slab model, the whole mixed layer moves with a vertically uniform horizontal velocity. The frictional force between the mixed layer and the layer below is much smaller than the sea-surface wind stress. Thus the τ_D terms in (8.7) are negligible.

Within our assumption in this chapter, the lower layer has an infinite depth and is motionless. We can eliminate the U_1, V_1 terms in (8.7) so that the free boundary condition (8.7) becomes

$$\gamma = -\tau^x/\tau^y \tag{8.8}$$

which means the free boundary is perpendicular to the local wind-stress vector. Physically, it is easy to understand that since the Ekman flux is perpendicular to the local surface wind stress so must be the free boundary which separates these two immiscible layers.

2) The interior Sverdrup flow

In the present case the upper layer occupies the region $\Omega_s: \{0 \le x \le x_e, 0 \le y \le .25\}$. Because $x = x_e$ is the eastern boundary, the interior Sverdrup solution is

$$\Psi_{in} = \lambda(x_e - x)\tau_y \tag{8.9}$$

$$D_{in}^2 = 2\lambda(x_e - x)(f\tau_y - \tau) \tag{8.10}$$

One can compare these two relations with (3.1) and (3.2). Putting (8.10) into (4.4) yields the relation between λ and x_e for the supercritical state (II). Fig. 1-6 shows some typical surfacing lines for such cases.

Near the western wall there is a western boundary current which has the classical structure discussed above. However, on the northern boundary of the upper layer there is a boundary current which needs special analysis.

3) The structure of the interior northern boundary current

Now the northern boundary for the upper layer water is the line $y = .25$ where $\tau = 0$, but $\tau_y \neq 0$. For the wind stress being used the Sverdrup relation gives a non-zero interior southward velocity on this northern boundary; therefore to satisfy the surfacing line condition $D = 0$, $\Psi = 0$ on $y = .25$, there must be a northern boundary current.

Using $D = 0$, $\Psi = 0$ on this northern boundary, the semi-geostrophy condition is

$$\Psi = D^2/2f_{ni} \tag{8.11}$$

where

$$f_{ni} = f_0 - 0.25 \tag{8.12}$$

The only appropriate boundary layer coordinate turns out to be (see Appendix A)

$$\eta = (0.25-y)/\varepsilon^{1/2} \tag{8.13}$$

and the main balance for the potential vorticity equation, (A.8), is

$$(\Psi_\eta/D)_\eta + \Psi_x = -\lambda\tau_y \tag{8.14}$$

Now $\tau_y = 2\pi$ at $y = .25$, thus (8.14) can be written as

$$(2f_{ni})^{-1/2}(\Psi^{1/2})_{\eta\eta} + \Psi^{1/2}(\Psi^{1/2})_x = -\pi\lambda \tag{8.15}$$

This nonlinear partial differentiation equation can be solved by numerical schemes with appropriate boundary conditions. However, if one is interested only in obtaining the global structure, this equation can be solved easily after linearization. The following analysis is basically an Oseen approximation. Instead of solving the nonlinear equation (8.15), one uses the following linearized equation

$$(2f_{ni})^{-1/2}(\Psi^{1/2})_{\eta\eta} + (\Psi_{in})^{1/2}(\Psi^{1/2})_x = -\pi\lambda \tag{8.16}$$

where

$$\Psi_{in} = 2\pi\lambda(x_e - x) \tag{8.17}$$

is the interior solution on the northern boundary (from (8.9)). Introducing a new independent variable

$$t = (2(x_e-x)/\pi\lambda)^{1/2} \tag{8.18}$$

yields a new equation

$$(2f_{ni})^{-1/2}(\Psi^{1/2})_{\eta\eta} + \pi\lambda = (\Psi^{1/2})_t \tag{8.19}$$

Defining a new dependent variable

$$\phi(\eta,t) = (\Psi)^{1/2} - \pi\lambda t, \tag{8.20}$$

one obtains a simple equation and the new boundary conditions:

$$\phi_t = (2f_{ni})^{-1/2}\phi_{\eta\eta} \tag{8.21}$$

$$\phi(0,t) = -\pi\lambda t \tag{8.22}$$

$$\phi(\infty,t) = 0 \tag{8.23}$$

for which the solution is

$$\phi = \pi\lambda t[(2f_{ni}/\pi^2)^{1/4}\int_0^{\eta t^{-1/2}} \exp(-(2f_{ni})^{1/2}u^2/4)du - 1] \tag{8.24}$$

Thus

$$\Psi = (8f_{ni})^{1/2}\lambda(x_e-x) \int_0^{(\pi\lambda/2(x_e-x))^{1/4}\eta} \exp(-(f_{ni}/8)^{1/2}u^2)du \tag{8.25}$$

gives the streamfunction within this northern boundary current. For the most part the Oseen approximation gives a good description of this boundary current. However, it is not valid near the surfacing line y = .25. The Oseen approximation is valid only for the far field, whereas near the "body" the linearization is no longer applicable. For our purposes, an Oseen approximation gives the global structure. Near the surfacing line, D is much less than the mixed layer thickness and our model is no longer valid.

Fig. 1-9 shows the typical streamline patterns for the supercritical state (II). The upper layer appears as a warm water pool in the south-west corner. This can be seen as a very crude two-layer model of the warm surface water pool in the subtropical ocean.
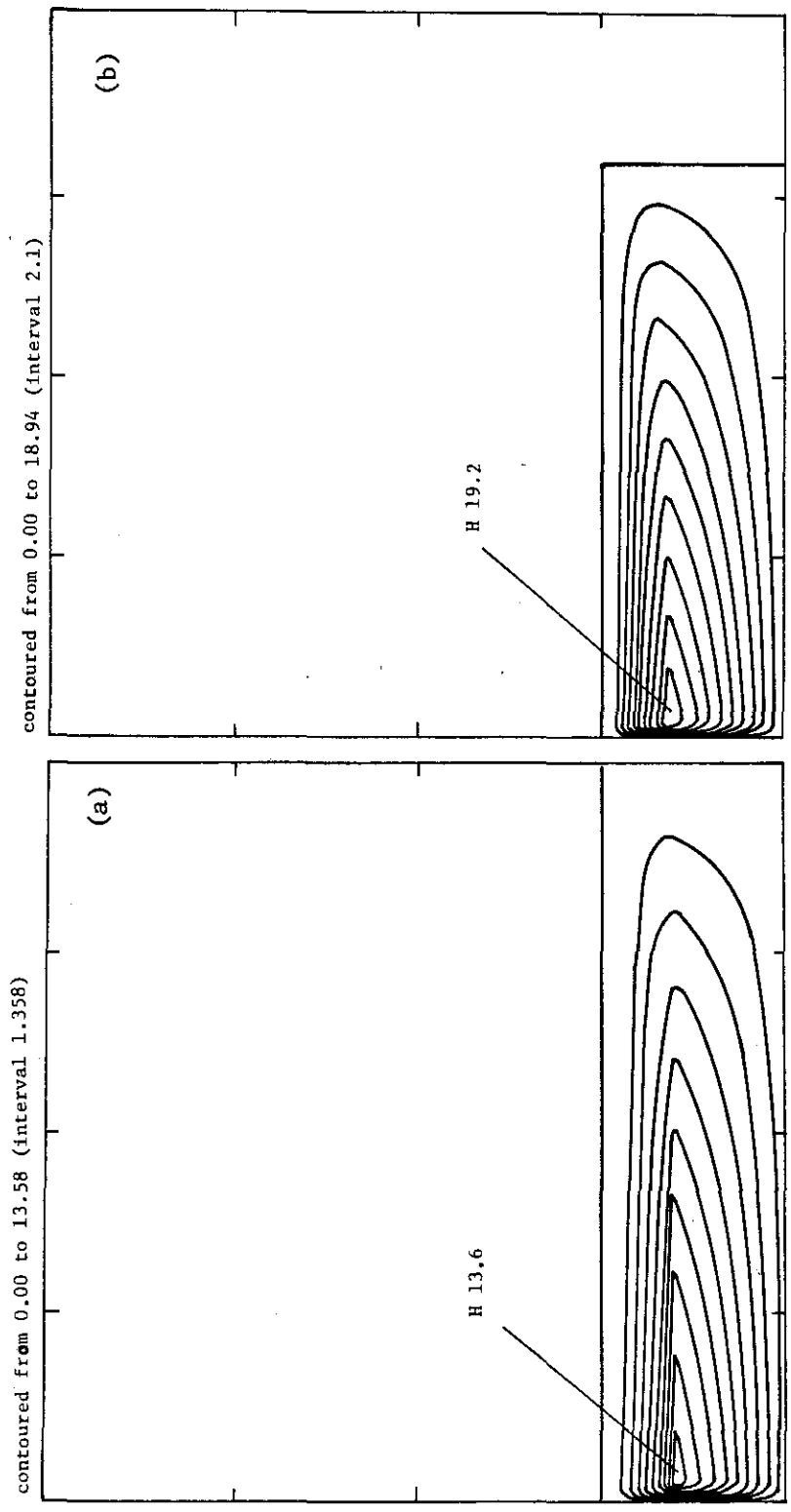
Fig. 1-9. Flow patterns for the second supercritical state of a subtropical-subpolar basin model. lambda = 2.627 (a); 5.13 (b), Xe = 1.0 (a); 0.8 (b).

9. Conclusions

The present model gives the complete scenario for a two-gyre basin thermocline and current structures. The state is assumed to be quasi-stationary. The process of increasing parameter λ can be interpreted either as: 1) A slow spin-up of a wind-driven two-gyre basin with a given amount of water in the upper layer and an infinitely deep lower layer; as the wind stress builds up gradually, the basin circulation evolves following the scenario. 2) A wind-driven two-gyre basin with fixed wind stress distribution; as the climatological atmospheric temperature distribution changes, the amount of upper layer water changes gradually. There are three basic states: the subcritical state, the supercritical state (I), and the supercritical state (II).

SUBCRITICAL STATE: For weak wind forcing and a large amount of upper layer water, the upper layer covers the whole basin. This is the classical flow pattern: an anticyclonic subtropical gyre with its western boundary current flowing northward and a cyclonic subpolar gyre with its western boundary current flowing southward.

SUPERCRITICAL STATE (I): For moderate wind forcing and a normal amount of upper-layer water, the lower layer outcrops within the subpolar basin. As λ increases the outcropping zone enlarges. Eventually, the outcropping zone extends into the subtropical basin, the subpolar gyre and the subtropical gyre unite into a single body. There is a continuous loop of boundary currents around the outcropping zone.

Fig. 1-10 shows the overall structure of a two-gyre basin for both

A - A

isolated w.b.c.
width ~ $0(\epsilon)$
spreading out

B - B

isolated n.b.c.
width ~ $0(\epsilon)$
linear profile

C - C

interior solution
no boundary layer

D - D

interior b.c.
width ~ $0(\epsilon)$

E - E

interior northern
boundary current
width ~ $0(\epsilon^{1/2})$
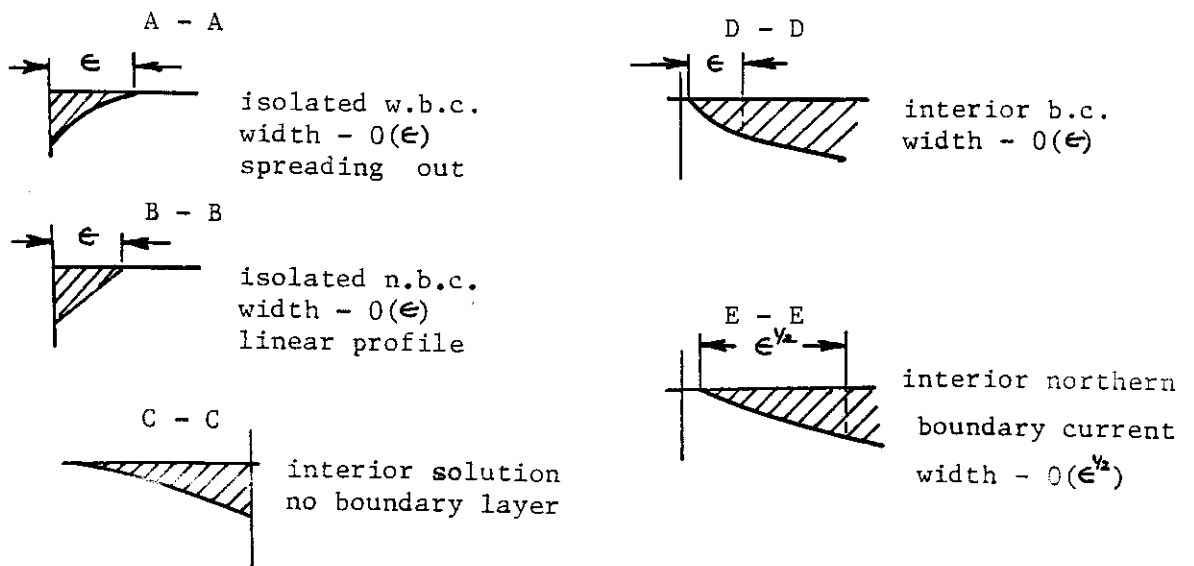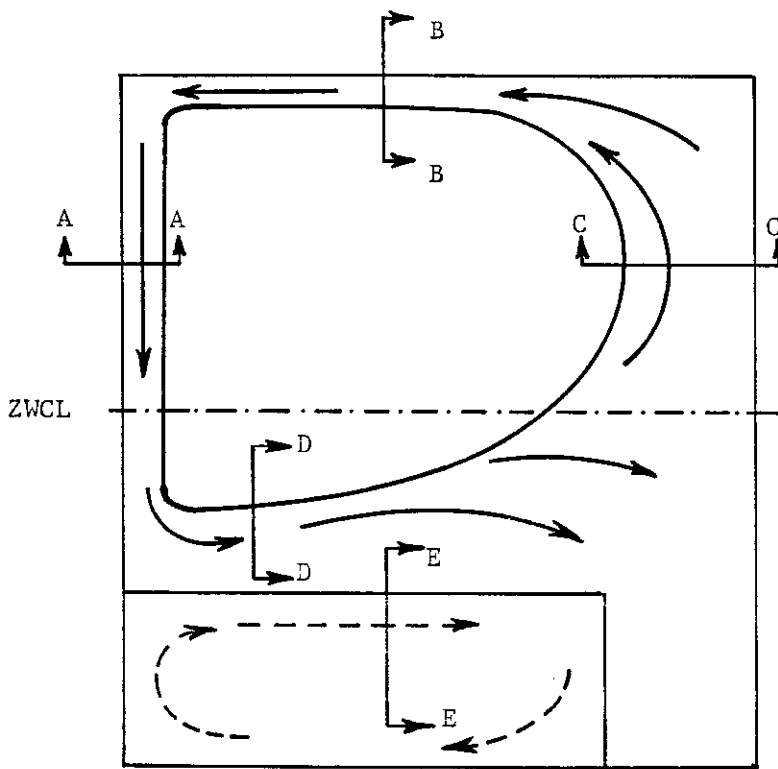
Fig.1-10. Dynamical structure of different kinds of boundary currents for subtropical-subpolar basin.

supercritical states (I) and (II), including all the boundary current structures.

The present model combines all these boundary currents into a dynamically consistent united body. The flow patterns we found have many features similar to the North Atlantic Ocean (or the North Pacific Ocean). The present model, in a sense, reproduces some features of the basin scale flow pattern that have been known for long time (see, for example, McCartney and Talley, 1984; Talley and McCartney, 1982).

1) The Gulf Stream is modelled as the strong internal jet which transports a large amount of warm water into the middle/high latitude interior ocean.

2) The North Atlantic Current moving northeastward as a continuation of the Gulf Stream System is represented by the internal boundary current within the subpolar basin. It consists of warm Gulf Stream water flowing all the way to the British Isles and into the Arctic Sea.

3) The eastern/western Greenland currents are seen as the isolated northern boundary current. It is a continuation of the North Atlantic Current. Actually, the Aleutian Current in the North Pacific Ocean is a better example of this kind of isolated northern boundary current.

4) The Labrador Current is seen as the isolated western boundary current that moves southward along the western coastline. Though the cold polar air reduces its temperature, and the run-off and precipitation modify its water mass property, the Labrador Current is still relatively warm (3-4 C) and saline (34.88-34.92) (Lazier,1982).

5) There is a water mass exchange across the ZWCL. Though the net north-south mass flux is zero across the entire longitude section, there is a

strong internal jet that goes across this line, bringing the warm water of the Gulf Stream into the subpolar gyre. In this model the Sverdrup relation is not satisfied where the internal jet crosses the ZWCL. However, it is consistent within our dynamical assumption. Because here the interfacial friction is very strong, the mass flux in the upper layer does not follow the same law as it does in the interior ocean.

6) If we make a hydrographic section across the Gulf Stream, the total mass flux should equal the interior Sverdrup transports, taking both the subtropical gyre and subpolar gyre into account. The increase in the mass flux of the Gulf Stream after its separation from Cape Hatteras is at least partially due to the joining of the Labrador Current from the north. The total mass transport of the Labrador Current is about $40 \times 10^6 M^3$/sec. (Leetmaa and Bunker, 1978; Ivers, 1975). Suppose that in a two-layer model two thirds of this mass flux is within the narrow isolated western boundary current. This current then will join with the Gulf Stream and increase the surface current mass transport. The most reliable estimation of the Gulf Stream mass flux is about $60-70 \times 10^6 M^3$/sec near Cape Hatteras; this volume flux increases to about $150 \times 10^6 M^3$/sec south of Nova Scotia (Worthington, 1976). According to our model one third of this increase comes from the subpolar gyre, and the rest, about $50 \times 10^6 M^3$/sec, comes from the compact recirculation gyre within the subtropical basin.

7) The subtropical gyre is bowl-shaped, while the subpolar gyre is shaped like an open dome with outcropping in the center of the gyre. During the late winter, the strong cyclonic circulation in the subpolar basin builds into a pre-conditioned phase for the deep water formation in the center of the gyre.

Most importantly, our model emphasizes the importance of the nonlinear interaction between the wind-driven circulation and the basic stratification within a subtropical-subpolar basin. The Gulf Stream is not only a result of the nonlinear advection terms, but also comes from the nonlinearity connected with the isopycnal outcropping. The Gulf Stream separation is not due to the local wind stress curl but is the result of the entire basin circulation balance. The ZWCL is no longer a boundary between two gyres, and the whole basin circulation becomes a united body.

SUPERCRITICAL STATE (II): For strong wind forcing or for a small amount of warm upper layer water, there is a warm water pool near the southwest corner of the basin. The eastern boundary of this warm water pool is a free boundary determined by the interaction between the local mixed layer dynamics and the large-scale geostrophic flow underneath.

Our model is highly idealized. Especially, all isolated boundary currents in the model strongly depend on the assumption of including the mixed layer. Therefore, the corresponding boundary current structures might be very sensitive to our assumptions and they are only meant to be a skeleton for the real oceans. Nevertheless, these boundary currents and the corresponding basin scale flow patterns are very interesting and important phenomena for further study.

Appendix A. The scaling of different kinds of northern boundary currents

For a general wind stress $\vec{\tau} = (\tau^x, \tau^y)$, after introducing the streamfunction the momentum equations for a two-layer model with an infinitely deep lower layer can be written as

$$-f\Psi_x = -DD_x + \varepsilon\Psi_y/D + \lambda\tau^x \qquad (A.1)$$

$$-f\Psi_y = -DD_y - \varepsilon\Psi_x/D + \lambda\tau^y \qquad (A.2)$$

where a simple Stommel friction has been used; other kinds of friction can be used without changing the essential part of the following analysis. Assuming that near the northern boundary $y = y_n$ there is a narrow northern boundary current with the length scale ε^k $(k > 0)$, i.e., the boundary layer coordinate is

$$\eta = (y_n - y)/\varepsilon^k \qquad (A.3)$$

(A.2) becomes

$$\partial/\partial\eta(-f\Psi + D^2/2) = O(\varepsilon^k) \qquad (A.4)$$

Integrating (A.4) across the boundary current yields

$$-f\Psi + D^2/2 = g(x) + \varepsilon^k h(x,\eta) \qquad (A.5)$$

where

$\quad g(x) = O(1)$ is the integration constant

$\quad h(x,\eta) = O(1)$.

Putting (A.5) into (A.1) gives

$$g'(x) = -\varepsilon^{1-k}D^{-1}\partial\Psi/\partial\eta + \lambda\tau^x \qquad (A.6)$$

From (A.1) and (A.2), by cross-differentiating, one obtains the potential vorticity equation

$$(\varepsilon \Psi_x/D)_x + (\varepsilon \Psi_y/D)_y + \beta \Psi_x = -\lambda(\tau_y^x - \tau_x^y) \tag{A.7}$$

For a northern boundary current $\partial/\partial x \ll \partial/\partial y$, so that (A.7) can be written as

$$\varepsilon^{1-2k} \partial/\partial \eta \cdot (D^{-1} \partial \Psi/\partial \eta) + \beta \Psi_x = -\lambda(\tau_y^x - \tau_x^y) \tag{A.8}$$

From (A.6) and (A.8) it is clear that the possible boundary layer scales are

$$k = 1, 1/2 \tag{A.9}$$

However, the appropriate scale depends on the matching boundary conditions that the boundary layer solution has to satisfy.

1) The classical northern boundary current (a non-isolated boundary current which exists when the wind-curl is non-zero near the northern wall) $k = 1/2$. The main balance for the potential vorticity equation is

$$\partial/\partial \eta \cdot (D^{-1} \partial \Psi/\partial \eta) + \beta \Psi_x = -\lambda(\tau_y^x - \tau_x^y) \tag{A.10}$$

a three-term balance between the relative vorticity, the planetary vorticity and the wind-curl.

For such a northern boundary layer, the integration constant $g(x)$ is a real function of x and the x-momentum balance is

$$g'(x) = \lambda \tau^x. \tag{A.11}$$

Thus the friction term is unimportant for this kind of boundary currents. The potential vorticity equation (A.10) describes a diffusion-like behavior and guarantees the smooth matching between the boundary current and the interior flow.

2) The interior northern boundary current $k = 1/2$. This is a degenerate case of the more general interior boundary current. The conventional scaling $k = 1$ for the ordinary interior boundary current is no longer valid because

41

now $D = 0$, $\Psi = 0$ on $\eta = 0$, so $g(x) = 0$. However, $\tau^x = 0$ for this

boundary current, so that the momentum balance equation (A.6) is

$$\varepsilon^k \partial h/\partial x = -\varepsilon^{1-k} D^{-1} \partial \Psi/\partial \eta \qquad (A.12)$$

Obviously, the only possible choice is $k = 1/2$ and the main balance for the

potential vorticity equation is the same as (A.10).

For the above two cases, the $\eta = (y_n - y)/\varepsilon^{1/2}$ coordinate gives a form

of exponential solution that can match the interior solution smoothly and the

boundary layers do not have any definite boundary.

3) The isolated northern boundary current $k = 1$. This case is different

from the above cases, because now the wind stress is non-zero near the

northern wall, and at the edge of this isolated current $D = 0$ and $\Psi =$

Ψ_m, a constant. Therefore, from (A.5) $g'(x) = 0$ and (A.11) becomes

inconsistent. This means it is no longer possible to balance the wind stress

with the downstream pressure gradient force within the classical scaling.

Actually, from (A.6) it is easy to see that $k = 1$ is the only possible scaling

and the momentum balance is between the wind stress and the friction term

$$0 = -D^{-1} \partial \Psi/\partial \eta + \lambda \tau^x(1) \qquad (A.13)$$

The potential vorticity equation is

$$\partial/\partial \eta \cdot (D^{-1} \partial \Psi/\partial \eta) = \varepsilon[-\beta \Psi_x - \lambda(\tau^x_y - \tau^y_x)] \qquad (A.14)$$

This equation appears not to show a balance within the lowest order

approximation, but one can notice that the wind-curl is order of ε here, and

(A.14) shows an x-independent structure which makes the planetary vorticity

term ineffective. The isolated northern boundary currents do not show the

conventional boundary layer form, because there is no interior geostrophic

42

flow matching requirement, so that the linear profile (A.11) works and the boundary current has a clear outer edge.

4) The isolated northern boundary current within a westerly.

For this case, to discuss all possible scaling for the boundary current structure we write (A.4) in details

$$\partial/\partial\eta[-f\Psi + D^2/2] = \varepsilon^{1+k}\Psi_x/D - \varepsilon^k\beta\Psi - \lambda\varepsilon^k\tau^y \qquad (A.15)$$

By our assumption $\tau^y = 0$, so that integrating (A.15) across the boundary current gives

$$-f\Psi + D^2/2 = g(x) + \varepsilon^{1+k}\int(\Psi_x/D)\ d\eta - \varepsilon^k\beta\int\Psi\ d\eta \qquad (A.16)$$

or

$$-f\Psi + D^2/2 = g(x) + \varepsilon^{1+k}P(x,y) - \varepsilon^k Q(x,y) \qquad (A.17)$$

where

$$P(x,y), Q(x,y) \sim O(1).$$

Putting (A.16) into (A.1)

$$g'(x) + \varepsilon^{1+k}\partial P/\partial x - \varepsilon^k\partial Q/\partial x = -\varepsilon^{1-k}D^{-1}\partial\Psi/\partial\eta + \lambda\tau^x \qquad (A.18)$$

However, for an isolated boundary current $g'(x) = 0$. Now $\lambda\tau^x$ is non-zero. Thus the only possible balances are $k = 0, 1$. Case $k = 1$ is impossible, because in (A.18) the friction term $-\partial\Psi/\partial\eta$ and the wind forcing term $\lambda\tau^x$ are both positive. Therefore, the only possible choice is $k = 0$. This means the current is not really a narrow current and the frictional term is unimportant. According to this analysis, the interior solution should be valid upon this outcropping line. Unfortunately, the interior solution cannot satisfy the kinematic condition: $\Psi = \Psi_m$ on line $D = 0$. This contradiction implies that there should be a special domain where there is some new force balance. In other words, it is not clear how the mass is

43

balanced when the northern boundary is within a westerly. No simple solution is available.

Chapter II

A Two Layer Model For the Thermocline and Current Structure

in Subtropical/Subpolar Basins

II. Lower Layer with Finite Depth

Abstract

A two-layer model with a finitely deep lower layer is studied for a
two-gyre basin. When the amount of upper-layer water is less than a critical
value, the lower layer outcrops. A continuous loop of boundary currents
completely surrounds the outcropping zone. These currents have quite different
dynamical structures, particularly the isolated boundary currents along the
northern and western walls. A first baroclinic mode of water mass exchange
exists across the zero-wind-curl-line (ZWCL). This baroclinic mode would be
important for a heat flux calculation. When the amount of upper water is less
than a second critical value, the upper layer water separates from the eastern
wall and becomes a warm water pool in the southwest corner and within this
region both layers are in motion.

Our model describes the thermocline structure for a two-gyre basin. The
surface temperature is determined from the dynamical balance of the entire
basin. The subtropical and subpolar gyres appear as a united body.

45

1. Introduction

The thermocline problem has been a classical and rather difficult problem in physical oceanography. In early theories of the thermocline, similarity solutions were tried which, though elegant mathematically, could not satisfy the boundary conditions for a three-dimensional basin. Recently there has been a renewal of enthusiasm about the thermocline problem. Among the new approaches to the problem are the ventilated thermocline theory by Luyten, Pedlosky and Stommel (1983) and the potential vorticity homogenization (non-ventilated thermocline) theory by Rhines and Young (1982). Both theories yield good descriptions of some aspects of the subtropical gyre. However, the subpolar gyre structure is not yet understood.

A third approach to the thermocline problem has been made by Parsons (1969), Kamenkovich and Reznik (1972), and Veronis (1973). In their models the ocean thermocline structure is represented by two immiscible layers and the upper layer has a specified amount of water. When the amount of warm upper-layer water is reduced below a critical value, the lower layer outcrops. The surfacing line which separates these two layers runs northeastward in a way similar to the Gulf Stream System. Parsons (1969) studies the simplest model, which has an infinitely deep lower layer, for the subtropical gyre. Parsons's model includes the basic ingredients for this kind of thermocline model, namely: 1) Two layer are immiscible; 2) the mixed layer is included; 3) the upper layer has a finite amount of water. Though Parsons's model has been extended, these basic assumptions are still made in the later models.

Veronis (1973) extends Parsons's model into a world ocean model. First, he generalizes the outcropping line condition for a two-gyre basin, taking into account of the interior Sverdrup flux in the subpolar gyre. Second, he tried to run a more realistic model by using more observational data, such as the climatological wind stress profile, the thermocline depth on the eastern wall, and the latitude at which the Gulf Stream separates from the coastline. Third, he improved Parsons's model by allowing the lower layer to be in motion when it is directly driven by wind. Although his solution is more realistic oceanically, its dynamical meaning is unclear. As shown in Chapter I, there is difficulty in finding a dynamically consistent picture for the wind pattern he used within our simple dynamics. There is also another inconsistency in his model: the lower layer is in motion when driven by direct wind forcing; however, it is motionless under the internal boundary current. Thus, the Sverdrup relation breaks down on the ZWCL near its intersection point with the internal jet. This inconsistency can be resolved with a model in which the lower layer has finite depth and dynamical consistency is required.

Kamenkovich and Reznik (1972) extend Parsons's model to include the pressure gradient in the lower layer. In their model the lower layer has a finite depth, so that the lower layer can be driven either directly by the wind stress when it outcrops or indirectly by the interfacial friction force underneath the strong surface boundary current. There are some interesting under currents in their model, such as those beneath the strong surface western boundary current and the internal jet stream. Although including pressure gradients in the lower layer should give a better picture of the Gulf Stream System, their pictures unfortunately show flow patterns which are worse

than Parsons's model: the Gulf Stream separates from the western wall too early compared with observations and has a northwest orientation near the northern boundary for the case when the ratio of layer thicknesses is not too large. The observed Gulf Stream has an northeast orientation at midlatitude. It seems inconsistent with the lower-order dynamical balance to have an internal boundary current going against the local wind in this model. This problem does not exist is our solution.

In the previous chapter we have analyzed a two-layer model with infinitely deep lower layer. Though that model gives an interesting description of the gyre structure, it has some shortcomings. First, the real ocean has a finite depth, so that direct wind forcing or interface friction can force significant velocities in the lower layer. As a result, the pressure gradient in the lower layer is not negligible and the whole flow pattern changes when we include the pressure gradient in the lower layer. Second, we made the assumption that the lower layer is infinitely deep and has a zero mass flux. As a result, the vertical integrated mass flux does not satisfy the Sverdrup relation on the ZWCL. This is obviously not true. No matter how deep the lower layer is, when it is being forced directly by winds or indirectly by interfacial friction, the vertically integrated mass flux will be a finite number. Thus a model with a finitely deep lower layer should give a better picture of the current structure, especially near the ZWCL and in the outcropping zone.

In this chapter we shall extend the purely wind-driven model for a two-gyre basin with an infinitely deep lower layer into the case with a finitely deep lower layer and study the whole flow pattern including all boundary currents. Our approach is parallel to Kamenkovich and Reznik's solution.

Just as in Chapter I, we study the structure of the flow pattern in a two-gyre basin as the non-dimensional number $\lambda = TL/g'\rho_0 d^2$ increases. Here, again, the increasing of λ can be a result of either the increasing of wind stress or the reducing of warm water in the upper layer.

When λ is small (weak wind forcing or a large amount of upper layer water) the system is in the subcritical state. The upper layer covers the whole basin, resulting in the classic picture (Welander, 1966): an anticyclonic subtropical gyre with its western boundary current flowing northward and a cyclonic subpolar gyre with its western boundary current flowing southward. There are narrow undercurrents along the western boundary in the lower layer.

When λ is moderate (normal wind forcing and normal amount of upper layer water) there is the supercritical state (I). The lower layer outcrops first near the western boundary in the subpolar basin. As λ increases further, the outcropping zone extends and intrudes into the subtropical basin. In the previous chapter the separation point of the internal boundary current can be as south as near the zero-wind latitude in the subtropical basin. It seems a poor simulation for the real Gulf Stream. Including the pressure gradient in the lower layer reshapes the outcropping line and moves it toward the ZWCL. Except for this point, the flow patterns in the upper layer are very similar to the patterns in Chapter I: two gyres with a continuous loop of boundary currents along the edge of the outcropping zone. The lower layer, however, is in motion now. There is a cyclonic gyre in the subpolar basin and a small anticyclonic gyre in the northwest corner of the subtropical basin. There are deep western boundary currents in the lower layer. Furthermore, there is a deep counter-current beneath the strong internal boundary current. Thus the

internal jet is more like the real Gulf Stream with its deep counter-current. The Sverdrup relation is now satisfied everywhere except near the western boundary; however, there is a first baroclinic mode of water mass exchange across the ZWCL. This is quite different behavior from the common eddy-resolving numerical models, since they generally use the quasi-geostrophic assumption. Such models always gives flow patterns which are symmetric with the ZWCL. Our model with the first baroclinic mode describes an asymmetric flow picture with a big outcropping zone in the subpolar basin and a continuous loop of boundary currents around this outcropping zone.

When λ is big (strong wind forcing or small amount of upper-layer water), the upper-layer water separates from the eastern wall and becomes a warm water pool in the southwest corner. Underneath the upper layer is the ventilated lower layer. The boundary between these two layers is a free boundary which is determined by the interaction between the local mixed layer and the large-scale circulation underneath it.

2. Basic Equations

In this section we consider the steady wind-driven circulation within a rectangular basin. The origin of a Cartesian coordinate system is at the southwest corner of the basin with the x-axis directed eastward and the y-axis northward. The continuous stratification in the real ocean is represented here by using two immiscible layers with uniform densities ρ_0 and ρ_1. The basin is a parallelepiped with $0 \le x \le L$, $0 \le y \le b$, $-h \le z \le 0$. The wind stress is assumed to be purely zonal: $\vec{\tau} = (\tau, 0)$, and $\tau = -\tau_0 \cos(2\pi y/b)$. The wind stress therefore drives two gyres within the basin. For simplicity, the following assumptions are made:

1) The pressure is hydrostatic.

2) Friction can be represented by a vertical diffusion term with a constant frictional coefficient. This is used in an Ekman model to derive stresses. The stresses now appear as body forces related to the layer thickness and the free surface elevation.

3) The flow within each layer can be represented by the vertically integrated velocity.

4) The Rossby number is very small, so that the non-linear momentum advection terms can be neglected.

The momentum equations and the mass conservation equations for these two layers are:

$$f \, \vec{k} \times \vec{v}_0 = -g\nabla\zeta + A\partial^2\vec{v}_0/\partial z^2 \qquad (2.1)$$

$$f \, \vec{k} \times \vec{v}_1 = g\nabla(\delta\rho D/\rho_0 - \zeta) + A\partial^2\vec{v}_1/\partial z^2 \qquad (2.2)$$

$$\nabla \cdot \vec{V}_0 + \partial w_0/\partial z = 0, \quad \nabla \cdot \vec{V}_1 + \partial w_1/\partial z = 0 \qquad (2.3)$$

where subscript "0" is for the upper layer, "1" is for the lower layer,

$f = f_0 + \beta y$ is the Coriolis parameter, A is the vertical turbulent friction

coefficient, ζ is the free surface elevation, D is the upper layer

thickness,

and $\delta\rho = \rho_1 - \rho_0 > 0$. The corresponding boundary conditions are

at $z = \zeta$

$$A\partial u_0/\partial z = \tau, \quad A\partial v_0/\partial z = 0 \tag{2.4}$$

$$w_0 = u_0\partial\zeta/\partial x + v_0\partial\zeta/\partial y \tag{2.5}$$

at $z = -D+\zeta$

$$w_0 = w_1 = -u_0\partial(D-\zeta)/\partial x - v_0\partial(D-\zeta)/\partial y \tag{2.6}$$

$$\vec{v_0} = \vec{v_1}, \quad \partial\vec{v_0}/\partial z = \partial\vec{v_1}/\partial z \tag{2.7}$$

at $z = -h$

$$u_1 = v_1 = 0 , \quad w_1 = 0 \tag{2.8}$$

After integrating (2.1,2,3,4) over the corresponding layer depths, we

find the vertically integrated momentum equations

$$fD \ \vec{k}\times\vec{v_0} = -gD\nabla\zeta+\vec{\tau}+\vec{\tau_0} \tag{2.9}$$

$$f(h-D+\zeta)\vec{k}\times\vec{v_1} = g(h-D+\zeta)\nabla(\delta\rho D/\rho_0-\zeta) - \vec{\tau_0} + \vec{\tau_b} \tag{2.10}$$

where $\vec{\tau_0}$, $\vec{\tau_b}$ are the friction forces on the interface and the bottom.

If one treats D and ζ as known functions, then $\vec{\tau_0}$ and $\vec{\tau_b}$ can be

written in terms of D and ζ by using the matching conditions (2.4, 5, 7, 8).

In the following analysis we use complex numbers to represent two-dimensional

vectors, for example $\nabla\cdot D = \partial D/\partial x+i\partial D/\partial y$, $\vec{\tau} = \tau^x+i\tau^y$. Using the

fact that $|\exp[-(h-D+\zeta)(1+i)(2A/f)^{-1/2}]| \ll 1$, we can find the

following relations:

$$\vec{\tau_0}=\tau_0^x+i\tau_0^y=-\tau e^{-\mu D}+(1-e^{-2\mu D})g\delta\rho/\rho_0\cdot(D_x+iD_y)/2\mu \tag{2.11}$$

$$\vec{\tau_b} = \tau_b^x + i\tau_b^y = -g[\partial(D\delta\rho/\rho_0-\zeta)/\partial x + i\partial(D\delta\rho/\rho_0-\zeta)/\partial y]/\mu \tag{2.12}$$

where

$$\mu = (1+i)/h_\varepsilon$$

$$h_\varepsilon = (2A/f)^{1/2} \tag{2.13}$$

It is important to notice that formula (2.13) is valid even if D goes to zero, and that $\vec{\tau_b} \to (-\tau,0)$ as $D \to 0$.

The amount of warm water in the upper layer is assumed to have a specified volume, i.e.

$$\int_0^b\int_0^L D\,dx\,dy = Lbh_0 \tag{2.14}$$

Vertically integrating the continuity equations, one obtains

$$\nabla(D\vec{u_0}) = 0 \tag{2.15}$$

$$\nabla[(h-D+\zeta)\vec{u_1}] = 0 \tag{2.16}$$

From the above relations, one can define the transport streamfunctions

$$\Psi_{0x} = Dv_0, \quad -\Psi_{0y} = Du_0 \tag{2.17}$$

$$\Psi_{1x} = (h-D+\zeta)v_1, \quad -\Psi_{1y} = (h-D+\zeta)u_1 \tag{2.18}$$

Introducing the following non-dimensional variables

$$(x,y) = L\,(x',y'), \quad D = h_0D'$$

$$f = L\beta f', \quad f' = f_0 + y' - 0.5, \quad f_0 = R\tan\Theta_0/L$$

$$(\vec{\tau}, \vec{\tau_D}, \vec{\tau_b}) = T\,(\vec{\tau}', \vec{\tau_D}', \vec{\tau_b}') \tag{2.19}$$

$$\zeta = h_0\zeta'\delta\rho/\rho_0$$

$$(\Psi_0,\Psi_1) = g\delta\rho h_0^2/\rho_0\beta L\cdot(\Psi'_0,\Psi'_1)$$

and dropping the primes, the non-dimensional system of equation becomes

$$-f\nabla\Psi_0 = -D\nabla\zeta + \lambda\vec{\tau} + \vec{\tau_D} \tag{2.20}$$

$$-f\nabla\Psi_1 = (\alpha-D)\nabla(D-\zeta) + \vec{\tau_b} - \vec{\tau_D} \tag{2.21}$$

53

where

$$\vec{\tau_D} = -\lambda\tau e^{-(1+i)D/\epsilon} + \epsilon/2(1+i)\cdot[1-e^{-2(1+i)D/\epsilon}](D_x+iD_y) \qquad (2.22)$$

$$\vec{\tau_b} = -\epsilon/(1+i)\cdot[\partial(D-\zeta)/\partial x + i\partial(D-\zeta)/\partial y] \qquad (2.23)$$

and

$$\epsilon = h_\epsilon/h_0 \ll 1$$

$$\alpha = h/h_0 \gg 1 \qquad (2.24)$$

$$\lambda = TL\rho_0/g\delta\rho h_0^2 \sim O(1)$$

are the non-dimensional parameters. In the following analysis we use a small parameter

$$\delta = 1/\alpha \ll 1 \qquad (2.25)$$

The integration constraint (2.14) becomes

$$\int_0^1\int_0^{b/L} Ddxdy = b/L \qquad (2.26)$$

In the following analysis, equations (2.20,21) with constraint (2.25) are solved with the assumed wind stress

$$\tau = (-\cos 2\pi y, 0) \qquad (2.27)$$

For convenience, we also assume L = b in the following analysis.

As we have discussed in Chapter I, when $\lambda < \lambda_c$ the upper layer covers the whole basin. For the lowest order expansion in ϵ, the interior flow is

$$\Psi_{0g} = 2\pi\lambda(1-x)\sin 2\pi y, \quad \Psi_{1g} = 0 \qquad (2.28)$$

$$D_g-\zeta_g = 0 \qquad (2.29)$$

$$D_g^2 = D_e^2 + 2\lambda(1-x)(2\pi f\sin 2\pi y + \cos 2\pi y) \qquad (2.30)$$

3. The Subcritical State and the Supercritical State (I)

If the amount of warm water is reduced, the flow will change in a similar fashion as in the case of an infinitely deep lower layer. Thus, if there is enough warm water, the upper layer covers the whole basin and the solution can easily be found from (2.28, 30). This is the subcritical state discussed by Welander (1966). Fig. 2-1 shows a schematic pattern for this state. In the upper layer are the anticyclonic gyre and the cyclonic gyre with their western boundary currents. The lower layer is stagnant for the large interior Sverdrup domain, except near the western boundary where strong interfacial friction drives two undercurrents in this layer.

As the volume of warm water is reduced to a critical value, the lower layer surfaces near the middle of the western boundary of the subpolar gyre. Around the edge of the outcropping zone is a loop of boundary currents. The general dynamical structures of these boundary currents are discussed in the Appendices. The shape of the surfacing line is determined by (B-62)

$$\Psi_{0g} = \Psi_m + [D_g^2/2 - \delta D_g^3/3 + O(\delta^2)]/f \tag{3.1}$$

where Ψ_{0g}, D_g constitute the interior solution for the upper layer, equations (2.28) and (2.30). For the case of an infinitely deep lower layer ($\delta = 0$), the surfacing line is symmetric with the zero-wind-line $y = .75$. Hence it is reasonable to assume that for small δ the surfacing line passes the line $y = .75$, so that (3.1) holds for this line. Then Ψ_m can be eliminated and the equation that determines the surfacing line follows

$$\Psi_{0g} - (D_g^2/2 - \delta D_g^3/3)/f = [\Psi_{0g} - (D_g^2/2 - \delta D_g^3/3)/f]_{y=0.75} + O(\delta^2) \tag{3.2}$$
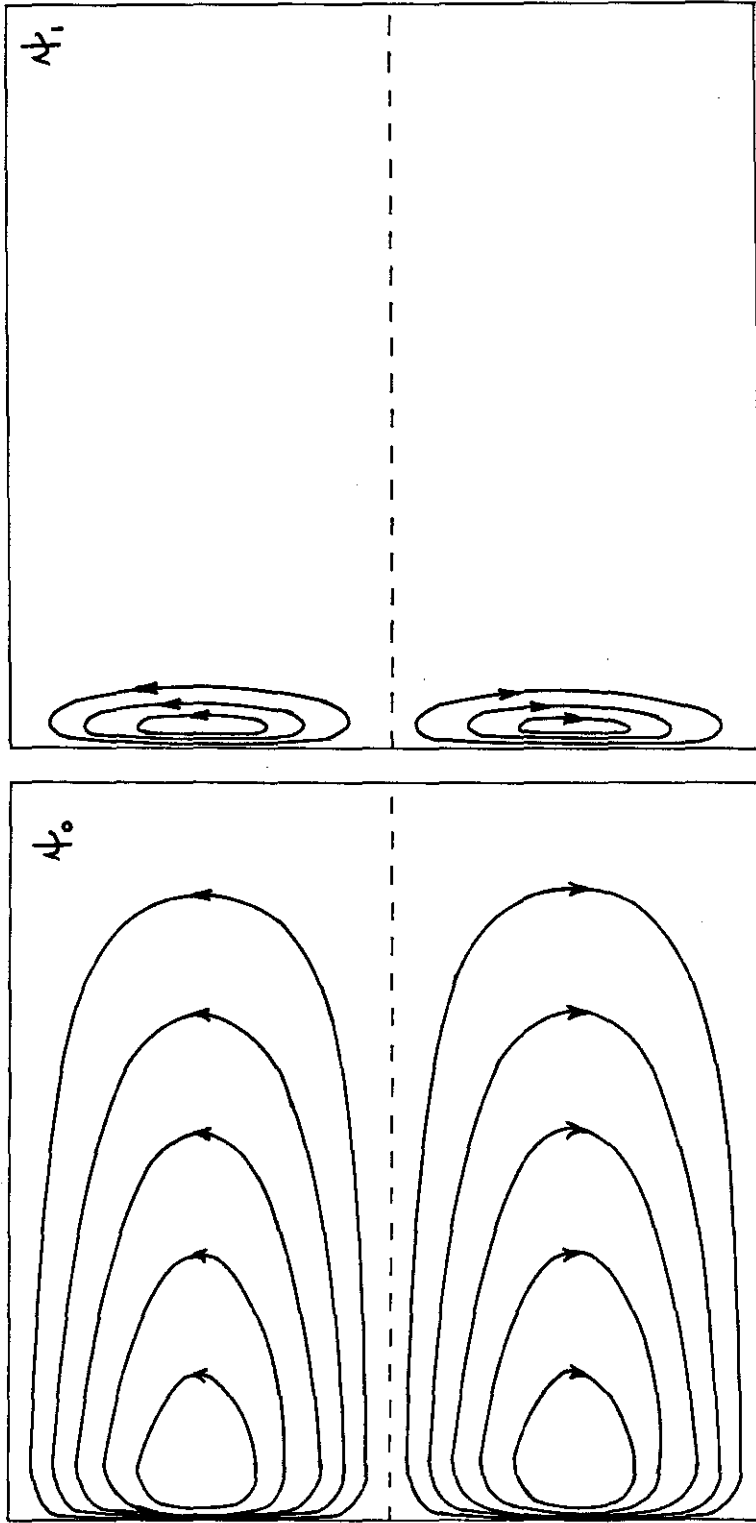
Fig. 2-1. Schematic flow patterns for a subtropical-subpolar basin, the subcritical state (Welander, 1966).

a) Upper layer streamfunction ψ_0.

b) Lower layer streamfunction ψ_1.

Equations (2.28, 30, 31) can be solved by an iterative process under the constraint

$$\iint_\Omega D_g \, dxdy = 1 \qquad\qquad (2.26')$$

where Ω is the region actually covered by the upper-layer water. From (2.24) it is clear that ε and α are inversely proportional to h_0, while λ is inversely proportional to h_0^2. The non-dimensional upper layer thickness D_e, as same as in Chapter I, increases initially as the volume of warm water decreases. Fig. 2-2 shows surfacing lines for typical cases. From this figure it can be seen that for a model with a finitely deep lower layer, in the subtropical basin the surfacing line moves northward compared to the case of an infinitely deep lower layer. This result differs from the result of Kamenkovich and Reznik (1972, Fig. 5 in their paper) in which the surfacing lines for $\delta>0$ move southward compared to the case $\delta=0$. We have run a model similar to theirs for the subtropical gyre and could not reproduce their result. For the solutions presented here, the boundary currents always flow downwind. This fact saves us from the seemingly paradoxical situation shown in Kamenkovich and Reznik's work, in which internal boundary currents may flow counter to the local wind stress forcing.

On the eastern side of the surfacing line and away from the internal boundary current, the interior solutions also satisfy (2.28,29,30). On the western side of the surfacing line $D = 0$ so that the equations describing the lower-layer flow are

$$-f\partial\Psi_1/\partial x = -\alpha\partial\zeta/\partial x + \lambda\tau + \varepsilon(\partial\zeta/\partial x + \partial\zeta/\partial y)/2 \qquad\qquad (3.3)$$

$$-f\partial\Psi_1/\partial y = -\alpha\partial\zeta/\partial y - \varepsilon(\partial\zeta/\partial x + \partial\zeta/\partial y)/2 \qquad\qquad (3.4)$$
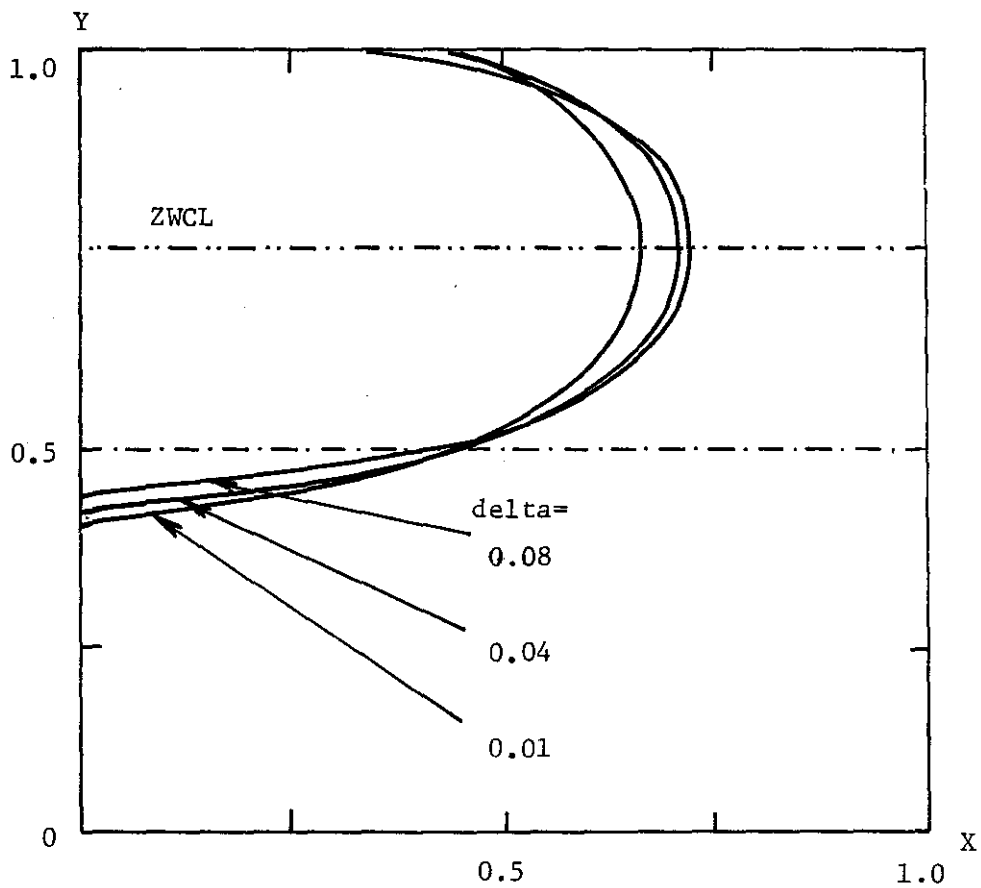
Fig. 2-2. Typical outcropping lines for a subtropical-subpolar
basin model with a finitely deep lower layer, lambda= 0.3.

For the interior ocean, bottom friction is unimportant, so that by cross-differentiating (3.3) and (3.4), one obtains

$$-\partial\Psi_{1g}/\partial x = -\lambda\partial\tau/\partial y \qquad (3.5)$$

The total streamfunction $\Psi = \Psi_0 + \Psi_1$ is continuous across the outcropping line because the bottom friction underneath the internal boundary current is small and the boundary currents in both layers cancel each other (as proved in Appendix B). Thus, to find Ψ_{1g}, ζ_{1g} one starts integrating from the boundary values (B-35) and (B-36), and obtains the following solution

$$\Psi_{1g} = 2\pi\lambda(1-x)\sin2\pi y - \Psi_m \qquad (3.6)$$

$$\zeta_{1g} = [D_e^2/2 + \lambda(1-x)(2\pi f\sin2\pi y + \cos2\pi y)]/\alpha \qquad (3.7)$$

Notice that $\Psi_0 = \Psi_m$ within the outcropping zone, thus

$$\Psi_0 + \Psi_1 = \Psi_g = 2\pi\lambda(1-x)\sin2\pi y \qquad (3.8)$$

on both sides of the surfacing line.

Fig. 2-3 shows the flow patterns for two typical cases. Figs. 2-3.a) and c) are the flow patterns for the upper layer. Notice the boundary current loop around the outcropping zone. Within the southern basin is the classical subtropical gyre with its western boundary current. On the subpolar western wall there is an isolated western boundary current whose position in the middle basin corresponds to the Labrador Current in the North Atlantic Ocean. As shown in Appendix D, this boundary current is quite wide laterally, consistent with observations of the Labrador Current. The isolated western boundary current in the subpolar gyre and the classical non-isolated western boundary current in the subtropical gyre meet somewhere below the ZWCL and form a strong internal jet flowing into the interior ocean. For the model with
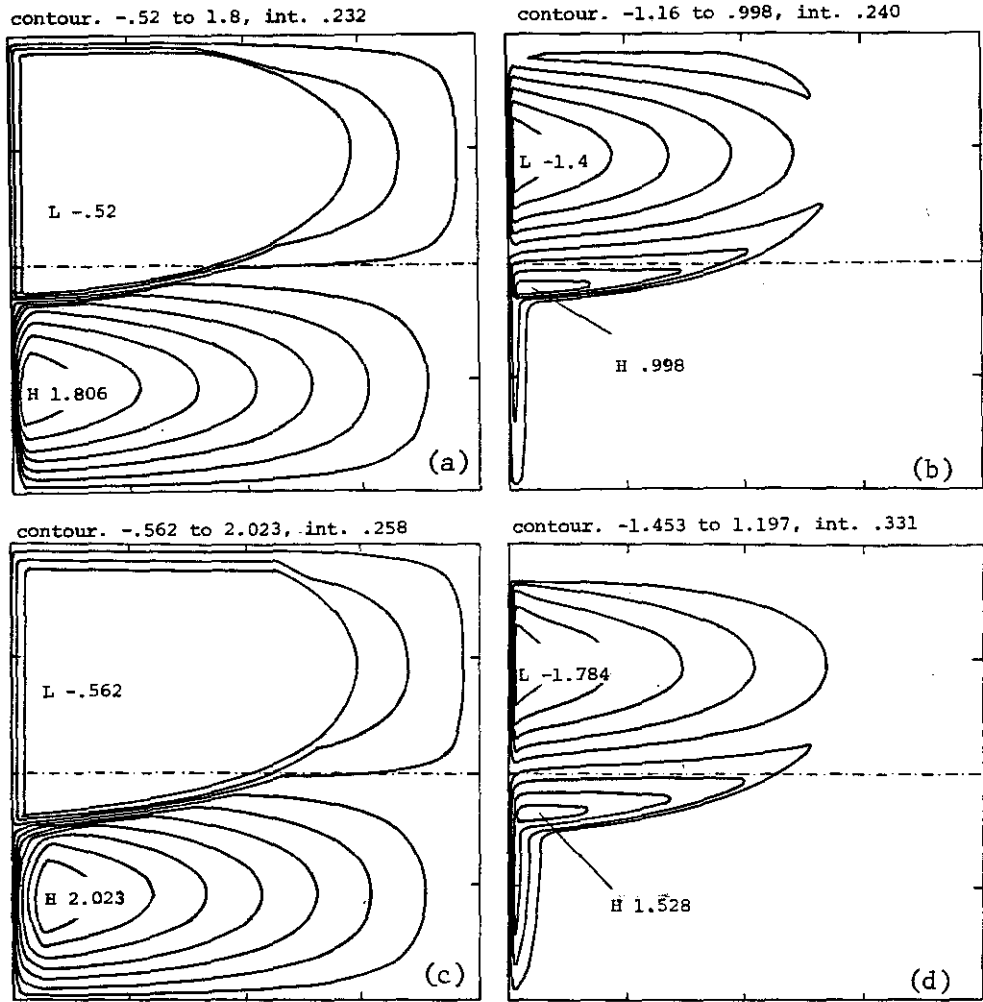
Fig. 2-3. Flow patterns for a subtropical-subpolar basin model
with a finitely deep lower layer: the upper layer (a,c);
the lower layer (b,d).

For case (a,b) delta= 0.1; epsilon= 0.03; lambda= 0.3,
    case (c,d) delta= .04; epsilon= 0.07; lambda= 0.35.

an infinitely deep lower layer, this internal boundary current can extend southward as far as the zero-wind-stress line y = .25. For a model with a finitely deep lower layer, the lower layer pressure gradient pushes this internal boundary current northward, so that the flow picture looks more like the real Gulf Stream System and saves us the conceptual trouble of a strangely shaped Gulf Stream which separates from the coastline too early. (In Kamenkovich and Reznik, 1972, the internal boundary current can separate from the coast as early as in the easterly zone and go against the local westerly near the northern boundary).

Fig. 2-3.b) and d) show the flow pattern in the lower layer. There are two gyres in this layer. Within most of the outcropping zone in the subpolar basin there is a strong cyclonic gyre. Near the western wall the strong interfacial friction drives a strong narrow western boundary current in the lower layer. Here the bottom friction is important. On the northern (southern) part of the outside edge of this boundary current the interfacial friction turns the current slightly northward (southward) before it joins the main western boundary current. Within the subtropical outcropping zone there is an anticyclonic gyre. This gyre penetrates underneath the western boundary current of the upper layer. The strong interfacial friction of the upper-layer western boundary current drives an undercurrent in the lower layer. This undercurrent is strong and narrow. Near the western wall the current flows in the same direction as the surface current, but offshore there is a strong counter-current which resembles the southward deep western boundary current observed in the Gulf Stream. In our formulation this western boundary current is very narrow, so that to show its detailed structure, the subtropical

boundary current coordinate in Fig. 2-3 has been exaggerated four times. On the eastern boundary of the outcropping zone, the interfacial friction drives a deep counter current. Here the bottom friction is unimportant; thus the sum of mass fluxes in both layers satisfies the Sverdrup relation. Due to the mass transport in this undercurrent, the boundary between the cyclonic and the anticyclonic gyres in the lower layer moves slightly northward from the ZWCL.

Of primary importance is the existence of a first baroclinic mode of water mass exchange across the ZWCL. Though the vertically integrated meridional mass flux is zero (from the Sverdrup relation), the warm Gulf Stream water flows northward within the upper layer and the cold lower layer water flows southward underneath the strong warm surface current. For most models examined previously, this ZWCL has been assumed to be a real boundary separating the subpolar gyre from the subtropical gyre. The existence of these baroclinic modes of water mass exchange across the ZWCL strongly suggests that the subpolar gyre and the subtropical gyre form a united, complicated system. For studies of the global ocean circulation and heat fluxes, a model which allows this kind of water mass exchange should be the best choice.

4. The Supercritical State (II)

As the amount of warm water in the upper layer is reduced, ε and α increase proportionately to $1/h_0$, while λ increases proportionately to $1/h_0^2$. When the amount of warm water decreases to a second critical value, the upper layer thickness at the eastern wall becomes zero. From that point on, if the volume of the upper-layer water is reduced further, the upper layer separates from the eastern wall (See Fig. 2-4.).

The upper layer has a minimum thickness ε on this edge, so that the slope of this free surfacing line is determined from the following relation (equation (8.7), chapter I)

$$\gamma = -(\lambda\tau^x - \varepsilon f V_1)/(\lambda\tau^y + \varepsilon f U_1) = \partial y/\partial x \qquad (4.1)$$

where the interior geostrophic flow in the lower layer (U_1, V_1) can easily be calculated by integrating from the eastern wall. Within domain II, by assuming $\zeta_{1g} = 0$ on the eastern wall, one then obtains

$$\Psi_{1g} = 2\pi\lambda(1-x)\sin 2\pi y \qquad (4.2)$$

$$\zeta_{1g} = \lambda/\alpha \, (1-x)(2\pi f \sin 2\pi y + \cos 2\pi y \,) \qquad (4.3)$$

Therefore

$$U_1 = -\Psi_{1gy} = -4\pi^2\lambda(1-x)\cos 2\pi y \qquad (4.4)$$

$$V_1 = \Psi_{1gx} = 2\pi\lambda\sin 2\pi y.$$

Putting (4.4) into (4.1)

$$\gamma = -(\cos 2\pi y - 2\pi f \varepsilon \sin 2\pi y)/4\pi^2 f \varepsilon (1-x)\cos 2\pi y \qquad (4.5)$$

which is independent of λ.

Within domain I, the upper layer is driven directly by the wind stress and the lower layer is in motion underneath the upper layer. This domain is the
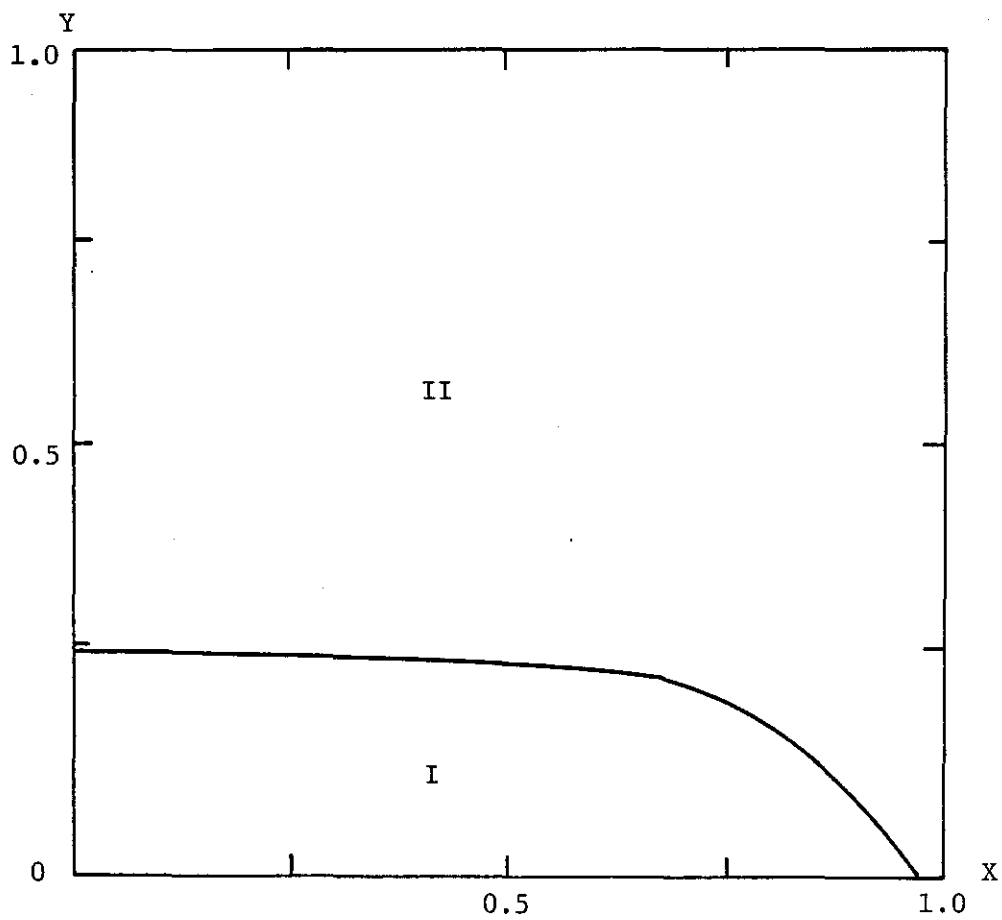
Fig. 2-4. Schematic diagram for the second supercritical state.
The region I for the upper layer and the region II for the
outcropping lower layer.

ventilated zone discussed by Luyten et al. (1983). However, instead of specifying the separating line $X_e = X_e(Y_e)$ in an ad-hoc fashion as in the LPS model, here we find this free boundary from a model which includes an advection-dominated interaction between the mixed layer and the large scale geostrophic flow.

In this domain both interfacial friction and bottom friction are unimportant, so that (2.20) and (2.21) become

$$-f\nabla\Psi_0 = -D\nabla\zeta + \lambda\vec{\tau} \tag{4.6}$$

$$-f\nabla\Psi_1 = (\alpha-D)\nabla(D-\zeta) \tag{4.7}$$

Adding (4.6) to (4.7), it follows that

$$-f\nabla(\Psi_0+\Psi_1) = \nabla[\ \alpha(D-\zeta)-D^2/2]\ + \lambda\vec{\tau} \tag{4.8}$$

Writing (4.6) in x, y components and cross-differentiating gives

$$- \partial(\Psi_0+\Psi_1)/\partial x = \lambda d\tau/dy \tag{4.9}$$

Thus, from (4.6) it follows that

$$\partial/\partial x[\alpha(D-\zeta) - D^2/2] = \lambda f d\tau/dy - \lambda\vec{\tau} \tag{4.10}$$

Using the boundary condition that on the "eastern boundary" $X_e = X_e(Y_e)$, $D = 0$ and $\zeta = \zeta_{1g}$, one obtains

$$\alpha(D-\zeta) - D^2/2 = -\lambda(1-x)(2\pi f\sin 2\pi y + \cos 2\pi y\ ) \tag{4.11}$$

To determine D and ζ, we need one more equation. Since the lower layer is sheltered from direct forcing, its potential vorticity is conserved

$$u_1\partial(f/(\alpha-D))/\partial x + v_1\partial(f/(\alpha-D))/\partial y = 0 \tag{4.12}$$

Using (4.7), this conservation relation can be written as

$$f/(\alpha-D) = G(D-\zeta) \tag{4.13}$$

where G is an arbitrary function which should be determined from the matching boundary condition on the free eastern boundary. Along $X_e = X_e(Y_e)$,

$D-\zeta = -\zeta_{1g}$ can be calculated from (4.3) and $f/(\alpha-D) = f(y)/\alpha$ on this line, so that the function G is completely determined. For a given λ, D and ζ can be obtained from the nonlinear equations (4.11) and (4.13). Again, one must apply the integration constraint

$$\iint_{I} D \, dxdy = 1 \tag{4.14}$$

The simplest way to do this is starting with the free surfacing line (4.5) which is not explicitly dependent on λ. By specifying the intersection point x_s on the southern boundary, the whole free surfacing line is determined. Afterward, an iterative process is used to find a value of λ which satisfies the constraint (4.14).

After calculating D and ζ, a simple integration gives the streamfunctions Ψ_0 and Ψ_1.

Near the western boundary are the western boundary currents. Within domain II, there is the classical western boundary current for a homogeneous ocean. Within domain I there are two western boundary currents. The detailed analysis is given in Appendix E.

Fig. 2-5 shows a typical example for the second supercritical case. Because h_0 might be very small for this case, ε is no longer much less than 1. Thus for a realistic h_0, the above ε expansion is not strictly valid. However, we can try to compare this case with the infinitely deep lower layer case and keep our arguments within a reasonable mathematical frame (we use the assumption $\varepsilon \ll 1$ explicitly) by choosing a very small Ekman layer depth h_ε that ensures ε remains small enough. In Fig. 2-5 shows the free eastern boundary which moves toward the southwest corner if the amount of upper layer water is reduced further. The flow pattern in the upper layer looks like the

contoured from -110 to 119.6 (interval 10.)

(b)

L -120.4

H 120.4

contoured from 0.00 to 47.46 (interval 4.75)

(a)

H 47.46
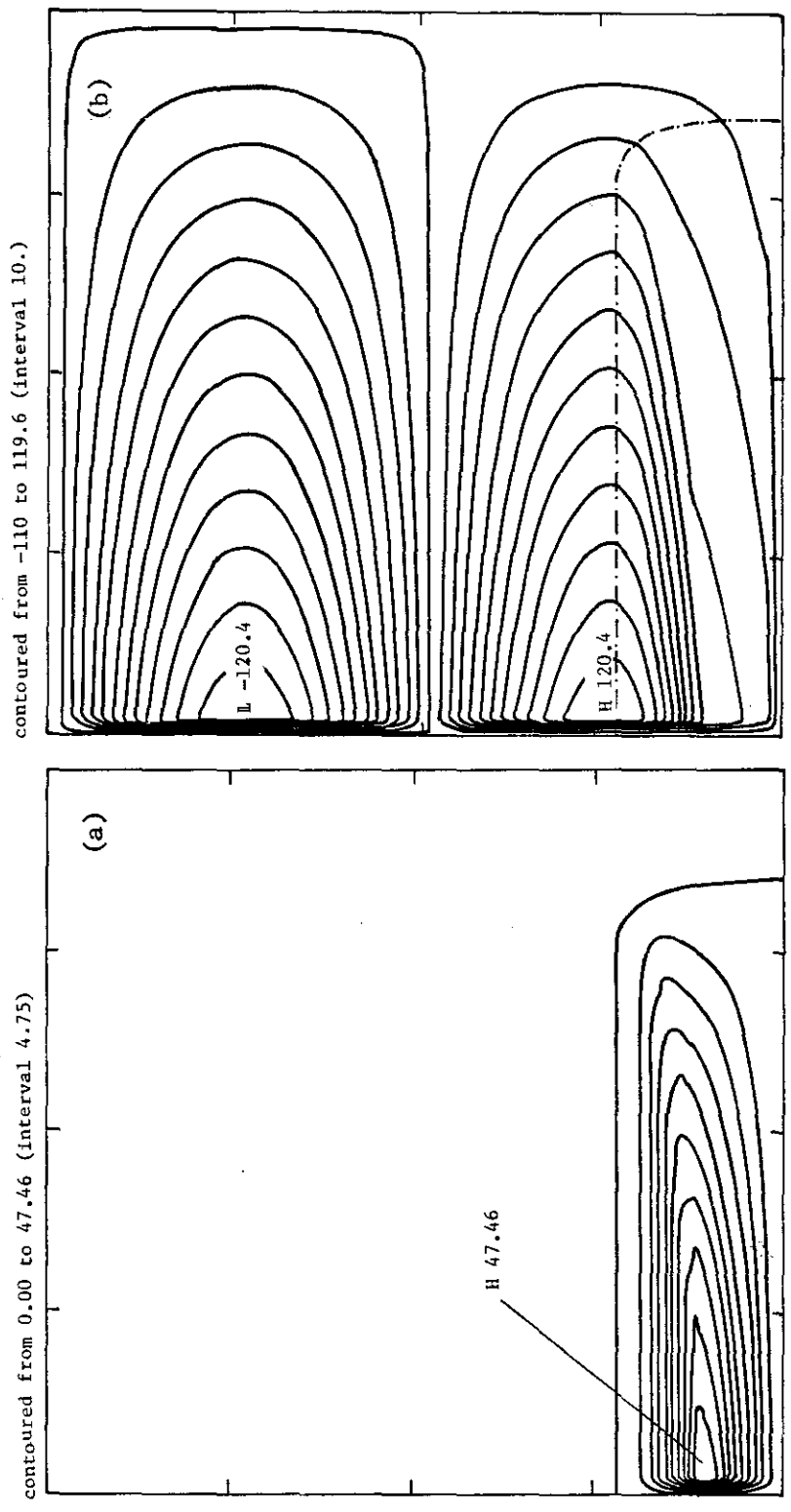
Fig. 2-5. Flow patterns for the second supercritical state: (a) the warm water pool (upper layer) in the south-west corner; (b) the lower layer with its ventilation below the warm water pool.

picture for the case with an infinitely deep lower layer (Chapter I), except that now the mass flux in the upper layer is only a small part of the total Sverdrup transport. Most of the mass flux goes into the ventilated lower layer. Underneath the upper layer, the lower layer has a relatively large ventilation velocity within the northern region, whereas within the southeast region the ventilation velocity is rather small. It can be seen that if the amount of upper-layer water increases slightly, the free surfacing line extends to the eastern wall, and this slowly ventilated region becomes the unventilated zone in the Luyten et al.(1983) model. Within the western boundary current region, as in the subpolar gyre, water particles turn slightly southward before they join the strong northward motion. However, it is within a very narrow region and is not an important feature. Thus, using a rather coarse grid for contouring, this feature does not appear. Though Luyten et al discuss the ventilated thermocline model, it is not clear how the water mass transport can be balanced by the western boundary current for a general case. Our model gives the first concrete example of a balanced two-gyre thermocline model with the surface density distribution determined by the intrinsic dynamics.

5. Conclusions

In the real oceans both subtropical and subpolar gyres exist and interact with each other. These two gyres have quite different structures. The subtropical gyre is anticyclonic and its thermocline is bowl-shaped; the subpolar gyre is cyclonic and its thermocline is dome-shaped. In the center of this dome-shaped thermocline isopycnals outcrop. Traditional quasi-geostrophic numerical models treat the thermocline structure as a perturbation to a basic state that has a constant stratification within the entire basin. Thus it cannot handle outcropping phenomena. The flow patterns from a quasi-geostrophic model are always symmetric with the ZWCL. Therefore, a simple two-layer model is used to investigation outcropping and the connected circulation pattern with a two-layer model, taking into account of the pressure gradient in the lower layer.

Our simple two-layer model easily includes the outcropping and gives an asymmetric flow pattern that is very similar to the observed ocean:

1) The subtropical gyre and the subpolar gyre unite into a single body which is asymmetric with respect to the ZWCL. After its separation the Gulf Stream is modelled as a combination of two western boundary currents. The separation takes place equatorward of the ZWCL. After separation the Gulf Stream flows northeastward and becomes the North Atlantic Current after its crossing the ZWCL. Our model extends the result of Kamenkovich and Reznik on the counter current underneath the strong surface current.

2) The model solution includes water mass exchange across the ZWCL. Though the Sverdrup mass flux is zero at this line, there is a baroclinic mode of

64

water mass exchange (appears in a form of a narrow internal boundary current). The warm upper layer water flows northward and the cold lower layer water flows southward across this line. This water mass exchange is very important for the thermocline structure and the water mass formation theory. The water mass exchange would, of course, also be important for a heat flux calculation.

3) Our model includes an isolated western boundary current bringing the Sverdrup transport in the warm water on the eastern side of the subpolar gyre southward past the ZWCL. This contributes to the Sverdrup flow when it joins with the Gulf Stream. In the oceans the Labrador Current may play a similar role.

4) The model can also be used to describe a warm water pool in the southwest corner and its connected ventilated zone.

All these features are essential elements for a global ocean model.

Of course, our model is a very simple model, so that the new theoretical features, such as the isolated western and northern boundary currents, and the first baroclinic mode of water mass exchange across the ZWCL, are different in detail from the real oceans. For example, the ZWCL in the North Atlantic Ocean is not a latitudinal line, but goes northeastward. The position of the Gulf Stream is strongly modified by nonlinear effects and also strong air-sea interaction. The mixed layer dynamics must include both advection (including the Ekman drift and the large scale geostrophic velocity below the mixed layer) and atmospheric exchange, so that the outcropping lines are determined by both dynamics and thermodyamics. To apply our model to the real ocean there are many steps to go before we can really compare the modelling result with the real data.

65

Appendix A. The Classical Western Boundary Current

D, ζ, Ψ_0, Ψ_1 are $O(1)$ within such a boundary current.

Introducing the boundary layer coordinate

$$\xi = x/\varepsilon \tag{A-1}$$

and expanding (2.20, 21, 22, 23) in power series of ε, the lowest order equations are

$$-f\partial\Psi_0/\partial\xi = -D\partial\zeta/\partial\xi \tag{A-2}$$

$$-f\partial\Psi_0/\partial y = -D\partial\zeta/\partial y - 1/4 \cdot \partial D/\partial\xi \tag{A-3}$$

$$-f\partial\Psi_1/\partial\xi = (\alpha-D)\partial(D-\zeta)/\partial\xi \tag{A-4}$$

$$-f\partial\Psi_1/\partial y = (\alpha-D)\partial(D-\zeta)/\partial y + 1/4 \cdot \partial D/\partial\xi + 1/2 \cdot \partial(D-\zeta)/\partial\xi \tag{A-5}$$

The corresponding boundary conditions are

$$\text{at } \xi = 0, \ \Psi_0 = \Psi_1 = 0 \tag{A-6}$$

$$\text{at } \xi \to \infty, \ \Psi_0 \to \Psi_{0g}, \ \Psi_1 \to 0, \ D \to D_g, \ \zeta \to \zeta_g \tag{A-7}$$

where $D_g = D_g(0,y)$, $\zeta_g = \zeta_g(0,y)$, $\Psi_{0g} = \Psi_{0g}(0,y)$ are known functions from (2.28, 29, 30). From (A-2) + (A-4) and (A-3) + (A-5), the total streamfunction satisfies

$$-f\partial(\Psi_0+\Psi_1)/\partial\xi = \partial[\alpha(D-\zeta)-D^2/2]/\partial\xi \tag{A-8}$$

$$-f\partial(\Psi_0+\Psi_1)/\partial y = \partial[\alpha(D-\zeta)-D^2/2]/\partial y + 1/2 \cdot \partial(D-\zeta)/\partial\xi \tag{A-9}$$

Using the relation (2.29), from (A-8) one finds the semi-geostrophic condition

$$-f(\Psi_0+\Psi_1-\Psi_{0g}) = \alpha(D-\zeta)+(D_g^2-D^2)/2. \tag{A-10}$$

By cross-differentiating (A-8) and (A-9) and integrating (using the assumption that $\partial(D-\zeta)/\partial\xi = 0$ as $\xi \to \infty$), we get another relation for the total streamfunction

$$(\Psi_0+\Psi_1-\Psi_{0g}) = 1/2 \cdot \partial(D-\zeta)/\partial\xi \tag{A-11}$$

From (A-10) and (A-11), by eliminating the streamfunction, the following relation is obtained

$$f/2 \cdot \partial(D-\zeta)/\partial\xi + \alpha(D-\xi) = (D^2 - D_g^2)/2 \qquad (A-12)$$

by cross-differentiating and subtracting from (A-2) and (A-3)

$$1/4 \cdot \partial^2 D/\partial\xi^2 + (D/f - \partial D/\partial y)\partial\zeta/\partial\xi + \partial D/\partial\xi \cdot \partial\zeta/\partial y = 0 \qquad (A-13)$$

Equations (A-10, 11, 12, 13) are four equations in four unknowns Ψ_0, Ψ_1, ζ, D. The corresponding boundary conditions are (A-6) and (A-7). Because $\alpha \gg 1$ (from equation (A-12)), one can see that it is a singular perturbation problem. Alternatively, equation (A-12) can be written as

$$\delta f/2 \cdot \partial(D-\zeta)/\partial\xi + (D-\zeta) = \delta(D^2 - D_g^2)/2 \qquad (A-14)$$

where

$$\delta = 1/\alpha \ll 1 \qquad (A-15)$$

is a small parameter. To solve this singular perturbation problem, we introduce the inner boundary coordinate

$$\Theta = \xi/\delta \qquad (A-16)$$

Now Ψ_0, Ψ_1, ζ, D can be expanded in series of δ . Considering equation (A-4), the Ψ_1 series should start from $1/\delta$ order term, so that the expansions are

$$\Psi_0(\xi,y) = \Psi_{00}(\Theta,y) + \delta\Psi_{01}(\Theta,y) + \delta^2\Psi_{02}(\Theta,y) + \ldots$$

$$\Psi_1(\xi,y) = 1/\delta \cdot \Psi_{1,-1}(\Theta,y) + \Psi_{10}(\Theta,y) + \delta\Psi_{11}(\Theta,y) + \ldots$$

$$D(\xi,y) = D_0(\Theta,y) + \delta D_1(\Theta,y) + \delta^2 D_2(\Theta,y) + \ldots \qquad (A-17)$$

$$\zeta(\xi,y) = \zeta_0(\Theta,y) + \delta\zeta_1(\Theta,y) + \delta^2\zeta_2(\Theta,y) + \ldots$$

Putting (A-17) into (A-10, 11, 12, 13), one can find the lowest order balance, the first order balance and so on.

1) δ^0 - order equations

$$-f\Psi_{1,-1} = D_0 - \zeta_0 \tag{A-18}$$

$$\Psi_{1,-1} = 1/2 \cdot \partial(D_0 - \zeta_0)/\partial\Theta \tag{A-19}$$

$$f/2 \cdot \partial(D_0 - \zeta_0)/\partial\Theta + (D_0 - \zeta_0) = 0 \tag{A-20}$$

$$\partial^2 D_0/\partial\Theta^2 = 0 \tag{A-21}$$

From (A-21), applying reasonable boundary conditions: $\partial D_0/\partial\Theta \to 0$ and $|D_0| < +\infty$ as $\Theta \to \infty$, one finds

$$D_0 = D_0(0,y) \text{ is independent of } \Theta. \tag{A-22}$$

The general solution for (A-20) is

$$D_0 - \zeta_0 = A_0(y)\exp(-2\Theta/f) \tag{A-23}$$

By (A-18), that means

$$\Psi_{1,-1} = -A_0(y)\exp(-2\Theta/f)/f. \tag{A-24}$$

However, from the boundary condition (A-6), $A_0 = 0$, so that

$$\Psi_{1,-1} = 0 \tag{A-25}$$

$$D_0 = \zeta_0, \text{ both are independent of } \Theta \text{ and } y. \tag{A-26}$$

2) δ - order equations

$$-f(\Psi_{00} + \Psi_{10} - \Psi_{0g}) = (D_1 - \zeta_1) + (D_g^2 - D_0^2)/2 \tag{A-27}$$

$$(\Psi_{00} + \Psi_{10} - \Psi_{0g}) = 1/2 \cdot \partial(D_1 - \zeta_1)/\partial\Theta \tag{A-28}$$

$$f/2 \cdot \partial(D_1 - \zeta_1)/\partial\Theta + (D_1 - \zeta_1) = (D_0^2 - D_g^2)/2 \tag{A-29}$$

$$\partial^2 D_1/\partial\Theta^2 = 0 \tag{A-30}$$

To derive (A-30) one uses relations (A-22) and (A-26). Applying the same argument as for D_0, one finds

$$D_1 = D_1(0,y) \text{ is independent of } \Theta \tag{A-31}$$

From (A-29)

$$\zeta_1 = D_1 - (D_0^2 - D_g^2)/2 - A_1(y)\exp(-2\Theta/f) \tag{A-32}$$

From (A-2), (A-26) and boundary condition $\Psi_0 = 0$ at $\Theta = 0$,

$$\Psi_{00} = 0 \tag{A-33}$$

Using (A-28,32), one obtains

$$\Psi_{10} = \Psi_{0g} - A_1\exp(-2\Theta/f)/f \tag{A-34}$$

Applying the boundary condition $\Psi_1 = 0$ at $\Theta = 0$, so that $A_1(y) = f\Psi_{0g}$ and

$$\Psi_{10} = \Psi_{0g}(1-\exp(-2\Theta/f)) \tag{A-35}$$

$$D_1 = D_1(y) \tag{A-36}$$

$$\zeta_1 = D_1(y) - (D_0^2 - D_g^2)/2 - f\Psi_{0g}\exp(-2\Theta/f) \tag{A-37}$$

The first non-zero term for the δ-series of Ψ_0 is Ψ_{01} which can be found from (A-2, 32) and the condition $\Psi_0 = 0$ at $\Theta = 0$:

$$\Psi_{01} = D_0\Psi_{0g}(1-\exp(-2\Theta/f)) \tag{A-38}$$

Now we go back to find the solution for the outer boundary layer. Using the standard boundary layer matching technique, the boundary conditions for the outer boundary layer solution are

$$\text{at } \xi = 0, \ \Psi_0 = 0, \ \Psi_1 = \Psi_{0g}, \ D = \zeta = D(y) \tag{A-39}$$

where $D(y)$ is an unknown matching function.

Again, we expand the outer boundary solution in δ-power series

$$\Psi_0(\xi,y) = \Psi_{00}^*(\xi,y) + \delta\Psi_{01}^*(\xi,y) + \ldots$$

$$\Psi_1(\xi,y) = \Psi_{10}^*(\xi,y) + \delta\Psi_{11}^*(\xi,y) + \ldots$$

$$D(\xi,y) = D_0^*(\xi,y) + \delta D_1^*(\xi,y) + \ldots \tag{A-40}$$

$$\zeta(\xi,y) = \zeta_0^*(\xi,y) + \delta\zeta_1^*(\xi,y) + \ldots$$

From (A-12)

$$D_0^* = \zeta_0^*\qquad\qquad\text{(A-41)}$$

Substituting (A-41) into (A-13), one finds the equation for D_0^*

$$\partial^2 D_0^*/\partial\xi^2 + 2/f\cdot\partial D_0^{*2}/\partial\xi = 0\qquad\qquad\text{(A-42)}$$

with the boundary conditions

$$D_0^*(0) = D_0(y),\ D_0^*(\infty) = D_g(y)\qquad\qquad\text{(A-43)}$$

The solution is

$$D_0^* = D_g(1 - C_1\exp(-C_2\xi))/(1 + C_1\exp(-C_2\xi))\qquad\qquad\text{(A-44)}$$

where

$$C_1 = (D_g - D_0)/(D_g + D_0)\ ,\ C_2 = 4D_g/f\qquad\qquad\text{(A-45)}$$

From (A-2), the lowest order streamfunction for the upper layer is

$$\Psi_{00}^* = \Psi_{0g} + (D_0^{*2} - D_g^2)/2f\qquad\qquad\text{(A-46)}$$

At $\xi = 0$, $\Psi_{00} = 0$, so that

$$D_0(y) = D_0^*(0,y) = (D_g^2 - 2f\Psi_{0g})^{1/2}\qquad\qquad\text{(A-47)}$$

Finally, from (A-11) one finds $\Psi_{10}^* = \Psi_{0g} - \Psi_{00}^*$.

Now we have found the entire solution:

1) When $\xi \sim O(\delta)$:

$$\Psi_0 = \delta D_0(y)\Psi_{0g}(1 - \exp(-2\theta/f)) + O(\delta^2)\qquad\qquad\text{(A-48)}$$

$$\Psi_1 = \Psi_{0g}(1 - \exp(-2\theta/f)) + O(\delta)\qquad\qquad\text{(A-49)}$$

$$D = D_0(y) + O(\delta)\qquad\qquad\text{(A-50)}$$

$$\xi = D_0(y) + O(\delta)\qquad\qquad\text{(A-51)}$$

2) When $\xi \sim O(1)$:

$$\Psi_0 = \Psi_{0g} + (D^2 - D_g^2)/2f + O(\delta)\qquad\qquad\text{(A-52)}$$

$$\Psi_1 = \Psi_{0g} - \Psi_0 + O(\delta)\qquad\qquad\text{(A-53)}$$

$$D = D_g(1 - C_1\exp(-C_2\xi))/(1 + C_1\exp(-C_2\xi)) + O(\delta)\qquad\qquad\text{(A-54)}$$

$$\xi = D + O(\delta)\qquad\qquad\text{(A-55)}$$

Appendix B. The Internal Boundary Current

The interior surfacing line is a western boundary for the upper layer, so that there is a strong internal boundary current to the right of the surfacing line. Here we discuss the boundary layer structure and the shape of the surfacing line.

A new set of orthogonal coordinates (r,s) is introduced such that $r = 0$ is the surfacing line and $r > 0$ to the right of the surfacing line. Assuming that the curvature radius of the surfacing line is much larger than the boundary layer width so that the curvature terms can be neglected, the basic equations (20,21) can be written

$$-f\partial\Psi_0/\partial r = -D\partial\zeta/\partial r+\lambda m_1[\tau^r(1-e^{-d}\cos d)+\tau^s e^{-d}\sin d]+$$

$$\varepsilon/4\bullet(1-e^{-2d}\cos 2d+e^{-2d}\sin 2d)\partial D/\partial r \qquad (B-1)$$

$$-f\partial\Psi_0/\partial s = -D\partial\zeta/\partial s+\lambda m_2[\tau^s(1-e^{-d}\cos d)+\tau^r e^{-d}\sin d]+$$

$$\varepsilon m_2/4m_1\bullet(-1+e^{-2d}(\cos 2d+\sin 2d))\partial D/\partial r \qquad (B-2)$$

$$-f\partial\Psi_1/\partial r = (\alpha-D)\partial(D-\zeta)/\partial r+\lambda m_1 e^{-d}(\tau^r\cos d+\tau^s\sin d)-$$

$$\varepsilon/4\bullet(1-e^{-2d}(\cos 2d-\sin 2d))\partial D/\partial r-\varepsilon/2\bullet\partial(D-\zeta)/\partial r \qquad (B-3)$$

$$-f\partial\Psi_1/\partial s = (\alpha-D)\partial(D-\zeta)/\partial s+\lambda m_2 e^{-d}(\tau^s\cos d-\tau^r\sin d)+$$

$$\varepsilon m_2/4m_1\bullet(1-e^{-2d}(\cos 2d+\sin 2d))\partial D/\partial r+\varepsilon m_2/2m_1\bullet\partial(D-\zeta)/\partial r \qquad (B-4)$$

where

$$d = D/\varepsilon$$

$$m_1 = ((\partial x/\partial r)^2+(\partial y/\partial r)^2)^{1/2}$$

$$m_2 = ((\partial x/\partial s)^2+(\partial y/\partial s)^2)^{1/2}$$

$$\tau^r = \tau/m_1\bullet\partial x/\partial r \qquad (B-5)$$

$$\tau^s = \tau/m_2\bullet\partial x/\partial s$$

In the following discussion, we assume that the boundary layer is very narrow and the new coordinates have the same length scale as the old coordinates so that $dr = ds = (dx^2 + dy^2)^{1/2}$; thus

$$m_1 = m_2 = 1 \tag{B-6}$$

The boundary conditions on the surfacing line are

$$D = 0, \ \Psi_0 = \Psi_m, \ \partial\Psi/\partial r \text{ is continuous at } r = 0. \tag{B-7}$$

where Ψ_m is an unknown parameter which will be determined later by an iterative process. The boundary layer is divided into two regions for discussion.

A) Region $D \sim \varepsilon$ and $\Psi_0 \sim 1$, $\Psi_1 \sim 1$.

Obviously, $\tau_D \sim \tau$ so that

$$\varepsilon \partial D/\partial r \sim \varepsilon^2/r \sim 1 \tag{B-8}$$

From the momentum equations for the upper and lower layers

$$\partial\Psi_0/\partial r \sim 1, \ \partial\Psi_1/\partial r \sim 1/\varepsilon \tag{B-9}$$

Thus, the appropriate inner boundary layer coordinate is

$$\eta = r/\varepsilon^2 \tag{B-10}$$

and the unknown functions have the following ε-power series expressions

$$\Psi_0(r,s) = \Psi_{00}(s) + \varepsilon\Psi_{01}(s) + \varepsilon^2\Psi_{02}(\eta,s) + \dots$$

$$\Psi_1(r,s) = \Psi_{10}(s) + \varepsilon\Psi_{11}(\eta,s) + \dots$$

$$D(r,s) = \varepsilon D_1(\eta,s) + \varepsilon^2 D_2(\eta,s) + \dots \tag{B-11}$$

$$\zeta(r,s) = \zeta_0(s) + \varepsilon\zeta_1(\eta,s) + \dots$$

Using the boundary condition (B-7), we find $\Psi_{00}(s) = \Psi_m$, $\Psi_{01} = 0$. Obviously, $\partial\Psi_1/\partial r = O(1)$ on the left side of the surfacing line, so that the continuity condition for $\partial\Psi/\partial r$ now turns out to be

$$\partial\Psi_1/\partial\eta = \varepsilon^2 \partial\Psi_1/\partial r = O(\varepsilon^2) \qquad \text{at } \eta = 0 \tag{B-12}$$

so that

$$\partial\Psi_{11}/\partial\eta = 0 \qquad\qquad \text{at } \eta = 0 \qquad\qquad\qquad (B-13)$$

Substituting the expansions (B-11) into equations (B-1,2,3,4), the lowest order balances are

$$-f\partial\Psi_{02}/\partial\eta = -D_1\partial\zeta_1/\partial\eta + \lambda[\tau^r + \exp(-D_1)(\tau^s\sin D_1 - \tau^r)]$$
$$+ 1/4\cdot(1-\exp(-2D_1)(\cos 2D_1 - \sin 2D_1)\partial D_1/\partial\eta \qquad (B-14)$$

$$\partial D_1/\partial\eta = 4\lambda[\tau^s(1-\exp(-D_1)\cos D_1) + \tau^r\exp(-D_1)\sin D_1]/$$
$$[1-\exp(-2D_1)(\cos 2D_1 + \sin 2D_1)] \qquad (B-15)$$

$$-f\partial\Psi_{11}/\partial\eta = \alpha\partial(D_1-\zeta_1)/\partial\eta \qquad\qquad\qquad (B-16)$$

$$-f\Psi_{01}/\partial s = \alpha\partial\zeta_0/\partial s + \lambda\tau^s + 1/2\cdot\partial(D_1-\zeta_1)/\partial\eta \qquad\qquad (B-17)$$

From (B-17), $\partial(D_1-\zeta_1)/\partial\eta$ is independent of η. Thus, from (B-16)
$\partial\Psi_{11}/\partial\eta$ is also independent of η. Now the boundary condition (B-13) gives

$$\partial\Psi_{11}/\partial\eta \equiv 0, \quad \partial(D_1-\zeta_1)/\partial\eta \equiv 0 \qquad\qquad\qquad (B-18)$$

Using boundary condition $D_0(0,s) = 0$, (B-15) can be solved numerically.
Asymptotically

$$D \to 4\lambda\tau^s\eta \qquad\qquad \text{as } \eta \to \infty \qquad\qquad\qquad (B-19)$$

Now (B-14) can be solved with D_1, $\partial\zeta_1/\partial\eta = \partial D_1/\partial\eta$ as known functions.
Asymptotically

$$\Psi_{02} \sim 8\eta^2(\lambda\tau^s)^2/f, \quad \text{as } \eta \to \infty \qquad\qquad\qquad (B-20)$$

Actually, the details of this inner boundary layer structure are unimportant for the large scale structure of the whole basin. The crucial aspect of the inner boundary analysis is the matching boundary condition for the outer boundary layer solution in the next section.

B) Region $D \sim 1$, $r \sim \varepsilon$.

We introduce the outer boundary layer coordinate

$$\sigma = r/\varepsilon \qquad\qquad\qquad (B-21)$$

73

From (B-1,2,3,4), we find the lowest order balance in ε-power

$$-f\partial\Psi_0/\partial\sigma = -D\partial\zeta/\partial\sigma \qquad\qquad\text{(B-22)}$$

$$-f\partial\Psi_0/\partial s = -D\partial\zeta/\partial s - 1/4\cdot\partial D/\partial\sigma + \lambda\tau^s \qquad\qquad\text{(B-23)}$$

$$-f\partial\Psi_1/\partial\sigma = (\alpha-D)\partial(D-\zeta)/\partial\sigma \qquad\qquad\text{(B-24)}$$

$$-f\partial\Psi_1/\partial s = (\alpha-D)\partial(D-\zeta)/\partial s + 1/4\cdot\partial D/\partial\sigma + 1/2\cdot\partial(D-\zeta)/\partial\sigma \qquad\qquad\text{(B-25)}$$

By the standard boundary layer matching technique, one can use the inner boundary layer solution in section A to find the matching boundary conditions for the outer boundary layer at $\sigma = 0$

$$D = 0, \quad \zeta = \zeta(s), \quad \partial(D-\zeta) = 0 \quad\text{at } \sigma = 0 \qquad\qquad\text{(B-26)}$$

$$\Psi_0 = \Psi_m, \quad \Psi_1 = \Psi_{10}(s) \qquad\text{at } \sigma = 0 \qquad\qquad\text{(B-27)}$$

As $\sigma \to \infty$, the boundary layer solution should match the interior solution, so that there are additional boundary conditions

$$D\to D_g(0,s), \quad \zeta\to\zeta_g(0,s), \quad \Psi_0\to\Psi_{0g}(0,s), \quad \Psi_1\to 0, \text{ as } \sigma\to\infty \qquad\text{(B-28)}$$

By adding (B-22) to (B-24) and (B-23) to (B-25), we find the following relations

$$-f\partial(\Psi_0+\Psi_1)/\partial\sigma = \partial[\alpha(D-\zeta)-D^2/2]/\partial\sigma \qquad\qquad\text{(B-29)}$$

$$-f\partial(\Psi_0+\Psi_1)/\partial\sigma = \partial[\alpha(D-\zeta)-D^2/2]/\partial\sigma + 1/2\cdot\partial(D-\zeta)/\partial\sigma + \lambda\tau^s \qquad\qquad\text{(B-30)}$$

Since the interior flow satisfies

$$D_g = \zeta_g, \qquad\qquad\text{(B-31)}$$

we have the following semi-geostrophic relation

$$-f[\Psi_0+\Psi_1-\Psi_{0g}(0,s)] = \alpha(D-\zeta)-[D^2-D_g^2(0,s)]/2 \qquad\qquad\text{(B-32)}$$

Cross-differentiating (B-29, 30) and substituting gives

$$-\beta_s\partial(\Psi_0+\Psi_1)/\partial\sigma = -1/2\cdot\partial^2(D-\zeta)/\partial\sigma^2 \qquad\qquad\text{(B-33)}$$

where $\beta_s = \partial f/\partial s$. Applying the boundary condition $\partial(D-\zeta)/\partial\sigma = \varepsilon\partial(D-\zeta)/\partial\sigma$ $= 0$ at $\sigma \to \infty$, we obtain the following equation

74

$$\beta_s[\Psi_0+\Psi_1-\Psi_{0g}(0,s)] = 1/2\cdot\partial(D-\zeta)/\partial\sigma \qquad (B-34)$$

Leting $\sigma \rightarrow 0$ in equation (B-32), we get

$$-f(\Psi_m+\Psi_{10}-\Psi_{0g}) = -\alpha\zeta(s)+D_g^2/2$$

Obviously, within this ε-order approximation the bottom friction is unimportant, so that the sum of the streamfunctions in the two layers should equal the Sverdrup transport thus

$$\Psi_{10}(s) = \Psi_{0g}(0,s)-\Psi_m \qquad (B-35)$$

$$\zeta_0(S) = D_g^2(0,s)/2\alpha \qquad (B-36)$$

After finding these matching functions, we discuss the outer boundary layer structure. Eliminating streamfunctions from (B-32, 34), we obtain

$$f/2\beta_s\cdot\partial(D-\zeta)/\partial\sigma+\alpha(D-\zeta) = (D^2-D_g^2)/2 \qquad (B-37)$$

Eliminating Ψ_0 from (B-22, 23), we have

$$1/4\cdot\partial^2D/\partial\sigma^2+(\beta_sD/f-\partial D/\partial s)\partial\zeta/\partial\sigma+\partial D/\partial\sigma\cdot\partial\zeta/\partial s = 0 \qquad (B-38)$$

Now equations (B-32, 34, 37, 38) are equivalent to the original system (B-22, 23, 24, 25). Because $\alpha \gg 1$, from (B-37) it is obvious that this is a singular perturbation problem. Again, we can introduce the stretched inner boundary layer coordinate

$$k = \sigma/\delta, \ \delta = 1/\alpha \ll 1 \qquad (B-39)$$

and expand D, ζ in power series of δ

$$D(\sigma,s) = D_0^+(k,s) + \delta D_1^+(k,s) +...$$

$$\zeta(\sigma,s) = \zeta_0^+(k,s) + \delta\zeta_1^+(k,s) +... \qquad (B-40)$$

Substituting (B-40) into (B-37), the lowest order relation is

$$\partial(D_0^+-\zeta_0^+)/\partial k+2\beta_s(D_0^+-\zeta_0^+)/f = 0 \qquad (B-41)$$

Applying the boundary condition (B-26), the solution for (B-41) is

$$D_0^+ = \zeta_0^+ \qquad (B-42)$$

The first order relation for the δ-power series is

$$f/2\beta_s \cdot \partial(D_1^+ - \zeta_1^+)/\partial k + (D_1^+ - \zeta_1^+) = (D_0^{+2} - D_g^2)/2 \qquad \text{(B-43)}$$

Using boundary condition (B-26) the solution is

$$D_1^+ - \zeta_1^+ = (D_0^{+2} - D_g^2)/2 \qquad \text{(B-44)}$$

Similarly, we have

$$D_2^+ - \zeta_2^+ = D_0^+ D_1^+ \qquad \text{(B-45)}$$

Substituting (B-40) into (B-38), the lowest order relation is

$$\partial^2 D_0^+/\partial k^2 = 0 \qquad \text{(B-46)}$$

Using the boundary condition that D_0^+ should be finite as $\Theta \to \infty$ and

$D_0^+(0) = 0$, the solution is

$$D_0^+ = \zeta_0^+ = 0 \qquad \text{(B-47)}$$

In (B-38) the first order balance for the δ-power series is

$$\partial^2 D_1^+/\partial k^2 = 0 \qquad \text{(B-48)}$$

Applying the boundary condition that $D_1^+ = 0$, at $k = 0$, $\partial D_1^+/\partial k = 0$ at

$k = \infty$, we find the solution

$$D_1^+ = 0, \quad \zeta_1^+ = D_g^2/2 \qquad \text{(B-49)}$$

Now we discuss the outer solution. Expanding D, ζ in power series of δ

$$D = D_0^*(\sigma, s) + \delta D_1^*(\sigma, s) + \ldots$$

$$\zeta = \zeta_0^*(\sigma, s) + \delta \zeta_1^*(\sigma, s) + \ldots \qquad \text{(B-50)}$$

Using the standard matching technique, the corresponding boundary condition at

$\sigma = 0$ can be found. Substituting (B-50) into (B-37), the lowest order balance

is

$$D_0^* = \zeta_0^* \qquad \text{(B-51)}$$

Putting (B-50) into (B-38) and using (B-51), one obtains a single equation for

D_0^*

$$1/4 \cdot \partial^2 D_0^* / \partial \sigma^2 + \beta_s / f \cdot D_0^* \partial D_0^* / \partial \sigma = 0 \qquad \text{(B-52)}$$

with the corresponding boundary conditions

$$D_0^* = 0, \qquad \text{at } \sigma = 0$$

$$D_0^* = D_g(0,s), \qquad \text{at } \sigma \to \infty \qquad \text{(B-53)}$$

The solution is

$$D_0^* = D_g(0,s)\tanh(n\sigma), \quad n = 2\beta D_g(0,s)/f \qquad \text{(B-54)}$$

Similarly, the first order relations are

$$D_1^* - \zeta_1^* = (D_0^{*2} - D_g^2)/2 \qquad \text{(B-55)}$$

$$\partial/\partial\sigma \cdot [\partial D_1^* / \partial\sigma + 4\beta_s / f \cdot (D_0^* D_1^* - D_0^{*3}/3)] = 0 \qquad \text{(B-56)}$$

with the boundary condition

$$D_1^*(0,s) = D_1^*(\infty,s) = 0 \qquad \text{(B-57)}$$

The solution is

$$D_1^* = D_g^2[\cosh(n\sigma) - 1 - 2Ln(\cosh(n\sigma)) - \sinh(2n\sigma)/2 - n\sigma]/3\cosh(n\sigma) \qquad \text{(B-58)}$$

After finding the solution for D and ζ, we can obtain the streamfunction Ψ_0 by integrating (B-22)

$$\Psi_0 = \Psi_m - 1/f \cdot \int_0^\sigma D \partial\zeta/\partial\sigma \, d\sigma \qquad \text{(B-59)}$$

By a simple manipulation, we have

$$\Psi_0 = \Psi_m + [D_0^{*2}/2 - \delta(D_0^{*3}/3 - D_0^* D_1^*) + O(\delta^2)]/f \qquad \text{(B-60)}$$

Using (B-51,55,58) and (B-32), the lower layer streamfunction is

$$\Psi_1 = \Psi_{0g} - \Psi_0 + \delta D_0^* / \beta_s \cdot \partial D_0^* / \partial\sigma + O(\delta^2) \qquad \text{(B-61)}$$

Letting $\sigma \to \infty$ in (B-60), we obtain the surfacing line condition

$$\Psi_{0g} = \Psi_m + [D_g^2/2 - \delta D_g^3/3 + O(\delta^2)]/f \qquad \text{(B-62)}$$

77

Appendix C. The Isolated Northern Boundary Current

This boundary current is a special case for the more general discussion in Appendix B. Assuming the surfacing line is $y_0 = y_0(x)$ and introducing the new coordinates

$$r = y-y_0, \quad S = -x \qquad (C-1)$$

we find a similar dynamical balance within this boundary layer as within the internal boundary layer. As in Appendix B, we divide the boundary layer into two regions. Region D~ε has exactly the same dynamical structure as the case in Appendix B, and we can write $\tau^s = -\tau$ explicitly. From the same argument, we obtain the matching condition for the outer boundary layer within region D ~ 1 where we define the new stretched coordinate

$$\eta = (y-y_0)/\varepsilon \qquad (C-2)$$

Substituting (C-2) into (B-1, 2, 3, 4), the lowest order expansions in ε are

$$-f\partial\Psi_0/\partial\eta = -D\partial\zeta/\partial\eta \qquad (C-3)$$

$$-f\partial\Psi_0/\partial s = -D\partial\zeta/\partial s - 1/4\cdot\partial D/\partial\eta - \lambda\tau(1) \qquad (C-4)$$

$$-f\partial\Psi_1/\partial\eta = (\alpha-D)\partial(D-\zeta)/\partial\eta \qquad (C-5)$$

$$-f\partial\Psi_1/\partial s = (\alpha-D)\partial(D-\zeta)/\partial s + 1/2\cdot\partial(D-\zeta)/\partial\eta + 1/4\cdot\partial D/\partial\eta \qquad (C-6)$$

Following the same argument as in Appendix B, the corresponding matching boundary conditions are

$$\Psi_0 = \Psi_m, \quad \Psi_1 = \Psi_{0g} - \Psi_m, \quad D = 0, \quad \zeta = \zeta_{1g} \text{ at } \eta=0 \qquad (C-7)$$

$$\Psi_0 = \Psi_1 = 0, \quad D = D_w, \quad \zeta = \zeta_w \qquad \text{at } \eta = \eta_w \qquad (C-8)$$

where $\Psi_{0g} \sim 0$ if the boundary layer is really very narrow.

Adding (C-3) to (C-5) and (C-4) to (C-6), we obtain the following relations

$$-f\partial(\Psi_0+\Psi_1)/\partial\eta = \partial[\alpha(D-\zeta)-D^2/2]/\partial\eta \qquad (C-9)$$

$$-f\partial(\Psi_0+\Psi_1)/\partial s = \partial[\alpha(D-\zeta)-D^2/2]/\partial s + 1/2\cdot\partial(D-\zeta)/\partial\eta - \lambda\tau(1) \qquad (C-10)$$

78

Integrating (C-9) under the boundary condition (C-8), we find

$$-f(\Psi_0+\Psi_1-\Psi_m) = \alpha(D-\zeta)-D^2/2-\alpha\zeta_{1g} \qquad (C-11)$$

Substituting (C-11) into (C-10)

$$1/2\bullet\partial(D-\zeta)/\partial\eta-\lambda\tau(1) = \alpha\partial\zeta_{1g}/\partial s|_{y=1} \qquad (C-12)$$

From (36)

$$\partial\zeta_{1g}/\partial s|_{y=1} = -\partial\zeta_{1g}/\partial x|_{y=1} = 1/\alpha \qquad (C-13)$$

Noting that $\tau(1) = -1$ and $\zeta = \zeta_{1g}$, $D = 0$ at $\eta = 0$, we have

$$D = \zeta_{1g}(s)-\zeta \qquad (C-14)$$

As for the northern boundary current in the case of a lower layer with infinite depth, if we had a single first -order differential equation for D, we could not determine two unknown constants. This problem can be solved if we include higher order terms in the equation. Alternatively, we can use the ageostrophic momentum equation directly. From (C-3,14), by integrating

$$\Psi_0 = \Psi_m+D^2/2f \qquad (C-15)$$

Puting (C-14,15) into (C-3)

$$\partial D/\partial\eta+4D\lambda/\alpha = \lambda \qquad (C-16)$$

The solution is

$$D = \alpha(1-\exp(-4\eta\lambda/\alpha)) \qquad (C-17)$$

$$\Psi_0 = \Psi_m+\alpha^2(1-\exp(-4\eta\lambda/\alpha))^2/2f \qquad (C-18)$$

$$\Psi_1 = 0 \qquad (C-19)$$

$$D_w = (-2f_n\Psi_m)^{1/2} \qquad (C-20)$$

$$\zeta_w = \zeta_{1g}+D_w \qquad (C-21)$$

The boundary layer width is

$$b_n = -\varepsilon\alpha Ln(1-(-2f_n\Psi_m)^{1/2}/\alpha)/4\lambda \qquad (C-22)$$

Appendix D. The Isolated Western Boundary Current

For this boundary current , the following coordinates are useful

$r = x_w - x$, $s = -y$.

As before, we divide the boundary layer into two regions. For region $D \sim e$, the dynamics are almost the same as before and the analysis of this region gives the matching conditions for the region $D \sim 1$. Here we discuss the region $D \sim 1$ only. For convenience, we redefine the coordinates as

$$\xi = x/\varepsilon, \quad s = y \qquad \qquad (D-1)$$

From the basic equations (20, 21), the lowest order balances for ε-power series are

$$-f \partial \Psi_0 / \partial \xi = -D \partial \zeta / \partial \xi \qquad \qquad (D-2)$$

$$-f \partial \Psi_0 / \partial y = -D \partial \zeta / \partial y - 1/4 \cdot \partial D / \partial \xi \qquad \qquad (D-3)$$

$$-f \partial \Psi_1 / \partial \xi = (\alpha - D) \partial (D - \zeta) / \partial \xi \qquad \qquad (D-4)$$

$$-f \partial \Psi_1 / \partial y = (\alpha - D) \partial (D - \zeta) / \partial y + 1/2 \cdot \partial (D - \zeta) / \partial \xi + 1/4 \cdot \partial D / \partial \xi \qquad (D-5)$$

By the same matching technique as before, the corresponding boundary conditions are

$$\Psi_0 = 0, \ \Psi_1 = 0, \ D = D_w, \ \zeta = \zeta_{1g} \quad \text{at } \zeta = 0 \qquad \qquad (D-6)$$

$$\Psi_0 = \Psi_m, \Psi_1 = \Psi_{1g}, D=0, \zeta=\zeta_{1g}, \partial(D-\zeta)/\partial\xi=0 \ \text{at} \xi=\xi_\infty \qquad \qquad (D-7)$$

Adding (D-2) to (D-4) and (D-3) to (D-5), we have

$$-f \partial (\Psi_0 + \Psi_1) / \partial \xi = \partial / \partial \xi \cdot [\alpha(D - \zeta) - D^2 / 2] \qquad \qquad (D-8)$$

$$-f \partial (\Psi_0 + \Psi_1) / \partial y = \partial / \partial y \cdot [\alpha(D - \zeta) - D^2 / 2] + 1/2 \cdot \partial (D - \zeta) / \partial \xi \qquad (D-9)$$

Introducing (D-8) and using boundary condition (D-7), we obtain

$$-f(\Psi_0 + \Psi_1 - \Psi_{1g} - \Psi_m) = \alpha(D - \zeta) - D^2 / 2 - \alpha \zeta_{1g} \qquad \qquad (D-10)$$

Cross-differentiating (D-8,9), integrating over(ξ, ξ_∞), using the boundary condition $\partial(D-\zeta)/\partial\xi = 0$ at $\xi = \xi_\infty$, we have

$$\Psi_0+\Psi_1-\Psi_{1g}-\Psi_m = 1/2\bullet\partial(D-\zeta)/\partial\xi \qquad\qquad (D-11)$$

From (D-10, 11), we obtain

$$f/2\bullet\partial(D-\zeta)/\partial\xi+\alpha(D-\zeta) = D^2/2-\alpha\zeta_{1g} \qquad\qquad (D-12)$$

Eliminating Ψ_0 from (D-2,3) gives

$$1/4\bullet\partial^2 D/\partial\xi^2+(D/f-\partial D/\partial y)\partial\zeta/\partial\xi+\partial D/\partial\xi\bullet\partial\zeta/\partial y = 0 \qquad\qquad (D-13)$$

Again, equation (D-12) implies the same singular perturbation character of this system. As in Appendix A, we introduce the inner boundary layer coordinate

$$\Theta = \eta/\delta, \; \delta = 1/\alpha \qquad\qquad (D-14)$$

and expand Ψ_0, Ψ_1, D, ζ in δ-power series

$$\Psi_0(\xi,y) = \Psi_{00}(\Theta,y) + \delta\Psi_{01}(\Theta,y) +...$$

$$\Psi_1(\xi,y) = 1/\delta\bullet\Psi_{1,-1}(\Theta,y) + \Psi_{10}(\Theta,y) + \delta\Psi_{11}(\Theta,y)$$

$$D(\xi,y) = D_0(\Theta,y) + \delta D_1(\Theta,y) + ... \qquad\qquad (D-15)$$

$$\zeta(\xi,y) = \zeta_0(\Theta,y) + \delta\zeta_1(\Theta,y) + ...$$

Notice that $\alpha\zeta_{1g}$ is order O(1), so that substituting (D-15) into (D-12,13) gives the lowest order relations

$$f/2\bullet\partial(D_0-\zeta_0)/\partial\Theta+(D_0-\zeta_0) = 0 \qquad\qquad (D-16)$$

$$\partial^2 D_0/\partial\Theta^2 = 0 \qquad\qquad (D-17)$$

Applying the boundary conditions: D, $\partial D/\partial\Theta$ are finite as $\Theta \to \infty$, we find

$$D_0 = D(0,y) \qquad\qquad (D-18)$$

$$\zeta_0 = D_0+A_0\exp(-2\Theta/f) \qquad\qquad (D-19)$$

The lowest order balance of equation (D-11) gives

$$\Psi_{1,-1} = 1/2\bullet\partial(D_0-\zeta_0)/\partial\Theta \qquad\qquad (D-20)$$

Using the boundary conditions (D-6), we find

$$\Psi_{1,-1} = 0, \; A_0 = 0 \qquad\qquad (D-21)$$

The next order solutions are

$$D_1 - \zeta_1 = D_0^2/2 - \alpha\zeta_{1g} + A_1\exp(-2\Theta/f) \tag{D-22}$$

Integrating (D-2) and using the boundary condition $\Psi_0 = 0$ at $\Theta = 0$, we obtain

$$\Psi_{00} = 0 \tag{D-23}$$

Substituting (D-23) into (D-11) and using (D-22), we have

$$\Psi_{10} = \Psi_{1g} + \Psi_m - A_1\exp(-2\Theta/f)/f \tag{D-24}$$

Using the boundary condition $\Psi_1 = 0$ at $\Theta = 0$, we find

$$A_1 = f(\Psi_{1g} + \Psi_m) \tag{D-25}$$

so that

$$\Psi_{10} = (\Psi_{1g} + \Psi_m)(1 - \exp(-2\Theta/f)) \tag{D-26}$$

Now we discuss the outer solution. From the inner solution, using the same matching technique, we find the boundary conditions for the outer layer solution

$$\Psi_0 = 0, \quad \Psi_1 = \Psi_{1g} + \Psi_m, \quad \zeta_0 = D_0 = D_0(y) \text{ at } \xi = 0 \tag{D-27}$$

$$\Psi_0 = \Psi_m, \quad \Psi_1 = \Psi_{1g}, \quad \zeta_0 = \zeta_{1g}, \quad D = 0 \text{ at } \xi = \xi_\infty \tag{D-28}$$

As in Appendix A, we expand the outer solution in δ-power series

$$\Psi_0 = \Psi_{00}^*(\xi, y) + \delta\Psi_{01}^*(\xi, y) + \ldots$$

$$\Psi_1 = \Psi_{10}^*(\xi, y) + \delta\Psi_{11}^*(\xi, y) + \ldots$$

$$D = D_0^*(\xi, y) + \delta D_1^*(\xi, y) + \ldots \tag{D-29}$$

$$\zeta = \zeta_0^*(\xi, y) + \delta\zeta_1^*(\xi, y) + \ldots$$

Substituting (D-29) into (D-12), we find

$$D_0^* = \zeta_0^* \tag{D-30}$$

From (D-13) we get

$$\partial^2 D_0^*/\partial\xi^2 + 2/f \cdot \partial D_0^{*2}/\partial\xi = 0 \tag{D-31}$$

Using boundary condition (D-27) and (D-28), the solution of (D-31) is

$$D_0^*(\xi,y) = D_0^*(0,y)/(1+2D_0^*(0,y)\xi/f) \tag{D-32}$$

From (D-2) we obtain

$$\Psi_{00}^* = \Psi_m + D_0^{*2}/2f \tag{D-33}$$

Thus

$$D_0^{*2}(0,y) = -2f\Psi_m \tag{D-34}$$

From (D-11)

$$\Psi_{10}^* = \Psi_{1g} + \Psi_m - \Psi_{00}^* \tag{D-35}$$

Appendix E. The Western Boundary Current for the

Supercritical State (II)

Within domain I of this case, the upper layer and the lower layer are both in motion. The purpose of the following analysis is to determine how the western boundary current can match the known interior flow. The analysis here basically parallels to the analysis in Appendix A, except here the matching boundary conditions are

$$\text{at } \xi = 0, \ \Psi_0 = \Psi_1 = 0 \tag{E-1}$$

$$\xi \to \infty, \ \Psi_0 \to \Psi_{0g}, \ \Psi_1 \to \Psi_{1g}, \ D \to D_g, \ \zeta \to \zeta_g \tag{E-2}$$

where D_g, ζ_g, Ψ_{0g}, Ψ_{1g} are known functions of y derived from the nonlinear equation system in Section 4. The interior flow has $D_g - \zeta_g \neq 0$, but it is a known function. Hence the semi-geostrophic condition is

$$-f(\Psi_0 + \Psi_1 - \Psi_{0g} - \Psi_{1g}) = \alpha(D-\zeta) - \alpha(D_g - \zeta_g) + (D_g^2 - D^2)/2 \tag{E-3}$$

From (E-3) and (A-11) , by eliminating the streamfunctions, we get

$$f/2 \cdot \partial(D-\zeta)/\partial\xi + \alpha(D-\zeta) = \alpha(D_g - \zeta_g) + (D^2 - D_g^2)/2 \tag{E-4}$$

which can be written as

$$\delta f/2 \cdot \partial(D-\zeta)/\partial\xi + (D-\zeta) = (D_g - \zeta_g) + \delta(D^2 - D_g^2)/2 \tag{E-5}$$

After introducing the inner boundary layer coordinate $\Theta = \xi/\delta$ and expanding Ψ_0, Ψ_1, D, ζ in power series of δ, one finds the lowest order and the first order balance.

1) δ^0-order balance

$$-f\Psi_{1,-1} = (D_0-\zeta_0)-(D_g-\zeta_g) \qquad\qquad\qquad\qquad (E-6)$$

$$\Psi_{1,-1} = 1/2\bullet\partial(D_0-\zeta_0)/\partial\Theta \qquad\qquad\qquad\qquad (E-7)$$

$$f/2\bullet\partial(D_0-\zeta_0)/\partial\sigma+(D_0-\zeta_0) = D_g-\zeta_g \qquad\qquad (E-8)$$

$$\partial^2 D_0/\partial\Theta^2 = 0 \qquad\qquad\qquad\qquad\qquad\qquad\qquad (E-9)$$

Following the same argument as in Appendix A, the solutions are

$$\Psi_{1,-1} = 0$$

$$D_0-\zeta_0 = D_g-\zeta_g \qquad \text{for any } \Theta \text{ and } y$$

$$D_0 = D_0(0,y) \qquad\qquad \text{is independent of } \Theta \qquad\qquad (E-10)$$

2) δ -order balance

$$-f(\Psi_{00}+\Psi_{10}-\Psi_{0g}-\Psi_{1g}) = (D_1-\zeta_1)+(D_g^2-D_0^2)/2$$

$$(\Psi_{00}+\Psi_{10}-\Psi_{0g}-\Psi_{1g}) = 1/2\bullet\partial(D_1-\zeta_1)/\partial\Theta$$

$$f/2\bullet\partial(D_1-\zeta_1)/\partial\Theta+(D_1-\zeta_1) = (D_0^2-D_g^2)/2 \qquad (E-11)$$

$$\partial^2 D_1/\partial\Theta^2 = 0$$

The solutions are

$$\Psi_{00} = 0$$

$$\Psi_{10} = (\Psi_{0g}+\Psi_{1g})(1-\exp(-2\Theta/f))$$

$$D_1 = D_1(y)$$

$$\zeta_1 = D_1(y)-(D_0^2-D_g^2)/2-f(\Psi_{0g}+\Psi_{1g})\exp(-2\Theta/f)$$

$$\Psi_{01} = D_0(\Psi_{0g}+\Psi_{1g})(1-\exp(-2\Theta/f)) \qquad\qquad (E-12)$$

For the outer boundary layer, the matching conditions are

at $\xi = 0$, $\Psi_0 = 0$, $\Psi_1 = \Psi_{0g}+\Psi_{1g}$

$$D = D(y), \quad \zeta = (\zeta_g-D_g)+D(y) \qquad\qquad\qquad (E-13)$$

at $\xi \to \infty$, $\Psi_0 = \Psi_{0g}$, $\Psi_1 = \Psi_{1g}$, $D = D_g$, $\zeta = \zeta_g$ (E-14)

After expanding all dependent variables in δ-power series, the lowest order balances for D_0 and ζ_0 are

$$D_0^* = \zeta_0^* \tag{E-15}$$

$$1/4 \cdot \partial^2 D_0^* / \partial \xi^2 + (D_0^*/f - \partial D_g/\partial y + \partial \zeta_g/\partial y) \partial D_0^* / \partial \xi = 0 \tag{E-16}$$

with the corresponding boundary conditions

$$D_0^*(0) = D_0(y), \quad D_0^*(\infty) = D_g(y) \tag{E-17}$$

where D_g and ζ_g are known functions of y from the interior solution. The solution of this equation is

$$D_0^* = (D_g - D_2 C_1 \exp(-C_2 \xi))/(1 - C_1 \exp(-C_2 \xi)) \tag{E-18}$$

where

$$C_1 = (D_0 - D_g)/(D_0 - D_2)$$

$$C_2 = 4[D_g - f \partial(D_g - \zeta_g)/\partial y]/f$$

$$D_0 = (D_g^2 - 2f\Psi_{0g})^{1/2}$$

$$D_2 = 2f \partial(D_g - \zeta_g)/\partial y - D_g \tag{E-19}$$

Thus the outer boundary layer solution is

$$\Psi_0 = \Psi_{0g} + (D_0^{*2} - D_g^2)/2f + O(\delta)$$

$$\Psi_1 = (\Psi_{0g} + \Psi_{1g}) - \Psi_0 + O(\delta)$$

$$D = (D_g - D_2 C_1 \exp(-C_2 \xi))/(1 - C_1 \exp(-C_2 \xi)) + O(\delta)$$

$$\zeta = D + O(\delta) \tag{E-20}$$

Addendum to Part I

On the Generalized Parsons's Model

By our definition, a generalized parsons's model is a two-layer model with

an outcropping zone in a two-gyre basin (the model we studied in Chapters I

and II). In a generalized Parsons's model there are four important assumptions:

1) Two layers are immiscible.

2) The Ekman layer is combined with the geostrophic flow below, and the

whole layer is treated as a vertically homogeneous layer.

3) The lower layer is motionless except when it is directly driven by the

wind force or underneath the the strong boundary currents. (The supercritical

state (II) is also an exception in which the lower layer is ventilated even

below the upper layer.)

4) The upper layer has a finite amount of water.

There are several boundary conditions that must be considered for all

thermocline problems, such as the upper boundary condition, the western

boundary condition, and the lower boundary condition. Most thermocline models

treat the mixed layer as a separate problem. It is rather difficult to match a

mixed layer with the geostrophic flow underneath because of the nonlinear

interaction between these two parts. It is even harder to build a model that

has a mass-balanced circulation. This difficulty also comes from trying to

match a western boundary current to the interior geostrophic flow. By

assumptions 1) and 2), the generalized Parsons's model avoids these

difficulties. Thus, by studying the vertically integrated flow, our model

successfully produces a mass-balanced circulation in a two-gyre basin with

outcropping. Of course, the disadvantage is losing track of the mixed layer structure and the connecting mechanism.

An essential step in establishing the entire circulation pattern is finding the shape of the outcropping line. An outcropping line is a very complicated phenomenon. The thickness of the upper layer becomes zero on that line and the lower layer rises to the surface. There is a very complicated three dimensional flow field near that line. In a model with two immiscible layers, the flow field is even more complicated because the water in the mixed layer has to turn around quickly to compensate for the flow in the geostrophic interior. Fig. Ad.-1 shows schematic pictures for flow patterns near an outcropping line for both the generalized Parsons's model and the LPS model. These pictures are for the cases in a subpolar basin and within the westerly. The upper-layer light water is on the right-hand side of the outcropping line. In the generalized Parsons's model, no water is allowed to cross the outcropping line. Consequently, to the north of the outcropping line the heavy lower layer water sinks down along the interface, and to the south of the outcropping line water upwells to compensate the southward Ekman transport in the mixed layer. In the LPS model water crosses the outcropping line on which its density decreases discontinuously because water densities on both side of the outcropping line are different according to the definition of an outcropping line. For the generalized Parsons's model, we do not have to worry about the three dimensional structure, and the entire circulation problem is much easier to solve. In a sense, the present model offers an alternative way of dealing the outcropping line. The outcropping line is not a streamline for the interior Sverdrup flow in this model. Hence there is an internal boundary

87

N   S

Mixed layer

⊙   ⊗

(a)

N   S

Mixed layer

⊙   ⊗
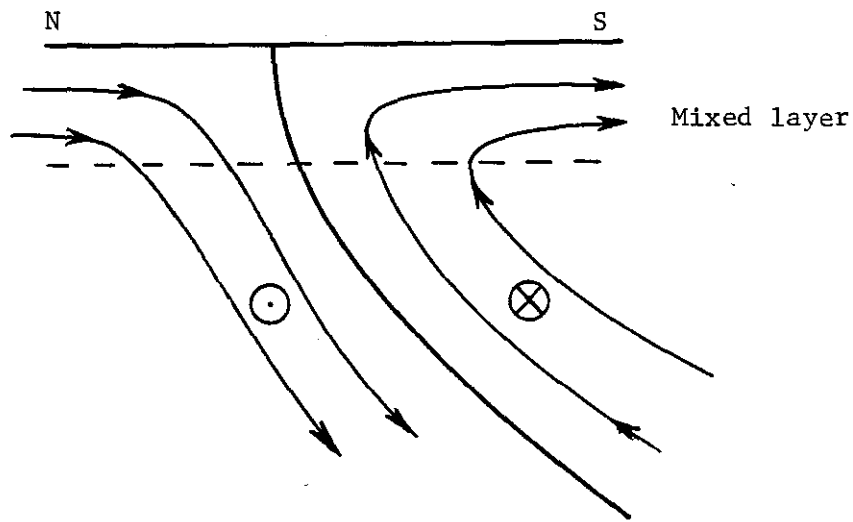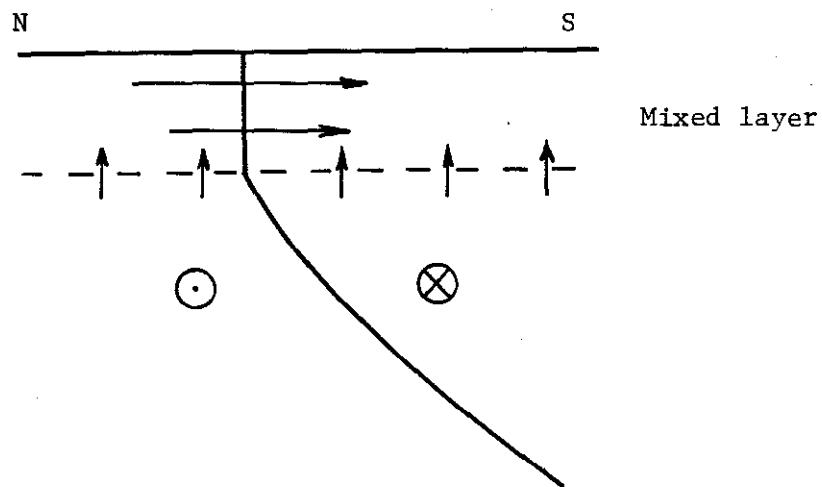
(b)

Fig. Ad.-1. Schematic pictures of flow field near an outcropping
    line in a subpolar basin. (a) The generalized Parsons' model;
    (b) the Luyten, Pedlosky and Stommel   model. ⊙ and ⊗ represent
    the geostrophic velocity vector componnent perpendicular to
    these sections.

current on the right-hand-side of the outcropping line because this line is a western boundary to the upper layer. This internal jet is very similar to the Gulf Stream in the North Atlantic Ocean.

However, one may try to consider other possible approaches for a two-gyre basin. One of these possible candidates is the LPS model. If one tries to apply the LPS model to a two-gyre basin, one immediately finds a puzzle (Pedlosky, personal communication): a line in which D is constant is also a streamline for the upper layer; thus, a question arises -- Does this argument apply to the D = 0 line? Assuming this argument does apply, there would be no internal boundary current, and the basin flow pattern would change dramatically.

Let us examine how the LPS model works in a subpolar basin. If there were only one active layer right upon the outcropping line, streamfunction would be constant along the outcropping line where D = 0. However, near the edge of the outcropping line, D → 0 and v → ∞, though the vertically integrated mass flux is still finite. This singularity is due to the assumption of a single active layer. Physically, v can not be infinite; therefore, there is motion below the upper layer. If we accept the second proposition, there is no more similarity near the outcropping line: the v-velocity remains finite on the outcropping line; the mass flux in the upper layer tends to zero there; meanwhile, most of the Sverdrup flux goes into the lower layer.

Apart from this minor singularity, a two-layer version of the LPS model works fine for a subpolar gyre. As long as we stick with the assumption that the lower layer is much thicker than the upper layer, the potential vorticity isopleths, f/(H -h), in the lower layer remain basically parallel to the

latitude circles. Therefore, only strong forcing, namely the direct wind forcing or the interfacial friction underneath the strong internal boundary current, can drive water particle across these potential vorticity isopleths. Within the LPS model, the outcropping line is a streamline; thus, there is no internal boundary current connected with it. Consequently, the lower layer is stagnant away from the outcropping zone, and a typical LPS solution for a two-gyre basin looks quite different from a typical solution for the generalized Parsosn's model.

After all, a question remains why there is an internal boundary current in the generalized Parsons's model. Veronis (1980) pointed out that including the Ekman flux is essential for a two-layer model to have the thermocline rising to the surface (within the subtropical gyre). In other words, including the Ekman flux causes the Gulf Stream - like internal jet to appear in a two-gyre basin model. Cutting out the mixed layer, of course, changes the entire model. Although the generalized Parsons's model is the only existed model that can produce the Gulf Stream - like internal jet, it is still possible to produce a similar kind of cross gyre mass flux with other models.

It is interesting to note that most previous models treat two gyres largely without cross-gyre interaction. The real oceans, however, behave in the other way. There are interactions between gyres. The following analysis gives simplest explanation.

First, the boundary between gyres can vary according to the model used. For the LPS model the boundary between gyres is the line where the Ekman pumping velocity vanishes. For the generalized Parsons's model, the mass flux is proportional to the wind-stress-curl; thus, the natural boundary between

gyres is the ZWCL. The relative positions of these two lines can be determined by the following relation

$$w_e = (\partial\tau^y/\partial x - \partial\tau^x/\partial y)/f + \beta\tau^x/f^2 \qquad\qquad (Ad.-1)$$

Generally, the subtropical-subpolar gyre boundary is located within the westerly region. Thus $\tau^x > 0$ and the zero-Ekman-pumping line is south to the ZWCL. Fig. Ad.-2a) shows a schematic diagram of a rectangular two-gyre basin. One can easily show that the distance between these two lines is much smaller than the north-south scale of the basin. For simplicity, let us assume that $\tau^y = 0$. By scale analysis the ratio between the first and the second term is order of $\beta L/f \cong L/R \ll 1$, where L is the north-south scale of a subtropical gyre, R is the Earth's radius. Therefore, these two intergyre boundaries are determined largely by the vanishing of the wind-stress-curl and located near each other.

Second, there are water mass exchanges across these natural boundaries determined above. Fig. Ad.-2.b) and c) show the corresponding pictures. As pointed above these boundaries are located in the westerly, so that there are southward Ekman flux within the mixed layer. On section A - A, where the wind-stress-curl is zero, the vertically integrated streamfunction (including the mixed layer) vanishes; thus, there should be a northward return flow within the geostrophic region underneath the mixed layer. A western boundary current is not a necessary part of a circulation system at this section. This is a first baroclinic mode of water mass exchange intrinsic to the generalized Parsons's model. On section B - B, where the Ekman pumping velocity is zero, the geostrophic mass transport vanishes. To balance the mass transfport, however, there should be a northward return flow somewhere. Therefore, as a

N

Subpolar gyre

A

B

Subtropical gyre

S

W   E

a)

$\nabla \times \vec{\tau} = 0$

$\nabla \times (\vec{\tau}/f) = 0$

mixed layer

A-A section

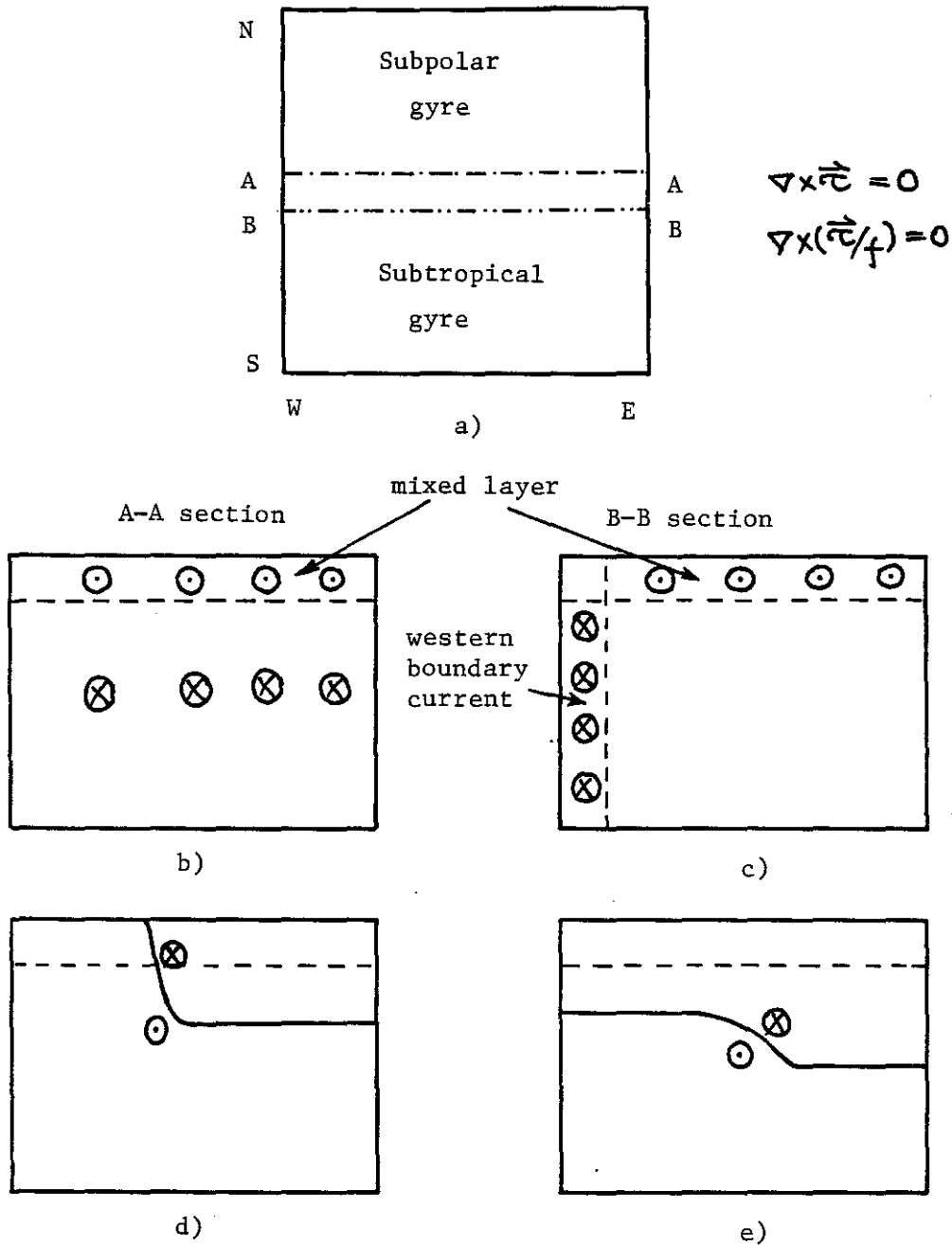B-B section

western boundary current

b)

c)

d)

e)

Fig. Ad.-2. Schematic picture for a two-gyre basin.
    a) Two possible choices for a natural boundary between gyres, the zero-wind-curl-line (A-A) and the zero-Ekman-pumping-line (B-B).
    b, c) Sverdrup flow patterns at sections A-A and B-B.
    d) first baroclinic mode of water mass exchange across the A-A section by the generalized Parsons' model.
    e) first baroclinic mode of water mass exchange across the B-B section (Pedlosky, 1984)

necessary part of the circulation system here, a northward western boundary current exists on this section.

The question, of course, is whether there are other kind of water mass exchanges across the gyre boundaries. There have been speculations about this kind of phenomena based on observations. Fig. Ad.-3 and Ad.-4 show the circulation diagram by Worthington (1976) and McCartney (1982). In these pictures the North Atlantic Current crosses the zero-Ekman-pumping line and the Labrador Sea water goes southward as a deep western boundary current. McCartney and Talley (1982) also point out that the subpolar mode water moves underneath the Gulf Stream and joins the subtropical anticyclonic gyre after crossing the Gulf Stream.

The generalized Parsons's model produces a first baroclinic mode of water mass exchange that is very similar to the case just described for the North Atlantic Current. As shown in Fig. Ad.-2d), this baroclinic mode appears as a strong, narrow internal boundary currents. It is also important to note that this baroclinic mode is quite different from the simple Ekman flux – geostrophic flux mode discussed above. Even the mass flux involved now is much bigger than the previous mode. From the concrete example in Chapter II, the mass flux in this baroclinic mode can be as big as a large fraction of the total Sverdrup transport for the subpolar gyre; while the baroclinic mode involved with the Ekman flux is much smaller than the total Sverdrup transport.

After the draft of this thesis had been finished the author become aware of Pedlosky's work on the first baroclinic mode of water mass exchange (within
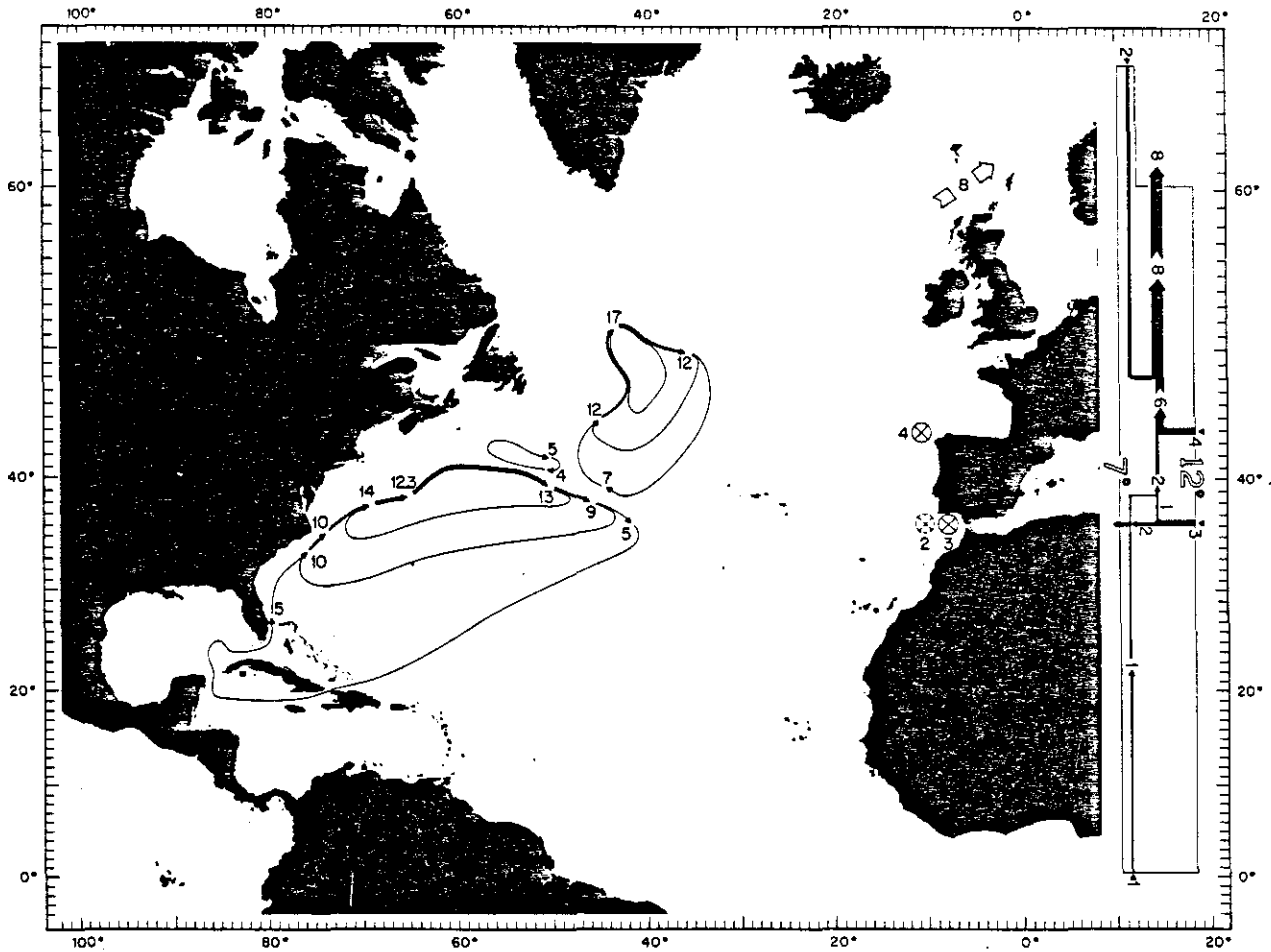
Fig. Ad.-3. Circulation diagram and box model for the mid-thermocline
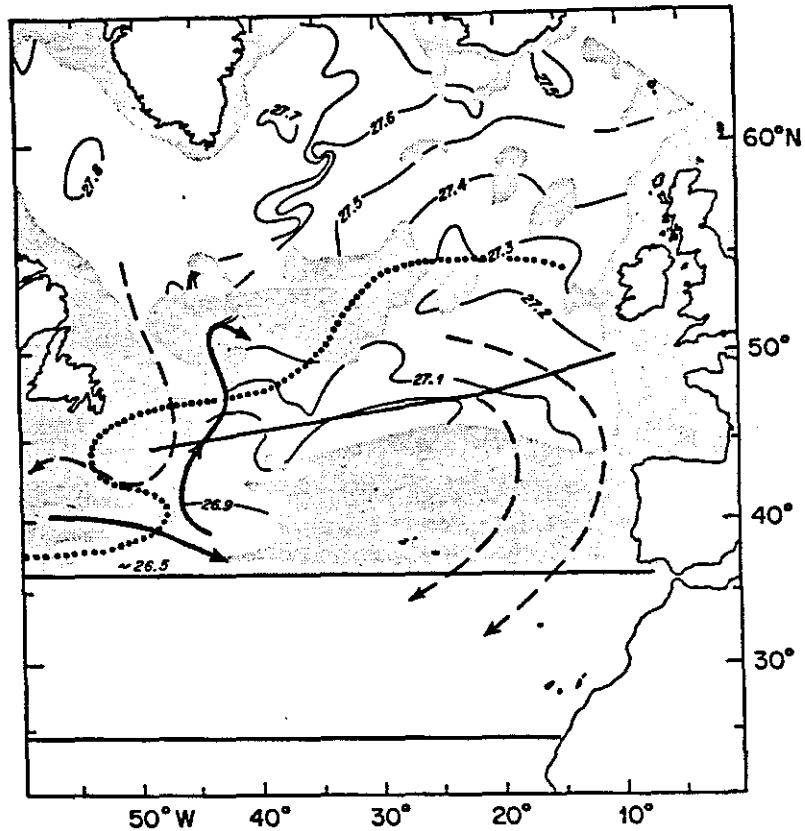layer (7-12^{0}C) in the North Atlantic (Worthington, 1976).

Fig. Ad.-4. Circulation pattern in the central and eastern North
Atlantic. The dotted line is the axis of zero Ekman pumping
from Leetmaa and Bunker (1978). The solid arrow is Worthington's
interpretation of the axis of the North Atlantic Current for
the temperature range $7-12^0$C. Two advection paths are
schematically indicated by dashed lines: a direct anticyclonic
recirculation from the winter outcropping between 27.0 mg/cm^3
and 27.2 mg/cm^3, and advection as part of the Deep Western
Boundary Current from the Labrador Sea southward inshore of the
North Atlantic Current. (McCartney, 1982)

the geostrophic region below the mixed layer) across the zero-Ekman-pumping line (Pedlosky, 1984). His solution is also shown in Fig. Ad. -2e).

In summary, the generalized Parsons's model provides a simple way of describing the Gulf Stream - like internal jet and cross-gyre water mass exchange with the basic circulation in a two-gyre basin. There are, of course, alternative way of describing the oceans. However, the generalized Parsons's model is the only known model that can reproduce the internal jet with simple algebra.

In the original Parsons's model the physical meaning of having a finite amount of warm water is not very clear. However, for a two-gyre basin its meaning is much clearer. Within a subtropical-subpolar basin, the basic air-sea interaction pattern is that of water being heated in the subtropical basin and being cooled in the subpolar basin. Cooling is not uniformly distributed over the whole subpolar basin. In the western basin extremely cold and dry air from the continents creates cold, dense water during the winter time. For a two-layer model, this water mass is represented by the outcropping lower layer. Meanwhile, the upper layer covers almost the entire subtropical basin and a small part of the subpolar basin. Each layer has only one temperature which is an averaged temperature determined by integration over the entire layer. Therefore, for a given wind forcing, if the averaged atmospheric temperature rises, the amount of warm water increases and, hence, the upper layer covers a larger area, and vice versa. In this sense, the amount of warm water reflects the climatological atmospheric temperature distribution in an average mean. Thus, the generalized Parsons's model does include some representation of the combination of thermodynamic forcing with

92

wind forcing and can give solutions for the entire basin, including the western boundary current and other boundary currents.

Since the flow pattern in a two-gyre basin is determined by both wind forcing and thermodynamic forcing, there are some interesting phenomena. For example, the position of the Gulf Stream changes in response to changes in both the wind stress curl and the amount of warm water. This occurs by two different mechanisms.

First, assuming the wind stress is unchanged, the position of the Gulf Stream and its strength depends on the amount of warm water in the upper layer. There are many parameters that control the amount of warm water, such as solar radiation, cloudiness and atmospheric temperature. The Gulf Stream separation point will change in response to changes in these parameters.

Second, assuming the amount of warm water is given, the position of the Gulf Stream and its strength depend on the wind forcing. For a weak wind forcing, the upper layer covers almost the entire basin. There is not much outcropping in the subpolar basin and the internal boundary current is fairly weak. For a moderate wind forcing, there is much more outcropping in the subpolar basin; the Gulf Stream appears as a strong internal jet that combines two gyres into a united body. One might conclude that the Gulf Stream becomes very strong if the wind forcing builds up further. This may not be the case. According to our model (remember that the nonlinear advection term has been ignored!) the non-dimensional streamfunction $-\psi_m$ increases with λ for $\lambda <$ λ_m; however, at $\lambda = \lambda_m$ it attains the maximum value $-\psi_m$ (see Section 7 of Chapter I and Fig. 1-5). When $\lambda > \lambda_m$, $-\psi_m$ decreases with λ and becomes zero at $\lambda = \lambda_s$. Assuming that the upper layer depth scale is

unchanged, the dimensional mass flux across the ZWCL is equal to $-\psi_m$ times

a constant factor. If the North Atlantic Ocean and the Gulf Stream can be

represented by the generalized Parsons's model, the corresponding λ is around

the range of 0.2 ~ 1 (see Fig. 1-6). As wind forcing becomes too strong

compared with the present value, the upper layer shrinks southward and the

cross ZWCL mass flux will decrease eventually. This phenomenon might have a

very important climatological meaning.

There have been many ice ages in our Earth's history. The dynamic reason

for this ice age - interglacial age cycle is not clear. Many theories have

been proposed, such as changes in the Earth's orbit and volcanic activity.

From the values of histograms of $\delta(^{18}O/^{16}O)$ from ice cores in Greenland

and the Antarctic, which are indicators of temperature changes during the past

100,000 years, Newell (1974) argues that there are two preferred modes of

temperature and circulation of the atmosphere-ocean system. These two modes

correspond to two modes of partitioning of the poleward energy flux between

the atmosphere and ocean. At present the ocean carries about 3/8 of poleward

hear flux at 30°N. In the cold mode, Newell suggested that the ocean carries

much less of the heat flux, and the atmosphere more, than at present.

Newell did not give a dynamic analysis for the ocean circulation pattern.

Can the generalized Parsons's model explains this atmosphere-ocean coupling

mode more clearly. For the present day circulation pattern, if the wind stress

is increased, then λ is increased. According to the generalized Parsons's

model, the upper layer shifts southward and the internal jet moves southward.

Assuming that the internal jet is the major mechanism for the poleward heat

flux across the gyre boundary, the decrease in the Gulf Stream strength

reduces the poleward heat flux and the average temperature in the subpolar basin. As the temperature in the high latitudes drops, the meridional temperature gradient increases. Hence, the available potential energy in the atmosphere increases. As a result, the wind speed is increased rapidly (Newell et al, 1981). This whole process is a positive feedback that can bring about a new ice age for a long period (on the order of 10,000 years).

As λ is larger than 2.63, all the upper layer water is confined within the subtropical basin. There is no intergyre jet and no poleward heat flux across the gyre. That is the cold mode of the atmosphere-ocean coupling model. It is uncertain how the wind stress pattern looked during that time. In the following argument we assume that the wind stress pattern was the same as present, except that the wind strength changed. Temperature maps of surface water in the North Atlantic for 18,000 B.P. have been reconstructed by transfer-function analysis of foraminiferal assemblages. Fig. Ad.-5 shows the sea-surface isotherm map for August 18,000 B.P.. The 22°C-isotherm was almost the same shape as predicted by our model for λ is larger than 2.63 (see Fig. 1-9), using the fact that the wind stress was about twice as present value and the amount of warm water was much less, say about 3/4 of the present value. Fig. Ad.-6 shows the temperature-anomaly map for August in the North Atlantic: 18,000 B.P. minus today's temperature. There was a big temperature decrease within the domain that is basically covered by the Gulf Stream System at present. During that period of time the oceanic poleward heat flux was cut down almost to zero near 35°N. It was not inconsistent with our model.

As the ice age persisted, the subpolar basin was largely frozen. There was no cold deep water formed, and the cold water upwelling stopped. Then, due to
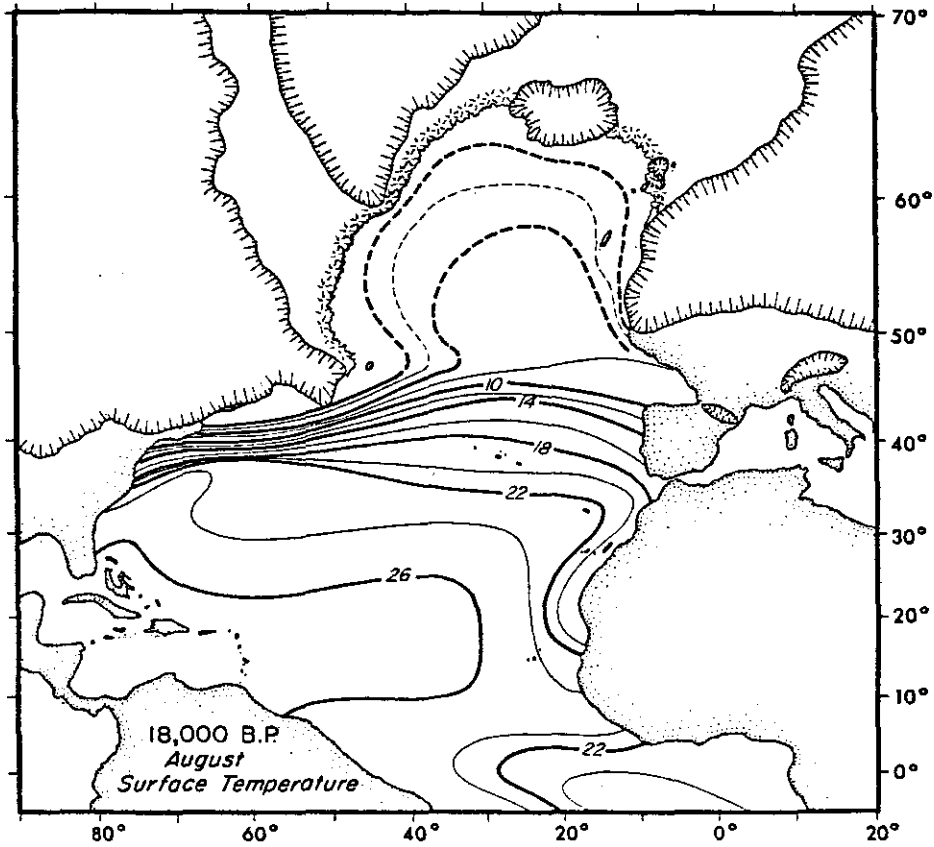
Fig. Ad.-5. Surface-water isotherm map for August 18,000 B.P.
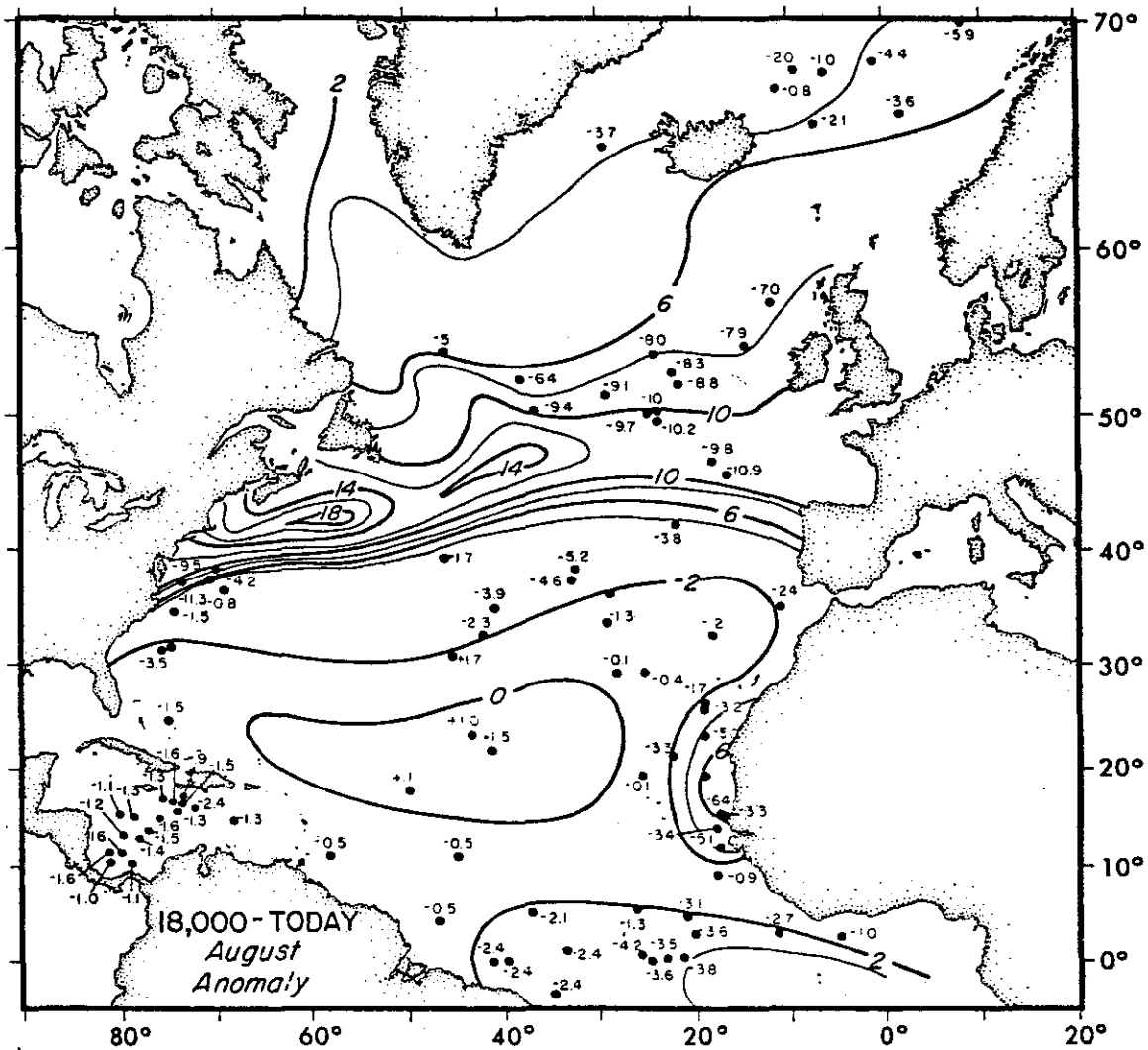(McIntyre and Others, 1976)

Fig. Ad.-6. Temperature-anomaly map for August in degrees Celsius.
Values were derived by subtracting average modern
surface-water temperatures from 18,000 B.P. (McIntyre
and Others, 1976).

the heating from the solar radiation in the subtropical gyre, the amount of warm water increased slowly. As long as there was a large mass of ice coverage at high latitude, the meridional temperature gradient remained basically the same and so did the wind speed. Therefore, according to our model the subtropical gyre expanded into the subpolar basin gradually, and transported much warm water into the subpolar basin. The warming-up period covered a long time. Finally, the warm Gulf Stream water transported enough heat to melt all the extra ice at high latitudes, and the warm mode of the interglacial period began.

The scenario above is only a simplified illustration of the complicated atmosphere-ocean coupling model. Further numerical investigation is underway to explain the details,.

In summary, the generalized Parsons's model is a very simple model that combines the dynamic effect of wind forcing and thermodynamic forcing. It is a model that can be used to study gyre circulation and climate. Further study is needed in order to explore all its dynamic meaning and potential for oceanic modelling and climatological study.

Chapter III

Exact Solution of the Ideal Fluid Thermocline
with Continuous Stratification

ABSTRACT

Welander's (1971a) solution and various generalizations are analyzed in detail. From examination of possible ways to satisfy the essential upper boundary conditions, a general way to solve the ideal fluid thermocline is proposed. Through specifying the functional form of $F(\rho,B)$ and the sea surface pressure on the western/eastern walls, the problem is reduced to one of repeatedly integrating two first order ordinary differential equations.

The present model, with appropriate choice of F, produces three-dimensional thermocline and current structures in a continuously stratified wind-driven ocean which are quite realistic. It also emphasizes the importance of diffusion and upwelling/downwelling in the western/eastern boundary currents and diffusion in the abyssal ocean. The model confirms the conjecture that to solve the ideal fluid thermocline problem, information is needed wherever fluid moves into (or out of) the domain.

The calculated results are very similar to the observed thermocline and current structures in subtropical/subpolar basins.

1. Introduction

Welander (1971a) was the first to discuss the exact solution for the ideal fluid thermocline with continuous stratification. By a simple conservation argument, a first integration is obtained

$$f\rho_z = F(\rho, B) \tag{1.1}$$

where

$$B = p + \rho g z \tag{1.2}$$

is the Bernoulli function and F is an arbitrary function. Equation (1.1) can be solved together with a second equation

$$p_z = -\rho g \tag{1.3}$$

Welander proposes an intuitive way to solve this first-order differential equation system, which consists of specifying the form of $F(\rho, B)$ and the initial value $\rho = \rho(x, y, 0)$, $B = B(x, y, 0)$. A simple downward marching then gives the whole solution.

As discussed in Addendum, however, a solution to the ideal fluid thermocline may have some discontinuities. The function $F(\rho, B)$ may have different forms for different domains. It is not clear how we can find the form of $F(\rho, B)$ from the observational data. Even if one knows the form of $F(\rho, B)$ for those water particles that can be traced back to the upper surface, one still faces the difficulty of not knowing the functional form of $F(\rho, B)$ for water particles that come into the domain through the lateral boundary (under the sea surface!).

The only successful way to solve this equation system thus far is to assume a specific simple form for the function $F(\rho, B)$. There are only a few

cases that can be integrated into finite analytical forms.

1) $f\rho_z = 0$.

There are two possible choices :

a) $\rho \equiv \rho_0$ within the whole layer. This gives the traditional homogeneous layer models in which ρ, u, v are constant within the whole layer; thus pressure p and vertical velocity w are linear functions of the vertical coordinate.

b) $\rho = \rho(x,y)$ within the upper layer. This gives the Pedlosky and Young (1983) model for a subpolar gyre. Though this model gives interesting hints about the subpolar gyre structure, it is unlikely to yield a stable solution.

2) $f\rho_z$ = const. This gives the Pedlosky and Young (1983) model with homogenized potential vorticity for layers underneath the directly wind-driven upper layer. This model is a continuous version of the original layer model with potential vorticity homogenization by Rhines and Young (1982). When the surface wind forcing is strong enough, there are closed geostrophic contours in the subsurface density layers. Within the purely ideal fluid thermocline theory, there is an infinite number of solutions. The potential vorticity homogenization theory helps us pick out a unique solution. This kind of solution is fairly close to the observational data. Huge potential vorticity plateaus exist in both the North Atlantic and the North Pacific Ocean (Holland, Keffer and Rhines, 1983); however, for the upper surface layer, potential vorticity is far from being homogenized due to the strong air-sea interactions. Thus, near the sea surface $F(\rho,B)$ should depend on both ρ and B. In fact, a realistic model should combine both situations into a

99

unified pattern.

    3) $f\rho_z = a\rho + bB + c.$ (1.4)

    The function $F(\rho,B)$ is a linear function of ρ and B; this is the logical step to take from the previous cases. Though Welander discusses a more general case with $F(\rho,B) = G(a\rho + bB + c)$, he gives no concrete example, except the degenerate case $F(\rho,B) = G(\rho)$. These were the only cases known previously for exact analytical solutions of the ideal fluid thermocline equation.

    In this chapter we first analyze Welander's solution and examine the implication of the failure to meet the essential dynamical upper boundary condition. An approach which permits satisfying the upper boundary conditions is discussed next. Thus we propose a general way to solve the ideal fluid thermocline problem. By specifying the function form of $F(\rho,B)$ and the sea surface pressure on the western (or eastern) wall, the sea surface pressure can be determined by integrating a first-order partial differential equation, using ρ_s and w_e as known functions, first suggested by Pedlosky (1983a). Then, using p_s and ρ_s as initial data, a simple downward marching gives the entire thermocline structure.

    This approach emphasizes the idea stated in Addendum that information is needed wherever fluid moves into (or out of) our domain and that different information corresponds to different thermocline structures. In this sense, for given ρ_s and w_e the ideal fluid thermocline problem is highly underdetermined: the ideal fluid thermocline cannot be solved without knowing the whole gyre structure. The interior thermocline structure and potential

vorticity distribution are determined by how the mass is balanced and how the diffusion modifies the water mass property within the entire basin.

By specifying p_s on the western (or the eastern) wall and the functional form of $F(\rho, B)$, we can find an ad-hoc solution that explains many observed features. Since the earliest period of thermocline theory, attempts have been made to explain the observed water mass distribution by either the ventilated thermocline theory or the diffusive thermocline theory. The present model confirms the ventilation theory idea that for the interior ocean the basic thermocline structure can be reproduced fairly successfully with an ideal fluid model. At the same time, however, the present model emphasizes the important role of diffusion within the western boundary layer and the abyssal ocean. In a sense, our model combines Welander's model, the LPS model and Rhines and Young's model into a unified picture. It also presents an interesting comparison with Cox and Bryan's (1983) numerical model of the ventilated thermocline.

Pedlosky and Young (1983) study a layer model that combines the LPS model with Rhines and Young's model. In principle, a multi-layer model might approximate a continuous model; however, the algebra involved is extremely complex. In some ways, the continuous case is actually simpler.

In the following analysis, we present some simple numerical solutions which are very similar to the thermocline structure in a subtropical/subpolar basin.

2. Welander's Solution

In this section we confine our discussion to the functional form (1.4). As discussed above, a solution to the ideal fluid thermocline can consist of many local solutions which match through some interfaces. Any physically sound solution should correspond to a function $F(\rho, B)$ which has fairly good analytical properties, including being expandable into Taylor series locally. Hence a knowledge of form (1.4) can give us much useful information about the thermocline structure.

The constant c in (1.4) is not essential, because any additional constant in the pressure field does not change the dynamical field at all. In the following analysis c is ignored.

By differentiating (1.4) with to z and using (1.3), a single second order ordinary differential equation in z is obtained. Integrating this equation twice gives the general solution for the density field:

$$\rho = \rho_s(x,y) + k(x,y)\int_z^0 \exp(-(t+z_0)^2 f_0/D^2 f)\, dt \qquad (2.1)$$

where

$$z_0 = a/bg, \quad D = (-2f_0/bg)^{1/2} \qquad (2.2)$$

This solution has two vertical scales. z_0 is the depth where the center of the thermocline is located. D is the vertical scale of the whole thermocline layer thickness. Actually, the local thermocline thickness scale is $D(f/f_0)^{1/2}$, which includes a factor $(\sin\theta)^{1/2}$. A thermocline solution with two vertical scales is, of course, a much better ocean model than the single scale exponential similarity solution. However, for a more realistic picture of the ocean, these two vertical scales should change horizontally

102

within the basin. We will come back to this point below.

Relation (2.2) can be written as

$$a = bgz_0 < 0, \quad b = -2f_0/D^2g < 0 \tag{2.3}$$

In (2.1), $\rho_s(x,y)$ is the surface density just below the Ekman layer. Most thermocline theories treat $\rho_s(x,y)$ as a given upper boundary condition.

By differentiating (2.1),

$$k(x,y) = -\rho_z(x,y,z)\exp(((z+z_0)/D)^2f_0/f)$$

$$= -\rho_z(x,y,-z_0) > 0. \tag{2.4}$$

Thus $k(x,y)$ is the absolute value of the vertical temperature gradient in the center of the thermocline. To determine $k(x,y)$ Welander proposes a second boundary condition

$$\rho \equiv \rho_0 \quad \text{as } z \to \infty. \tag{2.5}$$

Therefore

$$k(x,y) = (\rho_0 - \rho_s(x,y))/\int_{-\infty}^{0} \exp(-(t+z_0)^2f_0/fD^2)dt \tag{2.6}$$

this relation can be put as

$$k(x,y) = (f_0/f\pi)^{1/2}(\rho_0 - \rho_s(x,y))/D/\text{erf}((2f_0/f)^{1/2}z_0/D) \tag{2.7}$$

where

$$\text{erf}(x) = (2\pi)^{-1/2}\int_{-\infty}^{x}\exp(-u^2/2)dx$$

The whole solution is now determined completely. The corresponding pressure and velocity fields can be calculated as following

$$p = p_s(x,y) - \rho_s(x,y)gz$$

$$+k(x,y)\int_z^0 ds\int_s^0 \exp(-(t+z_0)^2f_0/fD^2)dt \tag{2.8}$$

Here, the pressure on the upper surface is not an independent new function. By putting (2.1) and (2.8) into (1.4) and calculating on $z = 0$, one obtains

$$-fk(x,y)\exp(-z_0^2f_0/fD^2) = a\rho_s(x,y) + b\rho_s(x,y) \tag{2.9}$$

103

Therefore

$$p_s(x,y) = -[a\rho_s(x,y)+fK(x,y)]/b \tag{2.10}$$

where

$$K(x,y) = k(x,y)\exp(-(z_0/D)^2 f_0/f) \tag{2.11}$$

The horizontal velocity is calculated from

$$u = -\partial p/\partial y/f\rho, \quad v = \partial p/\partial x/f\rho \tag{2.12}$$

The vertical velocity is obtained by

$$w = -(u\partial\rho/\partial x + v\partial\rho/\partial y)/\partial\rho/\partial z. \tag{2.13}$$

Here the entire solution is totally determined by specifying z_0, D and $\rho_s(x,y)$, and therefore the vertical velocity on the upper surface does not necessarily satisfy the Ekman pumping condition (Welander, 1971a; Pedlosky, 1983a). Actually, the vertical velocity on the upper surface is

$$w(z=0)= [\partial\rho_s/\partial x\bullet\partial(fK)/\partial y-\partial\rho_s/\partial y\bullet\partial(fK)/\partial x]/fKb\rho_s \tag{2.14}$$

Using (2.7) and (2.11)

$$w(z=0) = [\partial\rho_s/\partial x\bullet\partial((\rho_0-\rho_s)G(y))/\partial y$$

$$-\partial\rho_s/\partial y\bullet\partial((\rho_0-\rho_s)G(y))/\partial x]/fKb\rho_s, \tag{2.15}$$

where

$$G(y) = (ff_0/\pi)^{1/2}/DAB \tag{2.16}$$

$$A = \exp((z_0/D)^2 f_0/f) \tag{2.17}$$

$$B = erf((2f_0/f)^{1/2}z_0/D) \tag{2.18}$$

so that

$$w(z=0) = (\rho_0-\rho_s)/fKb\rho_s\bullet\partial\rho_s/\partial x\ \partial G/\partial y$$

$$= \partial\rho_s/\partial x/b\rho_s f^{1/2}A\bullet Bd(f^{1/2}/AB)/dy \tag{2.19}$$

Because f increases as y increases, both A and B decrease as y increases. Noting that b < 0, one observes that for $\partial\rho_s/\partial x > 0$, w(z=0) < 0. For the

104

special case when $\partial\rho_s/\partial x = 0$, there can be no Ekman pumping $w(x,y,0) = 0$. In any case, the vertical velocity is totally determined and does not satisfy the Ekman pumping condition for the general case.

The longitudinal velocity on the upper surface is

$$u(x,y,0) = [-a\partial\rho_s/\partial y - \partial(fK)/\partial y]/f(-b)\rho_s$$

$$= [-a\partial\rho_s/\partial y + \partial/\partial y\{(ff_0/\pi)^{1/2} \cdot (\rho_s-\rho_0)/DAB]/f(-b)\rho \qquad (2.20)$$

One can make an estimate of the sign for u. Now $\Delta\rho \sim 10^{-3}$, but $(\rho_s-\rho_0) \sim -.01$, so that the second term is the order of $-.01f_0/D\Delta y$. From $a = bgz_0 = -2f_0z_0/d^2$, the order of the first term is $.001f_0/D\Delta y$. Thus all the surface velocity is westward.

From the analysis above, one can see that although Welander's solution gives a good meridional density section, the corresponding velocity field is unreasonable.

The original ideal fluid thermocline equation is a third-order partial differential equation to z, so that one expects to have to specify three vertical boundary conditions. Through giving the function form of $F(\rho,B)$, the equation becomes a second-order ordinary differential equation. Thus the form of $F(\rho,B)$ may imply a kind of boundary condition that the corresponding solution can satisfy. However, one faces the difficult problem of choosing two vertical boundary conditions from three.

The commonly accepted vertical boundary conditions for the ideal fluid thermocline are the upper boundary conditions

$$\text{at } z = 0 \quad \rho = \rho_s(x,y), \quad w = w_e(x,y) \qquad (2.21)$$

There are also commonly used lower boundary conditions. Considering the case

when both z_0 and D are much smaller then the ocean depth, the lower boundary condition can be proposed as

at $z \to -\infty$, $\rho \to \rho_\infty$, $w \to 0$ $\hspace{4cm}$ (2.22)

If our solution can only satisfy two vertical boundary conditions, Welander's choice seems better. However, as discussed above, the corresponding velocity field is so unrealistic that we have to try the other vertical boundary condition.

3. How to Satisfy the Ekman Pumping Condition

We begin with a solution in the form of (2.1). Instead of satisfying the lower boundary condition at z = -∞, here we apply the Ekman pumping condition on the upper surface (Pedlosky, 1983a), first suggested this possibility). To find the solution, one can rewrite (2.14) as a first-order partial differential equation for fK

$$\partial \rho_s/\partial y \cdot \partial(fK)/\partial x - \partial \rho_s/\partial x \cdot \partial(fK)/\partial y = -b\rho_s W_e(fK) \tag{3.1}$$

where $\rho_s(x,y), W_e(x,y)$ are specified upper boundary conditions. This equation can be solved by a standard characteristic method. The corresponding characteristics are defined by

$$dx/ds = \partial \rho_s/\partial y, \quad dy/ds = -\partial \rho_s/\partial x \tag{3.2}$$

Hence, along a characteristic

$$dy/dx = -\partial \rho_s/\partial x \ / \ \partial \rho_s/\partial y = (dy/dx)\big|_{\rho_s = \text{const.}} \tag{3.3}$$

Therefore, on z = 0 surface any constant density line is a characteristic. Along a characteristic the original equation becomes

$$d(fK)/ds = -b\rho_s W_e(fK) \tag{3.4}$$

If we specify fK on the boundary where fluid comes into our domain, (3.4) can be integrated by standard methods; in the numerical solution below, we use the improved Euler method.

Physically, imposing data about fK(x,y) on either the western boundary or the northern/southern boundaries implies giving information about the density structure for fluid particles that move into (or out of) the domain from the lateral boundary and under the sea surface.

For the special case when ρ_s and w_e are independent of x, (3.4) becomes a simple ordinary differential equation

$$dK/dx = -bw_e\rho_s K/ \, d\rho_s/dy, \qquad (3.5)$$

and the solution is

$$k(x,y) = k(0,y) \exp(-bw_e\rho_s x/ \, d\rho_s/dy) \qquad (3.6)$$

The entire solution for the upper layer is now fully determined if we specify ρ_s, w_e, z_0, D and k(0,y). Using (3.6), one finds k(x,y) and hence the whole density structure. The corresponding pressure and velocity fields are uniquely determined.

However, this solution can only apply to the upper part of the ocean. The lower boundary presents problems in matching. We will return to the lower boundary condition below.

In addition, this kind of solution has unpleasant features. Firstly, the isopycnal surfaces all are deeper on the eastern side. This can be seen easily for the case with $\rho_s = \rho_s(y)$. From (3.6), because b < 0, w_e< 0 for the subtropical gyre, we have k(x,y) < k(0,y). Thus the isopycnal surfaces are deeper in the eastern basin than in the western basin. Secondly, there is a contradiction between having a good meridional density profile and a reasonable anticyclonic horizontal velocity pattern. The longitudinal velocity on the sea surface is

$$u(x,y,0)=[-a\partial\rho_s/\partial y-\partial/\partial y(f\exp(-(z_0/D)^2 f_0/f)k(x,y))]/f(-b)\rho_s \qquad (3.7)$$

By examining the right-hand side of (3.7), one finds that $d/dy(f\exp(-(z_0/D)^2 f_0/f)) > 0$, $-a\partial\rho_s/\partial y > 0$, so that to have an anticyclonic gyre, $\partial k/\partial y$ must be positive in the southern basin. However, this kind of k(x,y) profile gives a very unrealistic thermocline shape.

Even if the surface density distribution is dependent on x, the same problem apperears. One cannot expect a thermocline formula with only two vertical scales to give a very realistic global picture.

4. General Cases of $F(\rho, B)$

Welander's model has two parameters a and b, and the corresponding thermocline structure has two vertical scales z_0 and D. A two-scale thermocline model can describe the ocean much better than other similarity solutions. Of course, two scales are still not quite enough, since above we have seen that a two-scale model has an unrealistic feature. In the real ocean, the depth of the thermocline and the thermocline thickness should change across the basin.

If one wants to describe the longitudinal thermocline structure, there must be a third length scale. To do this, one can try to solve a function $F(\rho, B)$ with more than two parameters. For example, if one could solve

$$f\rho_z = a + b\rho + cB + d\rho^2 + eB^2 + f\rho B \tag{4.1}$$

the solution would have five length scales and one would expect a much more complex thermocline pattern.

We shall now describe a more general procedure for obtaining solutions to the ideal fluid thermocline model. First consider how to satisfy the upper boundary conditions with an arbitrary function F. In Section 3, we have discussed the way to satisfy the Ekman pumping condition for a special form of F. This approach can be generalized as following. On the upper surface' the density conservation equation gives

$$u\partial\rho_s/\partial x + v\partial\rho_s/\partial y + w_e\partial\rho/\partial z = 0. \tag{4.2}$$

Using

$$u = -1/f\rho_s\cdot(\partial p_s/\partial y), \quad v = 1/f\rho_s\cdot\partial p_s/\partial x, \tag{4.3}$$

(4.2) can be written as a first-order partial differential equation for p_s

$$\partial\rho_s/\partial y\cdot\partial p_s/\partial x - \partial\rho_s/\partial x\cdot\partial p_s/\partial y = -\rho_s w_e F(\rho_s, p_s) \tag{4.4}$$

Introducing the characteristic

$$dx/dt = \partial\rho_s/\partial y, \quad dy/dt = -\partial\rho_s/\partial x \tag{4.5}$$

the equation for p_s is

$$dp_s/dt = -\rho_s w_e F(\rho_s, p_s) \tag{4.6a}$$

or

$$Dp_s/Dx = -\rho_s w_e F(\rho_s, p_s)/\,\partial\rho_s/\partial y \tag{4.6b}$$

where the characteristic line is $\rho_s(x,y)$ = constant. It is interesting to

note that this first-order differential equation can be integrated either

eastward or westward. It is also important to emphasize that this equation can

apply only to a steady and non-dissipative case. Accordingly, given p_s on

the western/eastern boundary (or even part of the northern/southern

boundaries), where fluid moves into (or out of) the domain, this first-order

differential equation can easily be solved numerically.

Based on these results, we can formulate two boundary value problems for

the ideal fluid thermocline:

1) BVP-A.

a) Specifying the functional form of $F(\rho,B)$.

b) Giving $\rho_s = \rho_s(x,y)$ and $w = w_e(x,y)$ on $z = 0$.

c) Specifying $p_s = p_s(0, y)$ on the western boundary where fluid

comes into the domain. (As discussed above, this condition can be more general.)

The BVP-A can be solved with two steps:

a) Integrating the first-order differential equation for the sea surface pressure

$$dp_s/dt = -\rho_s w_e F(\rho_s, p_s)$$

$$p_s = p_s(0, y) \tag{4.7}$$

b) Solving the following two-equation system

$$f\rho_z = F(\rho, B)$$

$$B = p_s + \rho g z + \int_z^0 \rho g \, dz \tag{4.8}$$

$$\rho(x,y,0) = \rho_s(x,y), \quad B(x,y,0) = p_s(x,y)$$

A simple downward marching gives the vertical density and pressure distribution. Afterward, the corresponding velocity field can easily be calculated from geostrophic condition.

2) BVP-B.

This is an alternative procedure in which p_s is specified rather than F.

a) Specifying ρ_s, p_s, and w_e on $z = 0$ surface.

b) Specifying $\rho = \rho(z)$ where water comes into the domain (on the western wall or part of the northern/southern wall).

The BVP-B can be solved with the following equations

$$u = -1/f\rho \cdot (\partial p/\partial y), \quad v = 1/f\rho \cdot (\partial p/\partial x)$$

$$\partial p/\partial z = -\rho g, \qquad \partial \rho/\partial z = -(u\partial \rho/\partial x + v\partial \rho/\partial y)/w$$

$$f\partial w/\partial z = \beta v \tag{4.9}$$

except on the singular interface where $w = 0$. This singularity leads to two difficulties: First, on this surface we cannot find the vertical density

111

gradient from the density conservation equation. Second, within a subtropical gyre we do not have information about the flow field below the w = 0 surface. It is unclear whether the ideal fluid thermocline equation apply to this region.

Here one also needs density data on the western wall, because calculating term $u\partial\rho/\partial x + v\partial\rho/\partial y$ requires upstream density data. What one is really dealing with is water that comes into the domain through the lateral boundaries.

Comparison between BVP-A and BVP-B:

Both problems include ρ_s and w_e as input data. However, there is still an infinite number of solutions. To solve BVP-A it is necessary to input $p_s(0, y)$, a one-dimensional array; and to specify the form of $F(\rho, B)$. Numerically, a two-dimensional array is necessary to specify the form of $F(\rho, B)$. In contrast, to solve BVP-B, $p_s(x, y)$ and $\rho(0, y, z)$ -- two two-dimensional data arrays -- are necessary. In some cases data on the northern/southern boundaries also may be necessary.

Presently, there is no accurate way to measure sea-surface pressure within a few cruises. Thus integration of BVP-B from data seems difficult. However, the satellite altimetry technique is developing so fast that within this decade sea surface pressure measurements will become routine procedure and BVP-B might become a useful approach (although the problem of the w = 0 singularity must still be resolved). In the following analysis we will concentrate on BVP-A. Again, it is difficult to specify F directly from data and we take the approach of choosing a parameterized form and selecting the one giving the most realistic results.

5. On the Boundary Conditions

One of the major difficulties intrinsic to the ideal fluid thermocline is to satisfy complicated boundary conditions in a basin. Although we proposed a way to satisfy the upper boundary conditions, there are other difficulties with the lateral and bottom conditions. In this section we will examine these conditions in details.

1) The eastern boundary condition.

The traditional approach for wind-driven circulations is to assume that the interior solution is applicable upon the eastern boundary. Thus $u = 0$, at $x = x_e$ and the interior solution is found by integrating from the eastern wall.

For the ideal fluid thermocline, the following simple partial differential equation (the M-equation, Welander, 1959) can be found through simple algebra

$$-M_{zy}M_{zzx} + M_{zx}M_{zzy} + \beta/f \cdot M_x M_{zzz} = 0 \tag{5.1}$$

where

$$p/\rho_0 = M_z, \qquad -g\rho/\rho_0 = M_{zz}$$

$$u = -M_{zy}/f, \quad v = M_{zx}/f, \quad w = \beta M_x/f^2$$

This equation is third order in z, first order in x and y. An intuitive way to specify the boundary conditions is to impose three boundary conditions in z and one in x and y.

Considering the boundary condition in x, a natural approach is to assume the ideal fluid thermocline equation to be valid on the eastern boundary. However, it will be demonstrated below that there is a problem in applying the boundary condition on the eastern wall. If the ideal fluid thermocline theory

is valid on the eastern wall,

$$u = 0, \text{ at } x = x_e$$

Assuming that wind stress has only a zonal component, from the y-momentum equation

$$\partial p / \partial y = 0 \text{ at } x = x_e \tag{5.2}$$

implying

$$\rho = \rho(z) \qquad \text{at } x = x_e \tag{5.3}$$

The density conservation equation is now

$$w \partial \rho / \partial z = 0, \qquad \text{at } x = x_e \tag{5.4}$$

so that

$$w = 0 \text{ or } \partial \rho / \partial z = 0, \quad \text{at} \quad x = x_e \tag{5.5}$$

Therefore, we have either $w = 0$ or $\rho = $ const. on the eastern wall (Killworth, 1983).

For layer models, these conditions are satisfied completely. In the top layer, $\rho \equiv$ const. and w is non-zero, and below this active layer there is no motion, $w = 0$. Thus, stratification can exist in the lower layer.

For a continuously stratified model, w is non-zero within the top part of the ocean, so that if one wants $u \equiv 0$ on the eastern wall, an ideal fluid thermocline solution must have a constant density ρ_e on the eastern wall. In such cases, the full solution may consist of several local solutions. Thus, under the active upper layer there can be a stagnant abyssal layer with continuous stratification even on the eastern wall.

However, $\rho_s = $ const. on the eastern wall is not consistent with real oceanic observations. Surface density distribution and the corresponding v-velocity in the ocean imply that setting $u = 0$ and $\rho = $ const. on the eastern

wall is not a good assumption. The other possible choice, then, is to match an eastern boundary layer to the interior solution. In this boundary layer, there is strong upwelling/downwelling and the other dynamical terms may play an important role in bringing the u-velocity to zero. In assuming there is an eastern boundary current, Pedlosky (1983b) relaxes the eastern boundary condition for layer models. Instead of requiring $u \equiv 0$ there, the new constraint requires

$$\int_{-H}^{0} u \, dz = 0 \tag{5.6}$$

on the eastern wall. As will be shown below, the lower boundary condition on our ideal fluid thermocline model is also not very clear. Therefore, we are not able to apply this constraint and the eastern boundary condition is still uncertain.

By examining (1.1), we see that specifying the form of $F(\rho,B)$ turns the original partial differential equation into a second-order ordinary differential equation in z. Therefore, there is little freedom left for any kind of lateral boundary condition. In other words, the form of $F(\rho,B)$ may imply a lateral boundary condition. This can be seen clearly from the following theorem.

Theorem I.

Functions in the form of

$$F(\rho,B) = (\rho-\rho_e)G(\rho,B) \tag{5.7}$$

can guarantee that $u = 0, \rho = $ const. on the eastern wall, if $\rho_s(x_e,y) = \rho_e$.

Proof:

Using (4-6.a) on the characteristic $x = x_e$ where $F(\rho_s,\rho_s) = 0$,

one finds that

$$p_s = \text{const. on } x = x_e$$

By equation (1.1), it follows

$$\rho \equiv \rho_e \text{ on the eastern wall.}$$

Q.E.D.

Welander's linear function $F(\rho,B) = a\rho+bB+c$ does not satisfy this criterion, so that if we use w_e as the upper boundary condition, the corresponding solution does not satisfy the $u = 0$ condition on the eastern wall. Welander's original solution does not, however, use w_e as an upper boundary condition, so that by imposing the condition that $\rho = \rho_e$ on the eastern wall his solution can satisfy $u = 0$ on the eastern wall.

From observation, u-velocity near the eastern boundary is rather small compared with the interior ocean. Therefore, in the following analysis, we try to find solutions that are not strictly subjected to the eastern boundary condition $u = 0$, but have a relatively small u-velocity on the eastern wall. By starting from the eastern boundary, one can satisfy roughly the eastern boundary condition (5.6). We assume that an eastern boundary current exists to match the interior solution to the real eastern wall. Because the lower limit of the ideal fluid thermocline solution and the structure of the corresponding eastern boundary current with continuous stratification are not clear, the eastern boundary condition for the ideal fluid thermocline is still an open question.

2) The western boundary condition.

From the discussion above the western boundary and the eastern boundary play the same kind of role in the ideal fluid thermocline theory. If one

116

starts from the eastern boundary, the behavior of the solution is completely

free on the western boundary. Even if one chooses to start from the western

boundary, the only input there is the pressure and density distribution on the

sea surface line. Below the sea surface the whole solution has a fairly

arbitrary structure.

The validity of our model, therefore, depends on the existence of the

corresponding western/eastern boundary currents, which can turn the water mass

back into the interior ocean at exact latitudes and depths.

3) The upper boundary condition.

According to the discussion above, the upper boundary condition is simply

the specification ρ_s, w_e on the sea surface and p_s on lateral boundaries

where fluid moves into (or out of) the domain under study. In the following

analysis we examine the topology of the solutions.

The first question is whether a closed ρ_s contour is possible.

Lemma 1.

There is no closed ρ_s contour for a steady ideal fluid thermocline

solution within the interior of a subtropical (or subpolar) basin.

Proof:

Suppose there is a closed contour C. Integrating (4-6.a) along this

closed line C, one has

$\int_c w_e F(\rho_s, p_s) ds = 0$

Because w_e is always negative (or positive in a subpolar basin), the sign of

$F(\rho_s, p_s)$ must change or $F(\rho_s, p_s) \equiv 0$. In the the first case, F

becomes negative, indicating an inertial instability. In the second case, $F \equiv$

0, indicating that near the sea surface isopycnals are vertical along the

closed line C, which is also an unstable condition.

Therefore, a stable solution of the ideal fluid thermocline has no closed constant density line on the upper surface.

<div align="right">Q.E.D.</div>

Lemma 1 excludes the possibility of having closed ρ_s contours in a subtropical (or subpolar) gyre. However, for a two-gyre basin there may be closed ρ_s contours that go across the ZWCL or that extend into the western boundary current. In the ideal fluid thermocline theory, the western boundary current is not included. Fortunately, the observed ocean does not have large scale closed ρ_s contours across the ZWCL. Therefore, the first step of integrating the ideal fluid thermocline can always be taken.

Remarks.   The above discussion applies to the planetary scale only. Even on the synoptic scale there are closed ρ_s contours, such as warm-core rings and cold-core rings. In most thermocline models, meso-scale eddies are treated as noise.

4) The lower boundary condition.

Specifying the form of $F(\rho,B)$ turns the original third order partial differential equation into a second-order ordinary differential equation in z. Therefore, if one specifies two upper-boundary conditions, the solution cannot satisfy an arbitrary lower-boundary condition. Even if we try different solutions for different domains, as long as they are solutions for second- or first-order differential equations, the lower boundary condition cannot be satisfied for general cases.

One way to solve this problem is to terminate the upper layer solution along an interface where $w = 0$. Across this interface the horizontal velocity

jumps to zero. Thus there is a density discontinuity across this interface. On the other hand, this approach does not necessarily give a solution with a totally stagnant abyssal layer. Because observation gives no evidence of the existence of this front at middle depth, we do not use this approach.

Another way to solve this problem is to find functions $F(\rho,B)$ that have attractive solutions. By definition of attractive solutions, as $t \to \infty$, any solution $x(t)$ of a differential equation $dx/dt = f(x,t)$ approaches a limit point x_∞ that is independent of $x(t_0)$.

A simple example is the equation

$$dx/dt = -\alpha(x-x_\infty), \qquad x(0) = x_0$$

The corresponding solution is

$$x = x_\infty + (x_0-x_\infty)\exp(-\alpha t).$$

For our model, we can use any attractive solution to satisfy the lower boundary condition $\rho(x,y,-\infty) = \rho_\infty$. The simplest choice is

$$f\partial\rho/\partial z = -\alpha(\rho_\infty-\rho) \qquad\qquad (5.8)$$

However, though $\rho \to \rho_\infty$ at $z = -\infty$, both the pressure p and the vertical velocity w cannot satisfy arbitrary lower-boundary conditions at $z = -\infty$. Welander's solution also has the same problem.

In principle, one can try to find some attractive solutions for the first-order differential equation system

$$\rho_z = F(\rho,B)/f < 0$$

$$B_z = gz\rho_z > 0 \qquad\qquad z: (-\infty,0]$$

Introducing the new variables

$$R = -B, \quad t = -z, \quad G(\rho,R) = -F(\rho,B)/f,$$

the system becomes

$$\rho_t = G(\rho, R) > 0$$

$$R_t = tG(\rho, R) > 0. \qquad\qquad t: [0, \infty)$$

Generally, this is a non-autonomous and nonlinear system. There may be special forms of $G(\rho, B)$ that make this system attractive. This means

$$\rho \to \rho_\infty, \quad R \to R_\infty \quad \text{as } t \to \infty.$$

In other words, density and pressure are horizontally uniform on the sea bottom.

However, though ρ, p might be constant on the bottom, the vertical velocity is not necessarily zero there

$$w(-H) = w_e - \beta/f^2\rho_0 \cdot \int_{-H}^0 p_x dz,$$

where

$$p_x = p_{sx} + g\int_z^0 \rho_x dz.$$

No solution that satisfies $w = 0$ on the bottom has thus far been found. We will discuss the lower boundary condition further in the next section.

In principle, one can include more and more parameters in the function $F(\rho, B)$. By adjusting these parameters, one might satisfy the lower-boundary condition $w = 0$ at a number of points on the bottom. This is a tedious nonlinear optimization problem, involving a large number of parameters.

The lower-boundary condition for the ideal fluid thermocline is not clear from the above analysis. From the physical point of view, the abyssal circulation is very slow, and horizontal and vertical diffusion may be dynamically important. Therefore, the ideal fluid thermocline is possibly not a correct model for the abyssal circulation. In this sense, the real lower-boundary condition for the ideal fluid thermocline is an open question.

Considering the above analysis, we will try to find some attractive

solutions that have a very small residual velocity in the abyssal layer and leave the exact formulation of the lower-boundary condition for a future study. One can terminate our solution at a middle depth and match it with a diffusive solution.

5) The northern/southern boundary conditions:

In the previous section we argued that density data might be needed on both the northern and southern boundaries. Thus, a single gyre box model is not strictly valid unless we can prove a-priori that there is no water mass exchange across the northern and southern boundaries. The following theorem is a sufficient condition for non-existence of water mass exchange.

Theorem II. If on $y = y_n(x)$, $w_e = 0$ and $\rho = \rho_n = const.$ and $F(\rho,B)$ is a single-valued function, there is no water mass exchange across the surface $y = y_n(x)$.

Proof:

$w_e = 0$, and $\rho = const.$ on $y = y_n(x)$, so that $y = y_n(x)$ is a characteristic. Using (4.6), one obtains

$dp_s/ds = 0$ on $y = y_n(x)$, $z = 0$.

Using $\rho_s = \rho_n$, $p_s = p_n$ to integrate $f\rho_z = F(\rho,B)$ from $z = 0$ downward, the solution is $\rho = \rho(z)$, $p = p(z)$. Therefore, $\partial p/\partial s \equiv 0$, and $v_n \equiv w \equiv 0$ on $y = y_n(x)$ interface.

Q.E.D.

Remarks: This theorem can apply to both the northern and southern boundaries.

One notices that if lines $\rho_s = const.$ cross the line $y = y_n(x)$ (where $w_e = 0$), there possibly is a baroclinic mode of water mass exchange across

this interface. Consequently, we have to specify ρ_s and p_s on these boundaries.

In passing, we see that the ventilated thermocline model of Luyten, Pedlosky and Stommel belongs to this special case with ρ_s = const. on both the northern and southern boundaries. According to our Theorem II, there is no water mass exchange across both the northern and the southern boundaries. As a result, a single-gyre model for the subtropical basin circulation can be studied.

6. The Existence of the Unventilated Thermocline and
the Determination of the Potential Vorticity

We will first define the term "unventilated". By an unventilated layer we mean that a layer is not Ekman-ventilated, i.e., not directly exposed to the air-sea interaction in the interior ocean. This definition implies the possibility of this layer being exposed to air-sea interaction in the western boundary current. Rhines and Young (1983) pose a model with closed streamlines, so that the weak vertical turbulent forces drive a circulation within the unventilated thermocline. However, the deep thermocline can also be ventilated by the strong western boundary current.

How deep the wind-driven circulation is and how a fluid below the directly wind-driven surface layer is set into motion have been very difficult problems in thermocline theory. In an ideal fluid thermocline model, as discussed in the LPS model, the upper part of the thermocline is driven by the wind. Therefore, the existence of subsurface motion can be explained if these water particles trace back to an outcropping region. However, there are other possible sources for the subsurface motion.

Let us consider a layer model of a stratified ocean. If there were no wind forcing, every layer would be level and potential vorticity isopleths in each layer would be parallel to the latitudinal circles. The whole ocean would be stagnant. If there is a weak wind forcing, the upper layer will be driven by the direct wind forcing. The interface between the first layer and the second layer will be deformed. Thus, the potential vorticity isopleths in the second layer will be slightly deformed, but all of them still meet the eastern wall,

making fluid motion impossible within this layer (and all layers below). As Rhines and Young (1982) point out, however, when the wind forcing is strong enough, the interface is strongly deformed and some closed potential vorticity isopleths develop within the second layer (or even layers below). Rhines and Young have discussed a model including these closed potential vorticity isopleths. In this model, motion in a deep ocean can only occur in a domain of closed potential vorticity contours within which motion is driven by small vertical friction forcing from the upper layer.

Although observations show fairly homogeneous potential vorticity plateaus in both the North Atlantic Ocean and the North Pacific Ocean (Holland, Keffer and Rhines, 1983), in large regions of these oceans potential vorticity is not uniform. The potential vorticity homogenization theory also has difficulty in coupling with a western boundary current (Ierley and Young, 1983). One, therefore, must try other possible explanations of the unventilated motion. A simple choice is to cut the closed potential vorticity isopleths in half, thus having potential vorticity isopleths coming from and returning to the western boundary current. In other words, when we have a subsurface motion ventilated by the western boundary current, the western boundary current picks up water particles from the southern basin and puts them back into interior circulation in the northern basin. Unknown upwelling/downwelling and diffusive processes within the western boundary current transport potential vorticity and other properties, redistribute them, and feed them back to the interior ocean at the right latitudes and depths.

There is no doubt that subsurface water does move. The problem is whether we can prove the existence of subsurface motion within the theoretical frame

work of the ideal fluid thermocline. Thus, we first discuss the existence of the unventilated thermocline. Afterward, our topic is the determination of the potential vorticity in a basin.

1) The existence of the unventilated thermocline in a subtropical basin.

For simplicity we discuss a special case when the sea surface density is independent of x and the northern boundary of the basin is the a latitudinal circle, $y = y_n$, and $\rho_s = \rho_n$ is constant along this line. Fig. 3-1 shows a north-south section of this case.

Lemma 2.

$w < 0$ on the interface $\rho = \rho_n$ (except on the sea surface).

Proof:

Using (4.2), at section A-A the v-velocity on the sea surface is

$$v_s = -w_e \rho_z / \rho_y \tag{6.1}$$

From the Sverdrup relation

$$\beta v = f(w_e - w)/h \tag{6.2}$$

where w is the vertical velocity on the interface $\rho = \rho_n$, v is the vertically averaged meridional velocity, and $v = v_s$ approximately.

By definition

$$h = -L\rho_y / \rho_z \tag{6.3}$$

Combining (6.1; 6.2; 6.3), one obtains

$$w = (1 - \beta L/f)w_e \tag{6.4}$$

or

$$w = (1 - L/R)w_e \tag{6.5}$$

where R is the Eath's radius.

Therefore, $w \sim w_e < 0$ for a subtropical gyre.

Q.E.D.

Fig. 3-1. A meridional section showing the density field
in the vicinity of a isopycnal outcropping line.

This lemma means that south of the ZWCL, a w = constant interface slopes down faster than a ρ = constant interface on a large scale.

Clearly, v and w are non-zero on the interface $\rho = \rho_n$. By our basic assumption, there is no density discontinuity within the whole ocean. Thus, from the thermal wind relation the water below the $\rho = \rho_n$ interface should move as well.

Recalling our assumption that ρ_s = const. on the northern boundary, $y = y_n$, and using Theorem II, one concludes that there is no water mass exchange across the northern boundary. Because the water particles below the $\rho = \rho_n$ interface have a density greater than ρ_n, they cannot have a source on the upper surface. Therefore, this subsurface current must have its source in the western boundary current. (The amount of deep water ventilated by the eastern boundary current is very small because there is no evidence of an eastern boundary current that can support a net meridional mass flux.) In summary, we have the following theorem.

Theorem III.

If the sea-surface density is constant along the ZWCL (which is the northern boundary of a subtropical gyre), and if $F(\rho,B)$ is a single-valued function, there is a unventilated thermocline below the directly wind-driven surface layer in a subtropical basin. The flow in this unventilated thermocline has its source in the western boundary current.

2) Ventilation in a subpolar gyre.

With all previous layer model (Veronis, 1973; LPS, 1983; Pedlosky and Young, 1983; and Chapter I and II of this thesis) the assumption has been used that in a subpolar gyre layers beneath the upmost layer are motionless (except

below narrow boundary current). This assumption makes these models simple enough to be worked out analytically. There is another possible assumption, however, that the lower layers are in motion before they outcrop (LPS mentioned this possibility, but did not give a real example). Although the assumption of single moving layer can be useful for layer model, a model with continuously stratification needs slightly different assumptions. In fact, it seems reasonable to assume that water particles below the upper surface are in motion even before they outcrop.

In this case the western boundary current sets up the potential vorticity field within these subsurface layers. The sole function of the ventilated and unventilated thermoclines in the subpolar gyre is to send water particles in these layers to the interior circulation. Some of these water particles outcrop in the interior, others move along a cyclonic path and return to the western boundary in the northern basin.

As can be seen from the concrete examples in the next section, the present model gives more similar circulation patterns for the subpolar and subtropical gyres than these layer models.

3) How deep is the total thermocline.

There have been several estimates of the thermocline depth (Welander, 1971b; Pedlosky, 1983a). One can make another simple estimate by using the present model.

Assuming $w = 0$ at depth $z = -H$ where $\rho = \rho_b$, one has

$$H = fw_e/\beta v_s \tag{6.6}$$

Combining (6. 6) and (6. 1) gives

$$H = -f\rho_y/\beta\rho_z \sim -R\rho_y/\rho_z \tag{6.7}$$

For the subtropical ocean the typical values are $\rho_y \sim 10^{-3}/2000km$, $\rho_z \sim 50 \cdot 10^{-9}/cm$, thus $H \sim 600$ meters.

At section A-A (Fig. 3-1) the ventilated thermocline depth is $h = -L\rho_y/\rho_z$. Introducing a ventilation ratio $v_r = h/H$, one obtains $v_r = L/R$. Therefore, for a subtropical gyre the overall ventilation ratio is

$$V_r = L_y/R \qquad\qquad (6.8)$$

Rhines (1983) first introduced a recirculation index $R_c = R/L_y = 1/V_r$ from a different point of view. According to our definition V_r is the ratio of the ventilated thermocline depth to the total thermocline depth for the entire basin. Obviously, $(1-V_r)$ also represents that portion of water which is recirculated within the unventilated thermocline and the western boundary current. For both the North Atlantic Ocean and the North Pacific Ocean, V_r is the order of $0.3 \sim 0.5$, which means that there are big unventilated water pools in both these two oceans. The water in these pools has its source in the western boundary currents or the subpolar gyres.

4) How the potential vorticity field is determined within a basin.

In the previous section we suggested a way to solve the ideal fluid thermocline for a entire basin by giving the functional form of $F(\rho,B)$ as an input data. There has been no conventional way of finding $F(\rho,B)$ from oceanic measurements. Even if we had a way of getting ρ_z on the entire sea surface, we still would face the difficulty of not knowing the ρ_z distribution on all lateral boundaries. The way we propose to solve this problem is rather ad-hoc. After all, a question remains whether it is possible to find the q-field for at least part of the ocean without solving the entire circulation problem.

At first glimpse, the LPS model seems able to determine the q-field fairly easily without solving the whole basin circulation. However, as we examine the LPS model in detail, this first impression turns out to be untrue.

Since the LPS model appeared, an important question has been how to transit from the layer model to a continuous model. A simple choice would be to divide the surface into more and more layers. Although it becomes more and more tedious to derive the corresponding equations, it can, in principle, be done. However, dividing the surface into more layers does little help in understanding the structure of the deep thermocline. The real problem is in the first moving layer near the northern boundary. Luyten et al. wisely chose to start the model there with a constant depth H_0 and assume that there is no water mass exchange across the ZWCL. Our Theorem II proves that their assumptions are consistent. Next, they assume that $w = 0$ on and below a constant density interface $\rho = \rho_b$. This assumption has never been proved as far as the author knows.

Let us examine section A-A in Fig. 3-1. There are two layers: the upper ventilated layer, in which the water all comes from the mixed layer, and the unventilated layer below. As discussed in great detail in the LPS model, if we treat these two layers as a vertically averaged single layer, for given H_0 the flow field at section A-A can be determined completely. However, as shown above, water mass within the unventilated thermocline on section A-A comes from the western boundary current. Thus, the q-field within the whole unventilated thermocline is unknown before solving the entire circulation. Without knowing the q-field in the second layer, solving the problem of the flow field is impossible.

Pedlosky and Young (1983) improve the LPS model by combining it with Rhines and Young's unventilated thermocline model. They propose to divide the unventilated thermocline into many layers each of which has a homogenized potential vorticity. Such a multi-layer model can be solved in principle, though the calculations are tedious.

Noting that layer thickness and potential vorticity have to be specified for each unventilated layer in Pedlosky and Young's model, it is easy to explain why potential vorticity functional relationship must be specified in a continuously stratified model. Between the directly ventilated and the unventilated thermocline with potential vorticity homogenized layers in real oceans, furthermore, there are transition zones where the potential vorticity is not homogenized. Even within the lower part of the thermocline there may be weak potential vorticity gradients; the deep oceans are not completely homogenized. The basic gyre-scale potential vorticity field is potentially unstable and there are meso-scale eddies moving around. Thus, our model chooses to specify a q-field that depends on both ρ and B, though there is a fairly low gradient potential vorticity pool in the middle of the so-called mode water region.

Classifying the ideal fluid thermocline equation as a non-strict hyperbolic system (see Addendum) also raises hopes that, if by some method we can find the q-field on part of the sea surface, we can find part of the solution by simply tracing streamlines along which the density, potential vorticity and Bernoulli function are conserved. Although this kind of standard characteristic approach might be valid for a time-dependent thermocline problem, the equation for steady ideal fluid thermocline has exceptional

properties. First, it has a triple characteristic that goes vertically and has
an unknown role in boundary value problems. Second, the single characteristic
is reversible. Thus, instead of getting q-field information from local
dynamics on the base of the mixed layer (assuming we can do this), we should
be equally able to find the q-field within the western boundary current and
let the information return to the mixed layer along the streamlines in the
ventilated thermocline. Certainly, it is still not a well-understood approach.

As discussed in Addendum, the functional form of $F(\rho,B)$ includes
information about the boundary conditions. There is no conventional way to
find the actual form of $F(\rho,B)$ for part of the domain without solving the
entire boundary value problem.

In summary, the q-field is a quality of the entire circulation balance. To
find the q-field one has to include the western boundary current and other
boundary currents. Giving a q-field is equivalent to giving the whole
solution. There seems no way of finding the q-field for some part of the
circulation by local dynamics.

7. Calculated Results

Before going into the details of numerical examples, let us examine the general criteria for the function $F(\rho, B)$ in order to fit the realistic oceanic data. First, we discuss the simplest form of $F = a\rho + bB + c$. A very natural choice is Welander's solution: $a < 0$ and $b < 0$. However, as pointed out in section 3, this kind of functional forms gives unpleasant feature: all isopycnal surfaces are deeper on the eastern side. This trouble comes from the negative sign of $\partial F/\partial B$. For simplicity, we assume $\rho_s = \rho_s(y)$. From (4.6b) ρ_s decreases eastward in a subtropical gyre. By definition, $B = \rho_s$ on the sea surface, so that B decreases eastward on the sea surface. Let us look at a longitudinal section. On the sea surface ρ is constant. Therefore, to have isopycnals slope westward. ρ_z should be smaller in the western basin than in the western basin. Hence, $\partial F/\partial B$ should be positive, meaning F is an increasing function of B. The simplest choice is

$$F(\rho, B) = a\rho + b(B_0 - B) \qquad \text{with} \quad a, b < 0 \tag{7.1}$$

However, a close examination of this functional form reveals that the solution blows up in the deep ocean because $|\rho_z|$ is unbounded. Thus, to find a nice-looking solution we have to match this solution to another solution. Actually, a typical vertical density profile in the subtropical oceans has a high gradient region near the sea surface -- the seasonal thermocline; a low gradient region below -- the mode water; a high gradient region again -- the permanent thermocline; and the almost homogeneous deep ocean near the bottom. Any successful model should take these regions into account.

Obviously, to find a solution that fits the observed oceans better, one has to include more parameters. Here, we try to emphasize that even a fairly simple functional form of $F(\rho, B)$ can give a picture very similar to observations. However, the actual form of F in a basin must be very complicated; the solutions here are not the exact flows in the real oceans.

1) Subtropical gyre.

Assuming a subtropical gyre from $20°N$ to $50°N$, we have

$f_0 = 0.0000837$ /sec, $\beta = 1.875 \cdot 10^{-11}$ /sec/m

and

$L_x = 6000$ km, $L_y = \pi R/6 \sim 3300$ km.

The surface density is the same as in the LPS model

$$\rho_s = 1.026 + .001y \qquad (7.2)$$

The Ekman pumping velocity is assumed to be x-independent

$$w_e = -.0001 \sin(\pi y) \text{ cm/sec} \qquad (7.3)$$

The sea surface pressure on the western or the eastern wall is given as a boundary value to start the integrating. As discussed above, there is no definite direction for the characteristic of the equation, so we can start from either the western or the eastern boundary. To compare with the LPS model, we choose to begin at the eastern boundary.

The u-velocity on the eastern boundary is generally fairly small. Thus we choose

$$p_s(1,y) \equiv 0 \qquad (7.4)$$

This boundary value guarantees that u is identically zero on the eastern boundary surface line. Vertically, we choose three different regions where the function $F(\rho, B)$ has different forms:

133

a) The buffer layer between the mixed layer and the mode water.

$$F(\rho, B) = -a_1(\rho-\rho_1)-b_1(B_1-B) \qquad \text{for } 1.026 < \rho < 1.027 \qquad (7.5)$$

b) The mode water layer.

$$F(\rho, B) = -a_2\rho-b_2(B_2-B)+b_3(B_3-B)(B_4+B) \text{ for } 1.027<\rho<1.028 \qquad (7.6)$$

c) The abyssal water.

$$F(\rho, B) = -a_3(1.0285-\rho) \qquad \text{for } 1.028 < \rho < 1.0285 \qquad (7.7)$$

Using ρ in units of g/cm^3 and B in units of m^2/s^2, the corresponding parameters are

$a_1 = 3.6 \cdot 10^{-7}$; $a_2 = 5 \cdot 10^{-11}$, $a_3 = -2 \cdot 10^{-6}$

$b_1 = 4.5 \cdot 10^{-11}$; $b_2 = 4 \cdot 10^{-11}$; $b_3 = 1.8 \cdot 10^{-12}$

$\rho_1 = 1.0265$

$B_1 = 9.4$; $B_2 = B_3 = 7$; $B_4 = 13$.

These functions are matched through smooth transitional regions:

$F = F_1$ for $1.0260 < \rho < 1.0270$

$F = dF_1+(1-d)F_2$ for $1.0270 < \rho < 1.0275$

     where $d = ((1.0275-\rho)/.0005)^3$

$F = F_2$ for $1.0275 < \rho < 1.0280$

$F = dF_2+(1-d)F_3$ for $1.0280 < \rho < 1.0285$

     where $d = ((1.0285-\rho)/.0005))^3$

Fig. 3-2 shows the functional relationship between F and ρ for B = -5, 0, 5 m^2/sec^2. The buffer layer basically represents the upper-layer structure. Therefore, the corresponding parameters determine how big the horizontal velocity is and hence the depth of the wind-driven gyre. The mode-water layer is the main body of the subtropical gyre. Within this layer the vertical density gradients are small, which means a low-potential
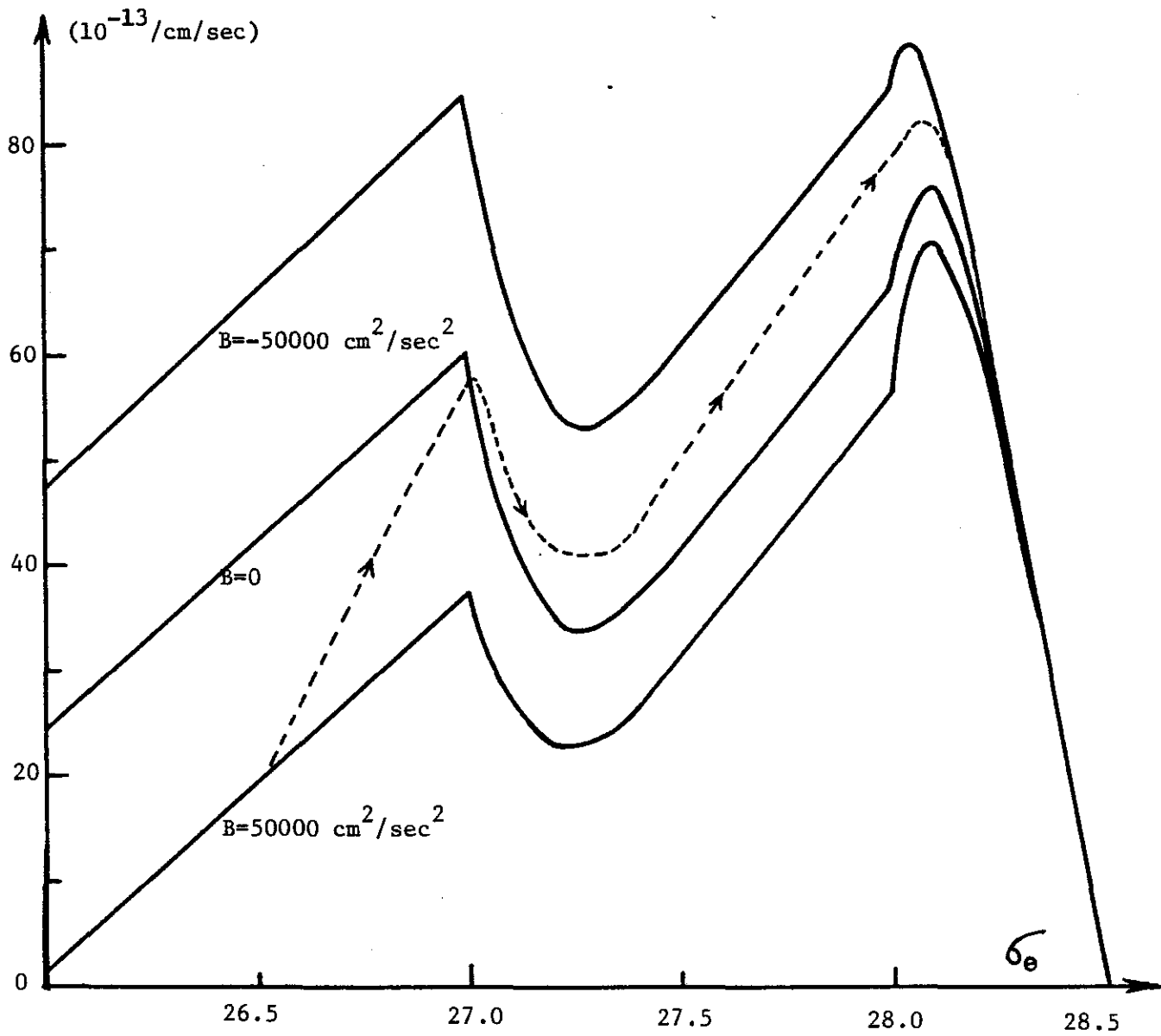
Fig. 3-2. Function $F(\rho, B)$ profiles for $B = -50000$, 0, 50000 cm^2/sec^2.
Broken line represents the potential vorticity change along a
vertical line (schematically).

vorticity pool. In principle we could try solution with homogenized potential vorticity; however, the solution here has a small potential vorticity gradient on middle-depth potential density surface. This gives slight differences between the Rhines - Young, Pedlosky - Young, and the present model. The transitional region between the mode water and the abyssal layer is the main thermocline. A dashed line in Fig. 3-2 represents the change of potential vorticity along a vertical line. Because the Bernoulli function decreases downward, this dashed line crosses constant-B lines in this figure. In the abyssal layer potential vorticity is uniform.

Here, we should emphasize that it is essential to have these three zones, the buffer layer, the mode water layer, and the abyssal water. The mode water region appears as a deep valley in the potential vorticity graph. The peaks on both sides of the valley are the seasonal thermocline and the permanent thermocline. The smoothing regions make all property profiles smooth and help to avoid unnecessary complications connected with matching solutions of quite different properties. The smooth steps used here are merely convenient rather than essential.

Fig. 3-3 shows the horizontal velocity field on the upper surface (the base of the mixed layer). As the eastern boundary condition requires, $u \equiv 0$ along the eastern boundary (a single line on the upper surface). This figure is a typical anticyclonic gyre with $u_{max} = 10 cm/sec$ and $|v|_{max} = 1.68 cm/sec$. Therefore, $u/v = 6$; unlike a simple scale analysis, this ratio is three times the geometrical aspect ratio $L_x/L_y = 1.8$.

Fig. 3-4 shows three meridional sections. From Fig. 3-4(a,c), one can see the density profile with a typical thermocline structure in a subtropical
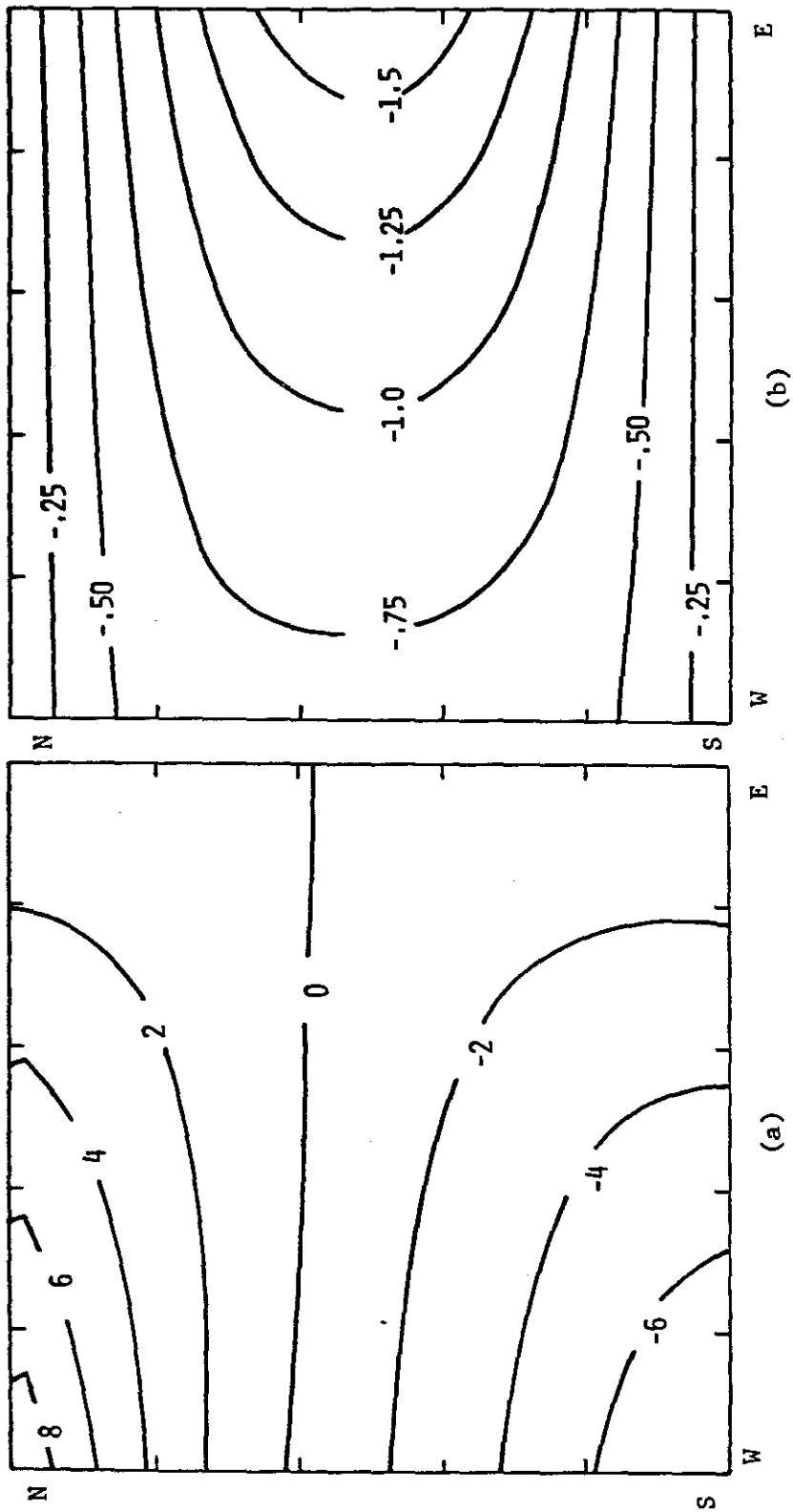
Fig. 3-3. Horizontal velocity on the upper surface of a subtropical gyre.
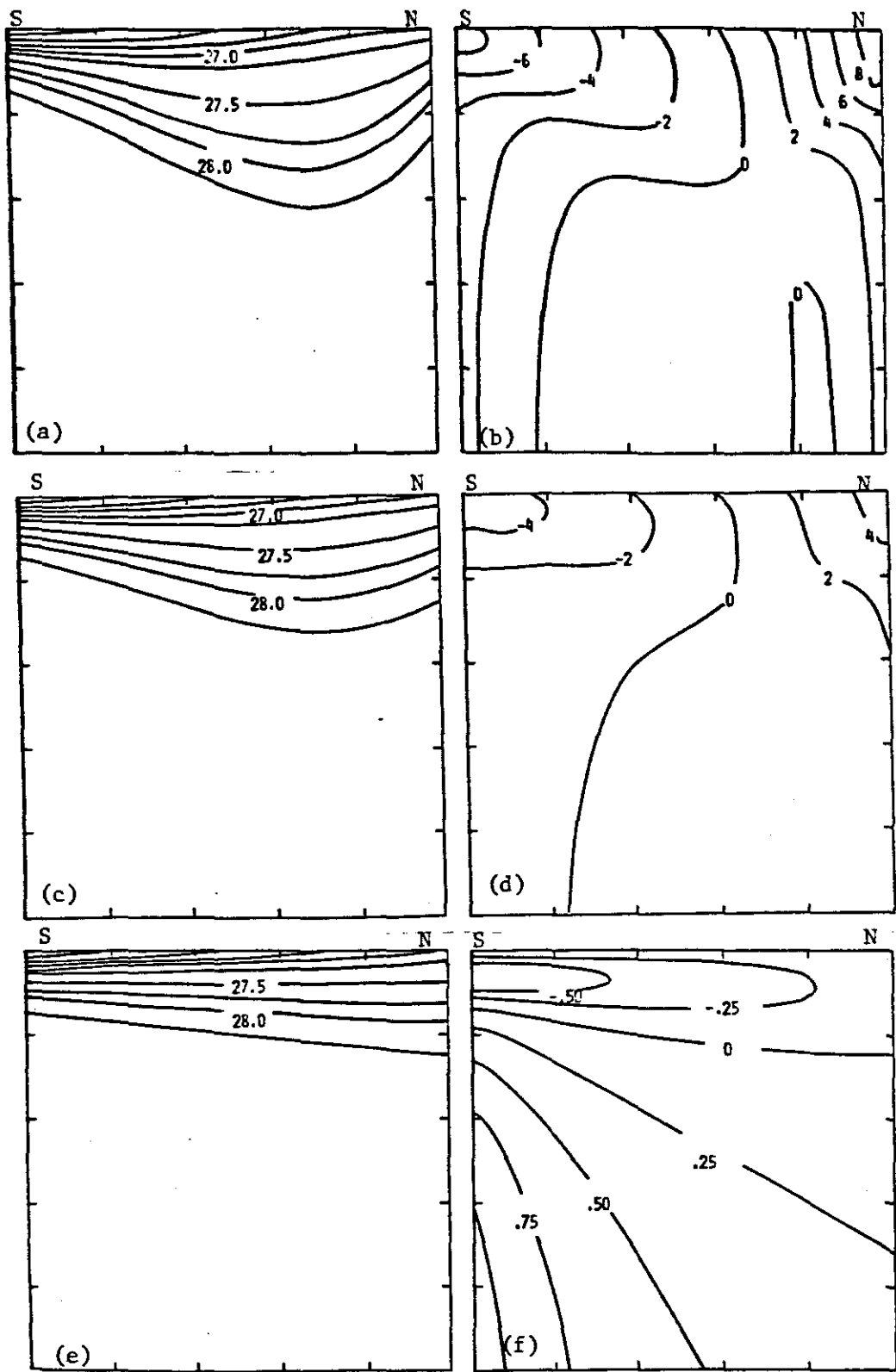a) u-velocity; b) v-velocity (in units of cm/sec).

135 - a

Fig. 3-4. Meridional sections of a subtropical gyre (H=3km).

a, c, e) Density profile at x=0, 0.5, 1.0 (sigma theta).

b, d, f) u-velocity profile at x=0, 0.5, 1.0 (in units of cm/sec).

gyre: a buffer layer on the top with the seasonal thermocline, a mode water layer with its thermostat and the main thermocline underneath the mode water. Below the main thermocline, density is almost homogeneous everywhere. From Fig. 3-4(b,d), one sees that the u-velocity is less than 2cm/sec below the main thermocline, except in a small region below the northern/southern boundaries. In principle, if we include more parameters in (7.5,6,7), we can find a better solution with the u-velocity nearly zero almost everywhere below the main thermocline. Therefore, as one can see from the thermal wind relation, the thermocline is the layer where the largest vertical velocity shear is located. Above the main thermocline the horizontal velocity is fairly barotropic. This result confirms the basic picture from a two-layer model with the main thermocline as the interface. Of course, the three dimensional picture here has a much richer structure.

Fig. 3-4(e,f) shows the structure on the eastern wall. For the parameters we choose, the density surface $\rho = 1.0275$ levels off and below this interface density surfaces tilt down northward. Because $p_s = 0$ on the upper surface, u < 0 within the top 600 meters and $-|u|_{max} = -.7cm/sec$. Below the first 600 meters, u becomes positive. Thus the vertical integrated longitudinal mass flux is near zero. If we add an eastern boundary current which allows upwelling to return the eastward mass flux in the lower layer to the westward mass flux in the shallow layer, the $u \equiv 0$ condition can be satisfied on the real eastern wall. However, as we will see below, our solution is valid only for the upper part of the ocean (depth < 300m on the eastern wall). This leaves the eastern boundary condition slightly uncertain.

Our model gives a continuous field near the eastern wall. However, the ideal fluid thermocline equation cannot describe the flow within this narrow eastern boundary current. To build a closed model, there should be an eastern boundary current to transport the necessary water mass. Within this eastern boundary current the upwelling/downwelling and diffusion are important. Of course, different eastern boundary currents can return the flow at different levels and reshape the interior potential vorticity field. Therefore, the interior thermocline and current structure depend on the eastern boundary current structure.

From observations in both the North Atlantic Ocean and the North Pacific Ocean, local wind forces an upwelling near the eastern boundary. By choosing a small eastward flow at the eastern boundary on the upper surface (just below the Ekman layer), our model can easily simulate this case. However, the interior thermocline structure will remain basically the same.

Fig. 3-5 shows two longitudinal sections. The isopycnals slope westward. Fig. 3-5(c, d) shows the velocity profiles. The wind-driven circulation should end somewhere around $w = 0$ (actually, the w-velocity becomes as big as $3 \cdot 10^{-4}$ cm/sec, though the number was not shown in these figures, in the eastern abyssal layer). Compared with Fig. 3-4(b,d), the $w = 0$ interface here is near the base of the main thermocline where the horizontal velocity is less than 2cm/sec. Below this domain, density is almost homogenized and water moves very slowly. This is the region of the thermohaline circulation where the horizontal and vertical diffusion terms might become important. The boundary between the ideal fluid thermocline and the diffusive thermohaline is not well defined. Considering that the upwelling velocity through the main thermocline
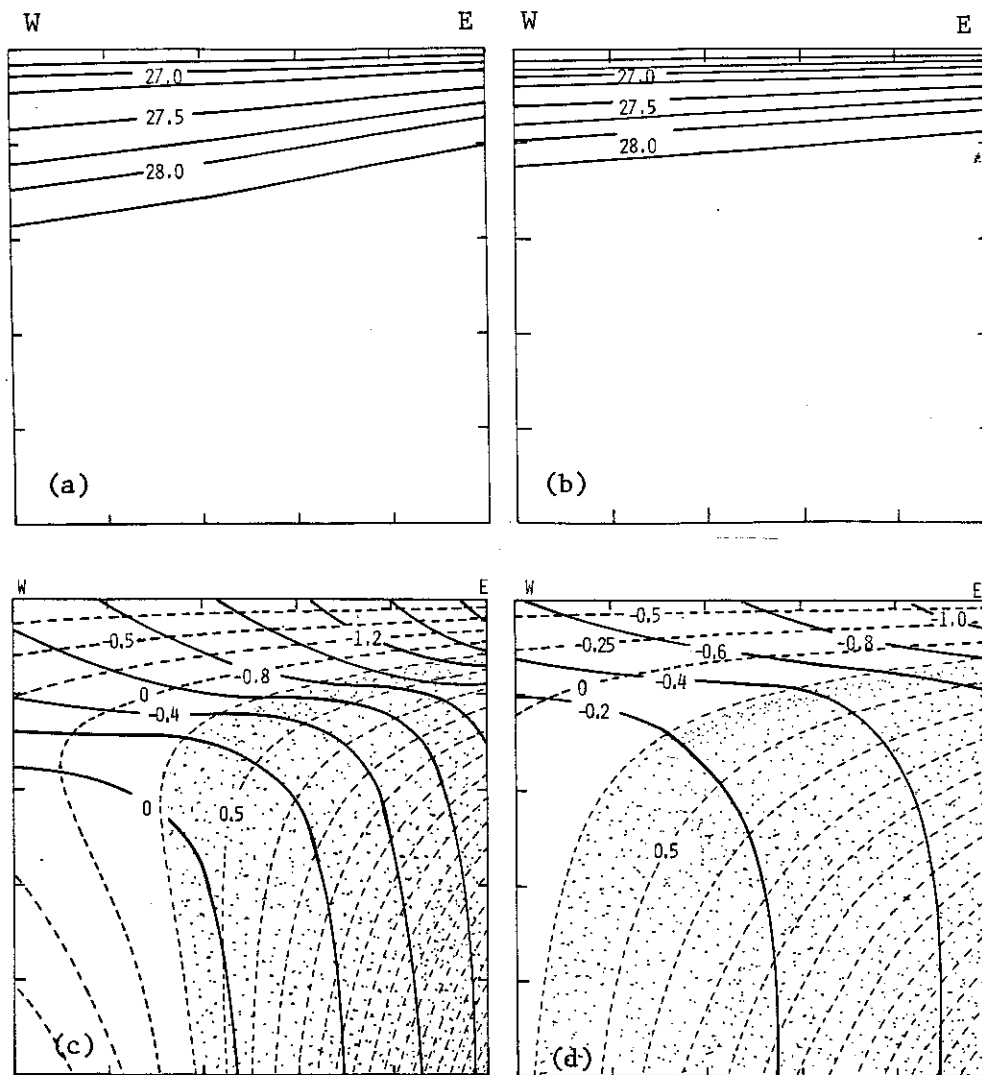
137

Fig. 3-5. Longitudinal sections of a subtropical gyre (H = 3km).

    a, b) Density profiles at sections y = 0.5, 0.25 (sigma theta).

    c, d) Velocity profiles at sections y = 0.5, 0.25.

            v-velocity contours (heavy line) in units of cm/sec;

            w-velocity contours (dashed line) in units of 0.0001 cm/sec and

            at intervals of 0.000025 cm/sec. w > 0.000025 cm/sec in stippled

            regions where the validity of the model is uncertain.

is only one-tenth of the Ekman pumping velocity, we place this boundary somewhere near w = 0.

Fig. 3-6 shows the flow structure on two density interfaces of the ventilated thermocline, ρ = 1.0264,1.0268. In Fig. 3-6.a) water particles enter the thermocline from the base of the mixed layer and move westward toward the western boundary. Fig. 3-6.c) describes the corresponding case in the northern part of the gyre. Water particles move eastward right after they enter the thermocline, then they move along an anticyclonic path. Fig. 3-6(b,d) shows the corresponding layer depths of these two density interfaces. The structure here is similar to the solution in the LPS model.

Fig. 3-7 shows two deep layers ρ = 1.0275, 1.028. Fig. 3-7(a,c) describes complete particle trajectories; they come out of the western boundary and follow an anticyclonic path until joining the western boundary again on the southern basin. These two levels represent unventilated thermocline regions. The LPS model does not produce this type of picture because it combines the unventilated thermocline and the first moving layer into a single layer. In the original LPS model only a small part of the circulation is ventilated by the western boundary current. This case apparent in Fig. 3-6.c) on the upper part of the western boundary. Our model also differs from Rhines and Young's model because we do not require potential vorticity homogenization. The strong upwelling/downwelling and diffusion within the western boundary current play an important role in setting up the potential vorticity field for the unventilated thermocline. In our model, this effect appears as specification of the potential vorticity on the fluid flowing out of the western boundary current. In this sense, the present model combines these two earlier models to create a more consistent picture.
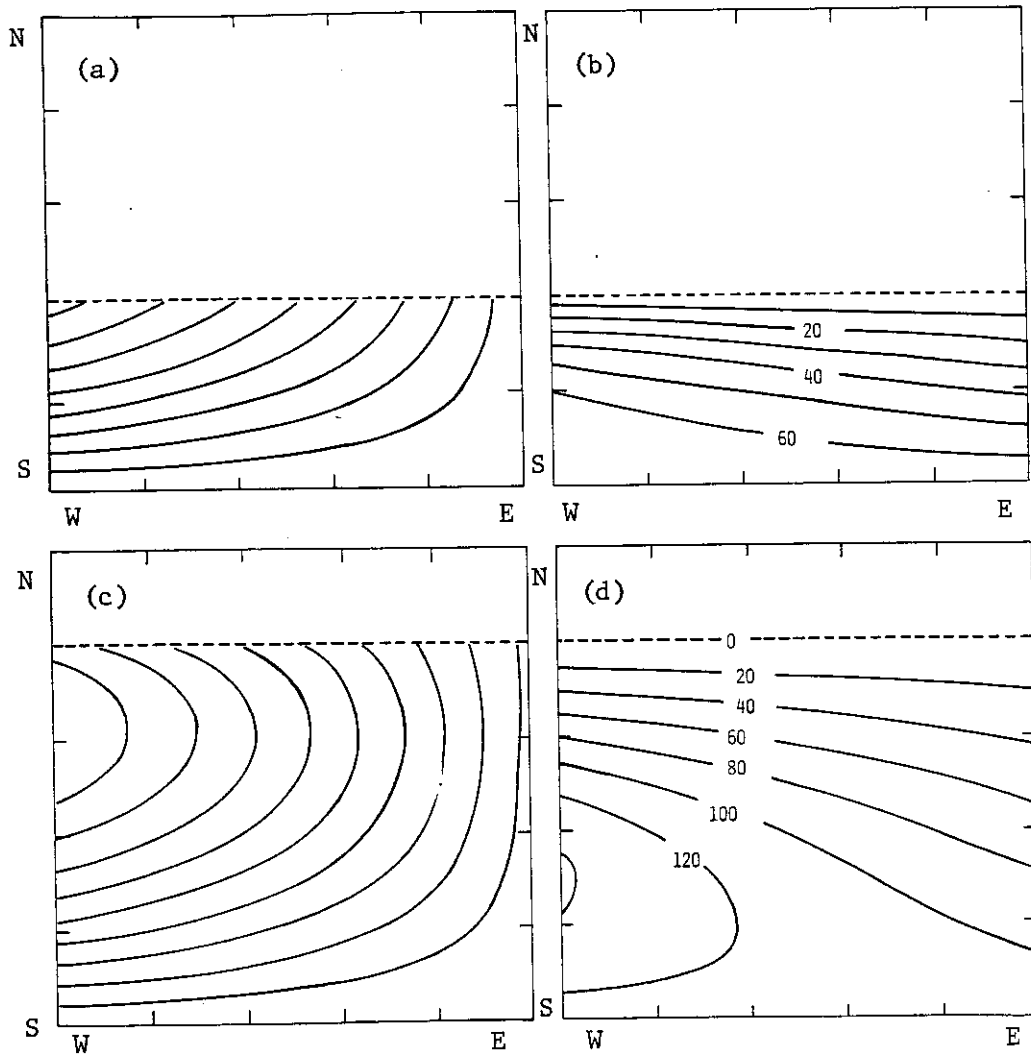
138

Fig. 3-6. Flow patterns on density surfaces σ_θ = 26.4 (a, b); 26.8 (c, d).

    a, c) Bernoulli function contours on σ_θ = 26.4 (a); 26.8 (c).

    b, d) Depth contours on σ_θ = 26.4 (b); 26.8 (d) (in units of meter).
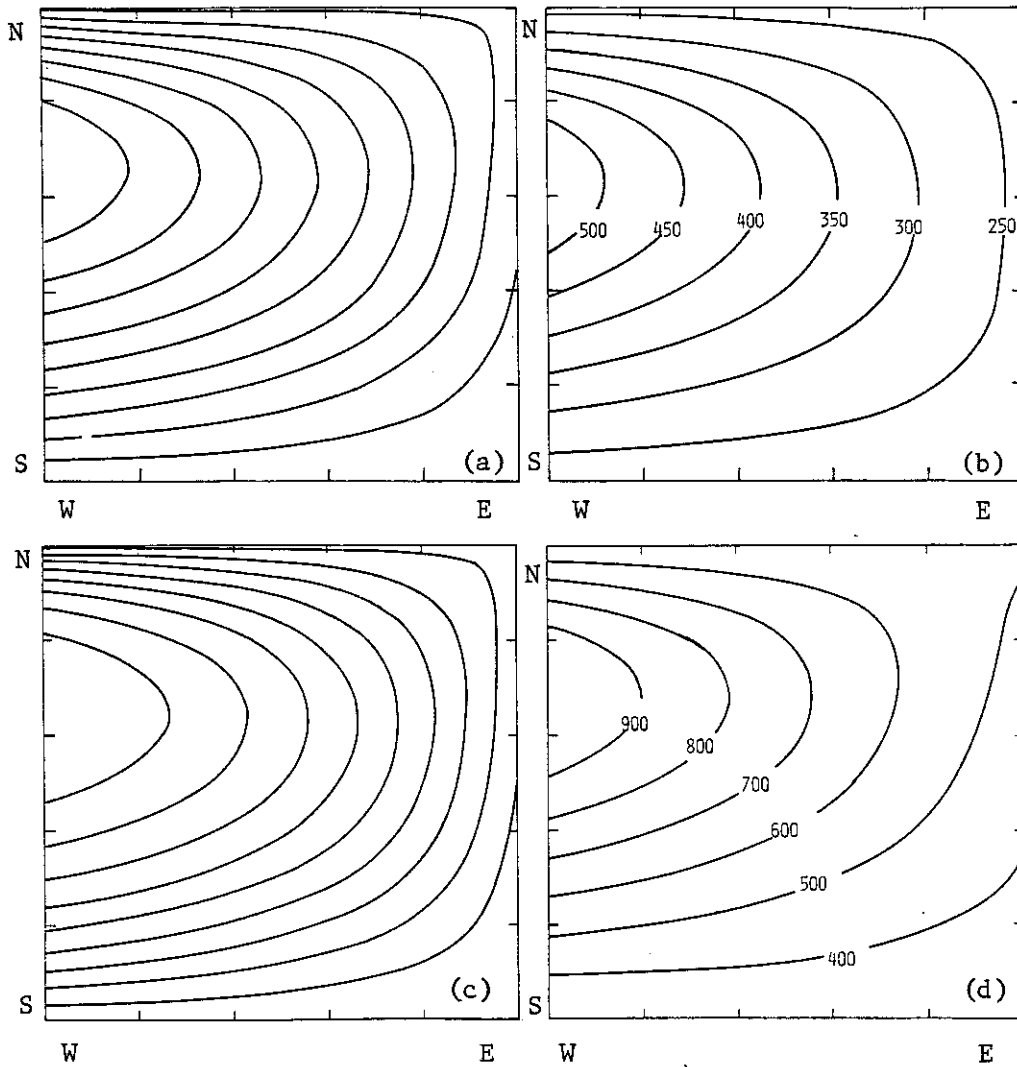
Fig. 3-7. Flow patterns on density surfaces σ_θ = 27.5 (a, b); 28.0 (c, d).

    a, c) Bernoulli function contours on σ_θ = 27.5 (a); 28.0 (c).

    b, d) Depth contours on σ_θ = 27.5 (b); 28.0 (d).

There is no shadow zone in the sense of a stagnant region in the present solution. This is due to the way we treat the eastern boundary current. Both the potential vorticity homogenization theory by Rhines and Young and the ventilated theory by Luyten, Pedlosky and Stommel predict the existence of shadow zone. There is also shadow zone in the generalized Parosns's model. In the real oceans there are large, poorly ventilated regions in the eastern basins. For continuously stratified model it is not clear whether a strict shadow zone can be found. Our present example shows slow ventilation near the eastern wall which is very similar to the numerical simulation by Cox and Bryan (1983).

Fig. 3-6(b,d) and 3-7(b,d) show the depths of these four density surfaces. We can see how the deepest points of these density bowls move northward compared to quasi-geostrophic model (northern intensification).

Fig. 3-8 shows how the horizontal velocity vector rotates vertically. Fig. 3-9 shows two examples of ß-spirals in the southern basin. These ß-spirals have the same structure as those observed by Schott and Stommel (1978). Counter-intuitively, u-velocity increases downward within the upper 300 meters, then it decreases. This phenomenon, which is quite appearent in Schott and Stommel's data, also can be seen from the meridional velocity profiles in Fig. 3-4(b,d). It can be explained by the thermal wind relation

$$u_z = g\rho_y/f > 0 \quad \text{for } \rho_y > 0.$$

Since within the southern basin $u < 0$, $|u|$ increases downward. Within the northern basin $u > 0$, so that $|u|$ decreases downward monotonically.

We have shown all the velocity and density profiles. In addition, we can also look at the potential vorticity field. As we pointed out earlier in this
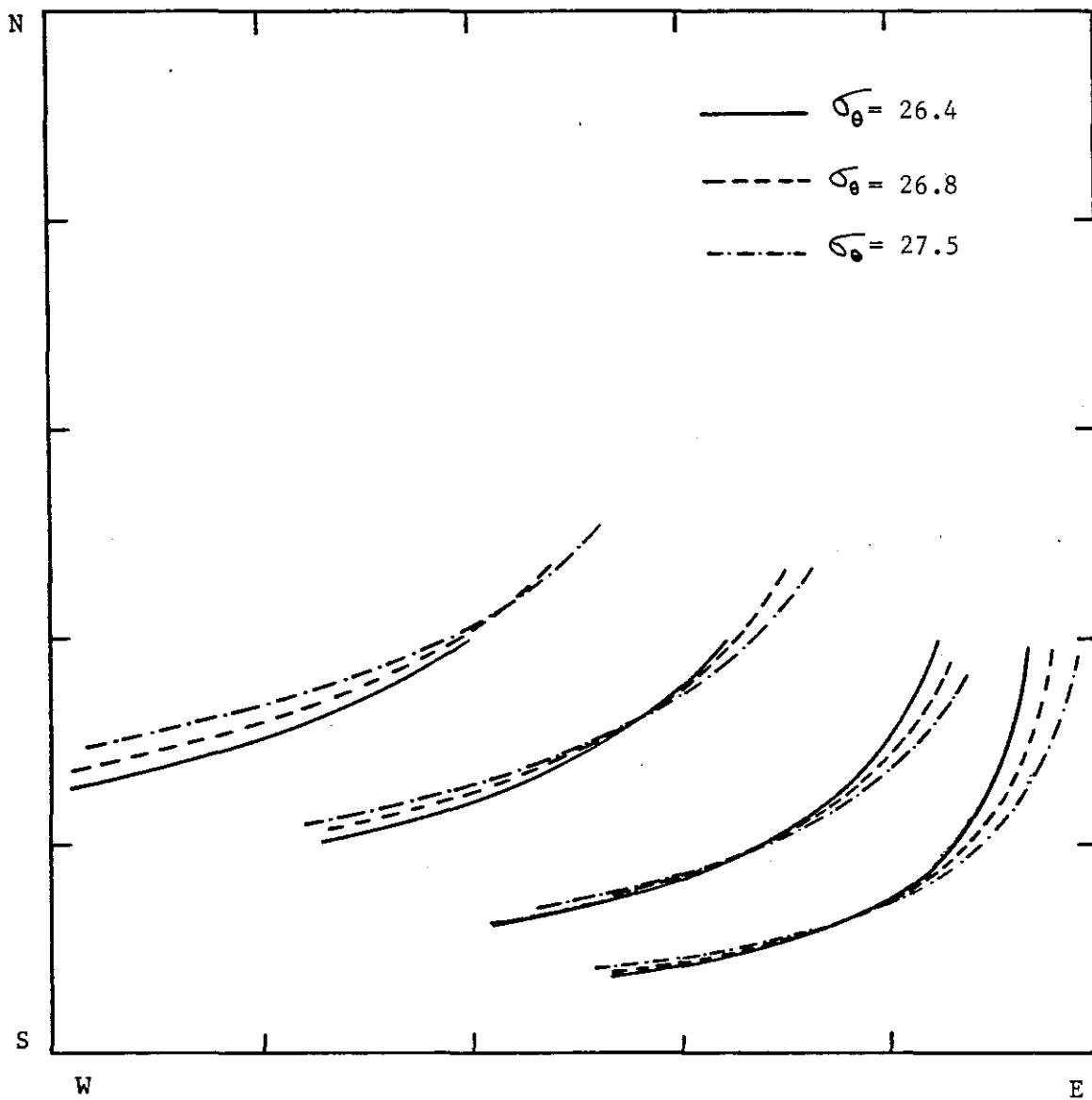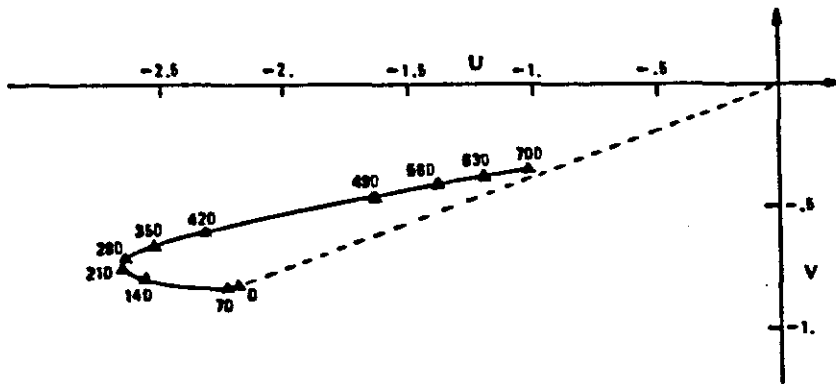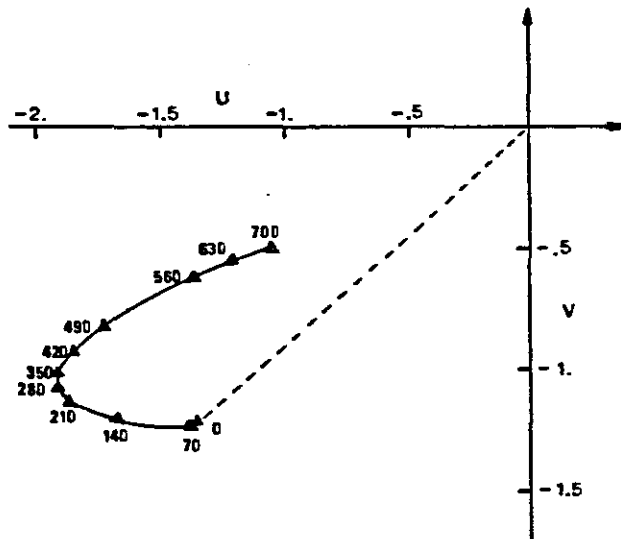
139

Fig. 3-8. Vertical rotation patterns of the horizontal velocity
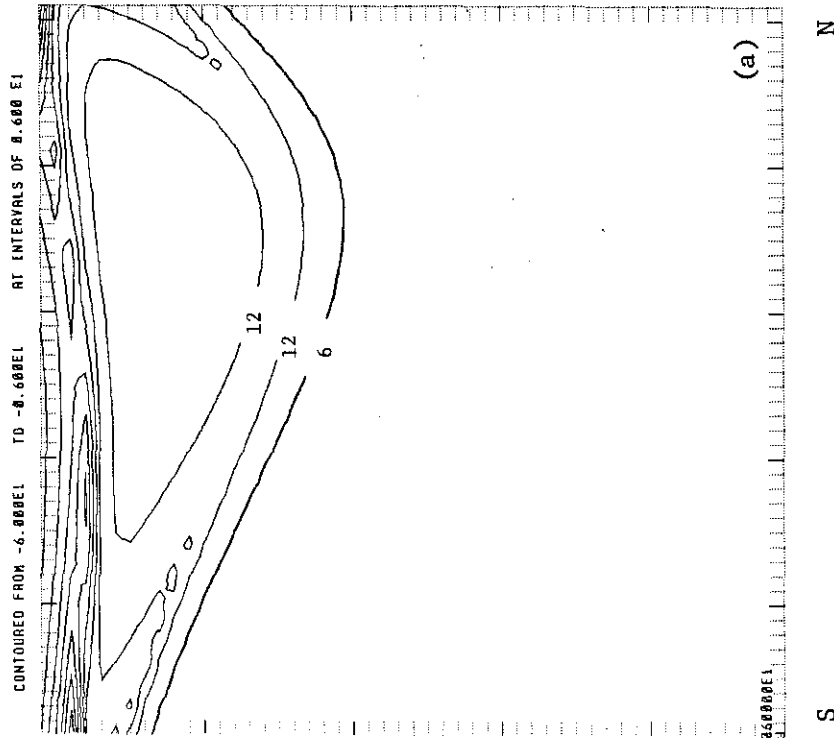vector in the southern basin of a subtropical gyre.

(a)

(b)

Fig. 3-9. Beta-spirals at two places. Numbers on curves are
depths in units of meter, velocity in units of cm/sec.
a) at x=0.72, y=0.20; b) x=0.72, y=0.38.

chapter, there is a slight difference between our numerical examples and Rhines and Young's theoretical model. Fig. 3-10 shows the corresponding potential vorticity profiles along the western boundary and a longitudinal section through the center. The potential vorticity profiles along the western boundary are very similar to the picture calculated from data (Keffer, Rhines and Holland, 1984). There is a bif low potential vorticity plateau in the western side of the subtropical basin. However, in our case the potential vorticity has not completely been homogenized. This feature can be seen more clearly from Fig. 3-11, in which potential vorticity isopleths are shown on two density surfaces. Density surface $\sigma_\theta = 27.5$ corresponds to the middle surface of the mode water region where the theoretically predicted low potential vorticity plateau is located. Obviously, the potential vorticity and its horizontal gradient here are much smaller than on the other density surface $\sigma_\theta = 27.0$. However, the horizontal potential vorticity gradient is not zero and has different signs within the subtropical basin. This means that the corresponding flow field is possibly baroclinically unstable. This is a real difference between the present model nad both Rhines and Young's model, and Pedlosky and Young's model. In these two theoretical models they assume the potential vorticity is totally homogenized in order to make a simple analytical model possible. The potential vorticity homogenization theory depends on a very special form of diffusion and other assumptions. Their models are very idealized. The real oceans, of course, do not behave in such a simple way. The potential vorticity is not completely homogenized. The basin flow field is baroclinically unstable. There are meso-scale eddies moving around the oceans. In a sense, our model gives a more realistic picture by fitting the data with an increasing number of parameters.

POTENTIAL VORTICITY ON Y=.5 SECTION.

POTENTIAL VORTICITY AT X=0 SECTION. (INTERVAL 6*E-11)

CONTOURED FROM -4.000E1   TO -0.600E1   AT INTERVALS OF 0.600 E1

CONTOURED FROM -6.000E1   TO -0.600E1   AT INTERVALS OF 0.600 E1

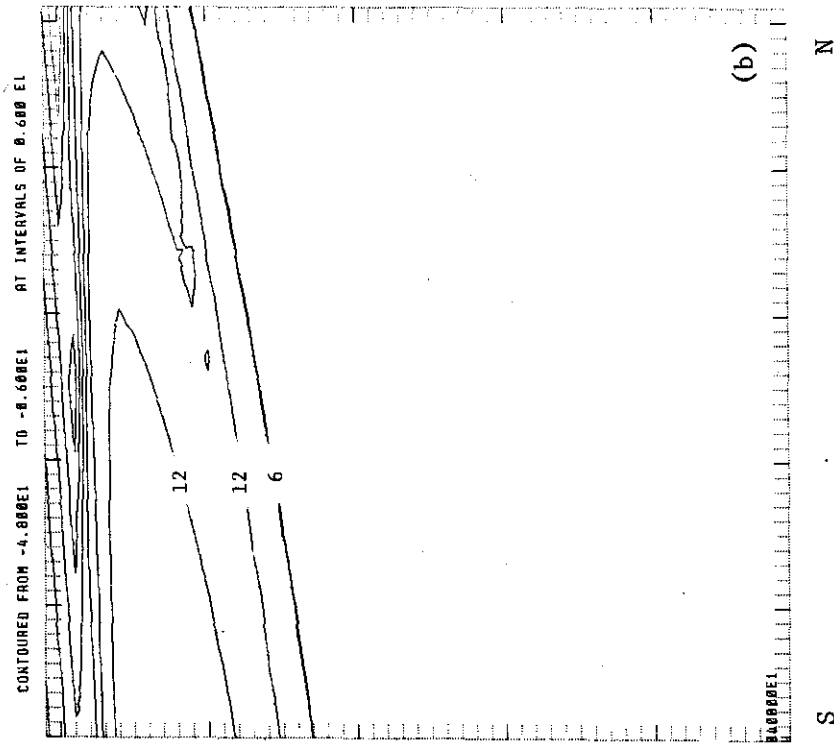Fig. 3-10. Potential vorticity contours (in units of 10^{-13}/cm/sec) at two sections of a subtropical basin model (H = 3km). a) Meridional section along the western wall. b) Longitudinal section through the center. There is a large low-potential-vorticity plateau that resembles the subtropical mode water found in the oceans.
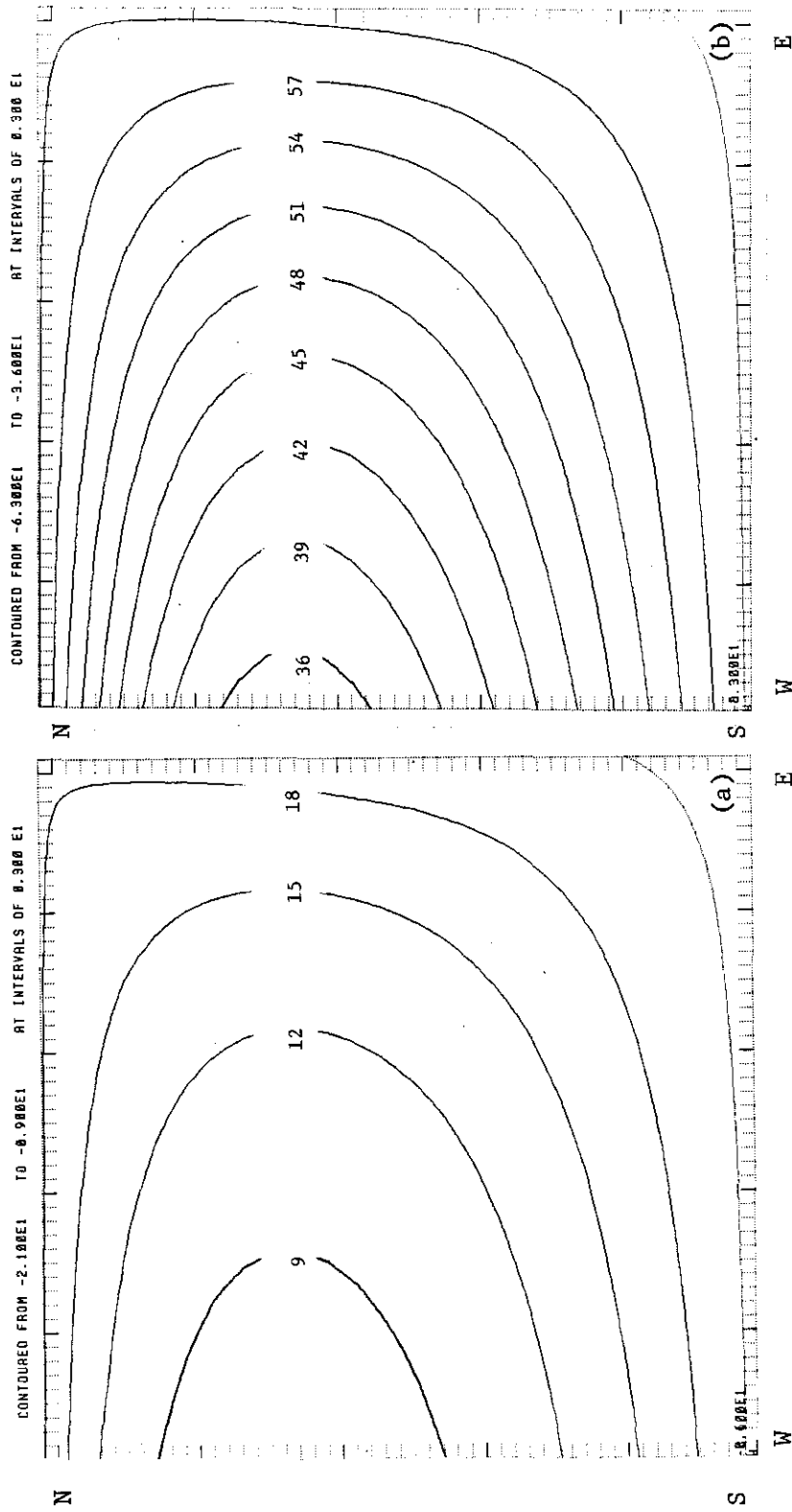
Fig. 3-11. Potential vorticity contours (in units of 10^{-13}/cm/sec) on density surface $\widetilde{\sigma_\theta}= 27.5$ (a) which is at the middle of the subtropical mode water region . The horizontal potential vorticity gradient here is much less than on other density surfaces, such as a shallower one $\widetilde{\sigma_\theta}= 27.0$ (b).

2) Subtropical/subpolar gyres.

Assuming the two-gyre basin covers roughly from 15°N to 75°N, we have

f_o = 0.000103 /sec, β = 1.61•10^{-11} /sec/m

and

L_x = 6000 km, L_y = $\pi R/6$ = 6600 km.

As in the first example, we choose a surface density distribution independent of x

ρ_s = 1.026+0.002y   (7.8)

The Ekman pumping velocity is

w_e = -.0001sin(2πy) cm/sec   (7.9)

For convenience, we impose ρ_s on the western wall and move eastward. The u-velocity on the western wall is a simple sinusoidal form, and the corresponding ρ_s is calculated by integrating the velocity.

The function F(ρ,B) has the same general form as in (65, 66, 67), but the parameters are slightly different.

Fig. 3-12 shows the horizontal velocity on the upper surface. There are two gyres: the anticyclonic subtropical gyre and the cyclonic subpolar gyre.

Fig. 3-13 shows three meridional density and u-velocity profiles. Many features compare well with observations from the North Atlantic Ocean, Fig. 3-14. There is a subtropical gyre with its bowl-shaped thermocline and a huge volume of mode water. The northern basin has a subpolar gyre with its dome-shaped isopycnals. There is isopycnal outcropping within the subpolar gyre.

Because of the strong vertical shear of the horizontal velocity within the subtropical gyre, there is not much flow below the main thermocline. In the
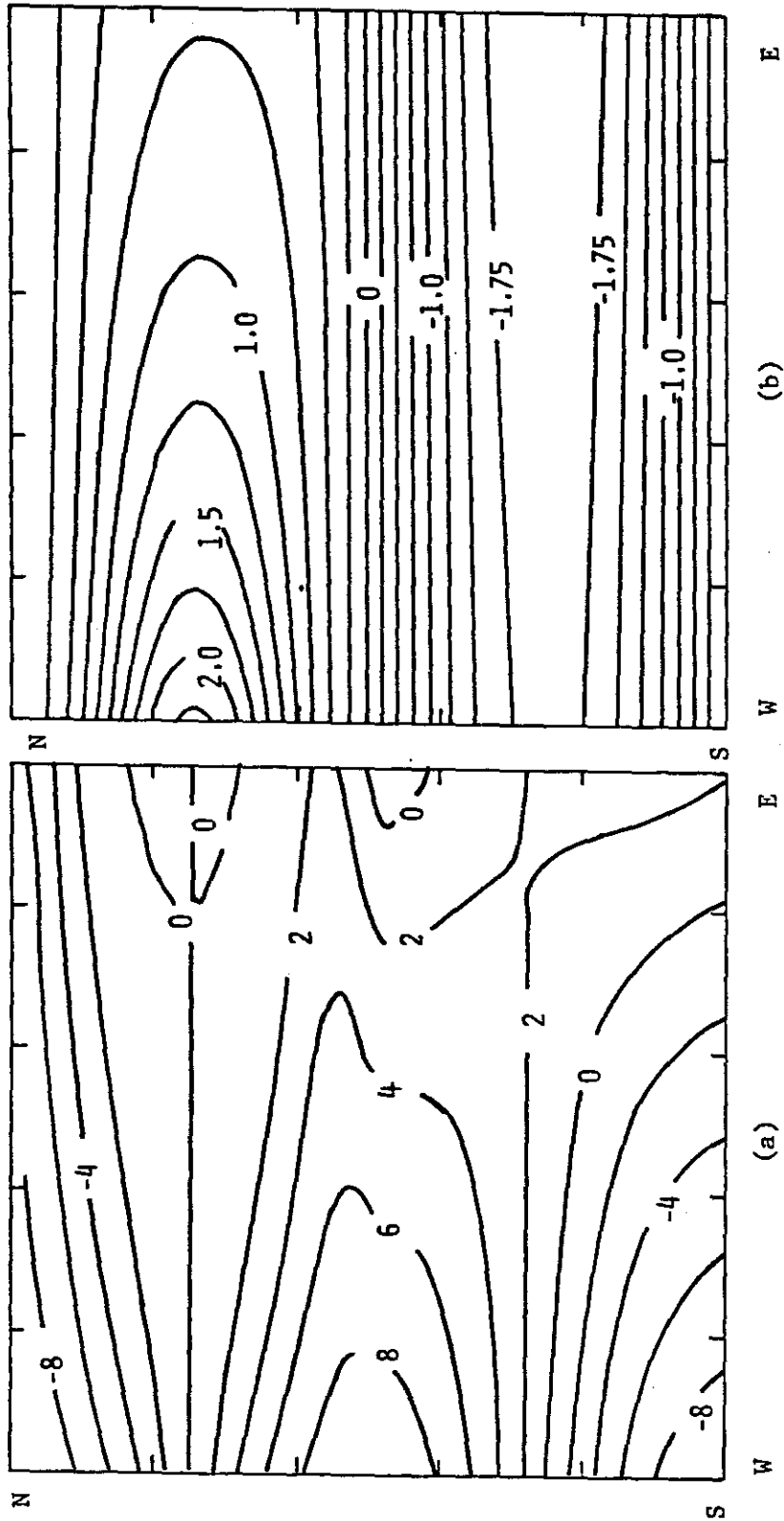
Fig. 3-12. Horizontal velocity on the upper surface of a subtropical/subpolar gyre. a) u-velocity; b) v-velocity (in units of cm/sec).
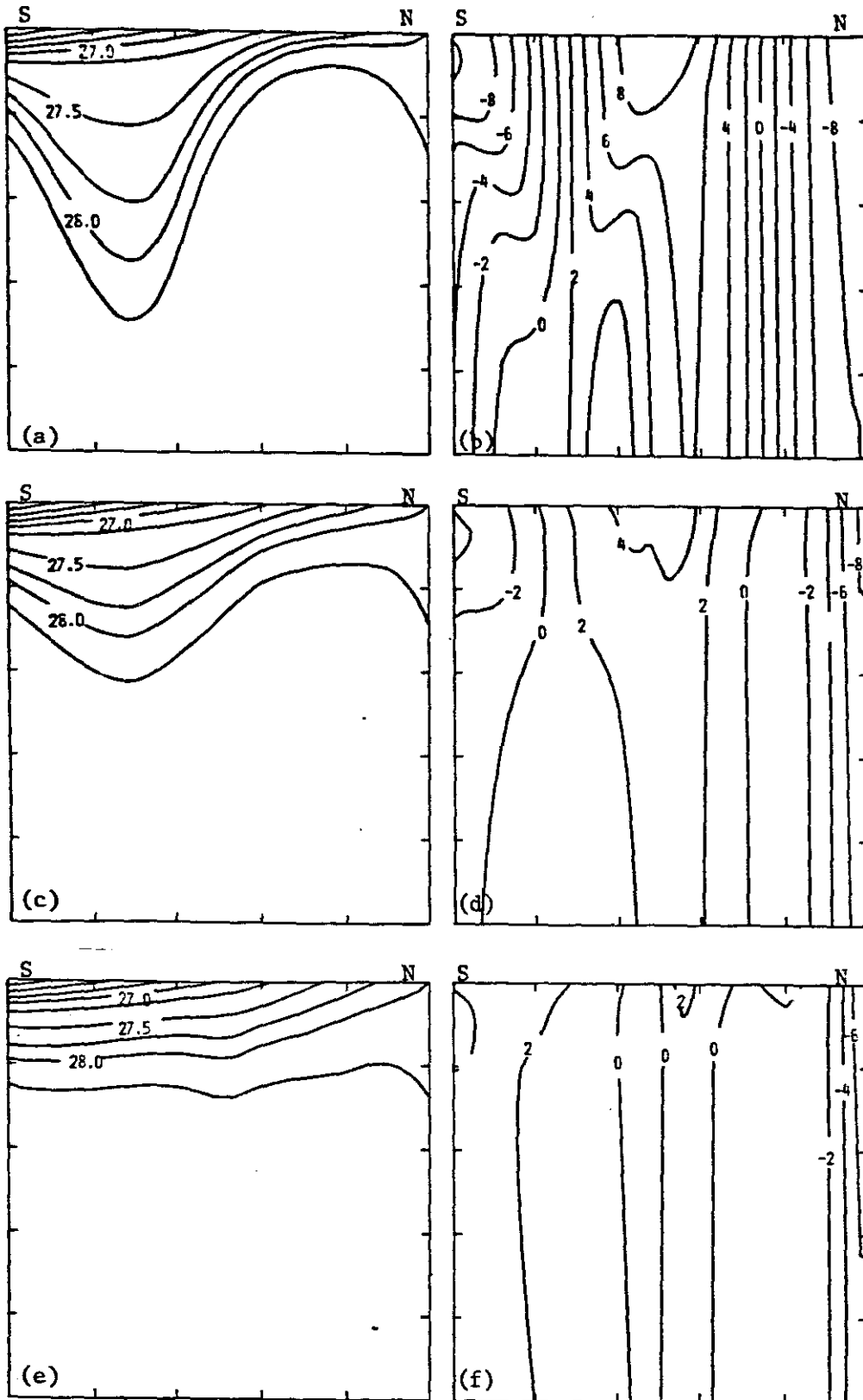
Surface density is independent of x.

Fig. 3-13. Meridional sections of a subtropical/subpolar gyre (H=2km).

a, c, e) Density profile at x=0, 0.5, 1.0 (sigma theta).

b, d, f) u-velocity profile at x=0, 0.5, 1.0 (in units of cm/sec).
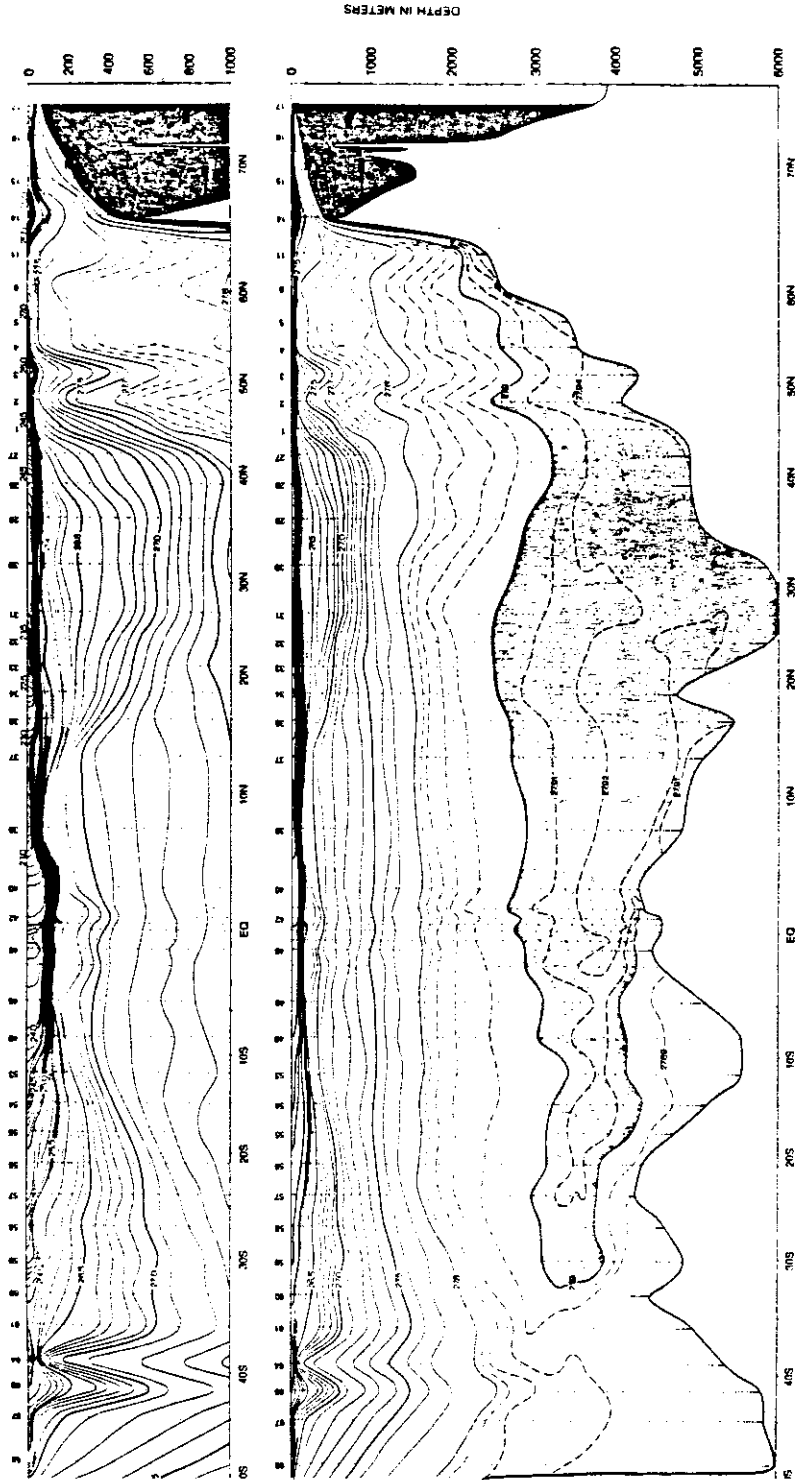
141 - b

Fig. 3-14. Density profile in the Western Atlantic Ocean (GEOSECS).

subpolar basin the thermocline layer is very thin and shallow; therefore the corresponding horizontal velocity is much more barotropic (Fig. 3-13(b,d,f)). On the eastern wall most isopycnals are level, and the u-velocity is very small (< 2cm/sec). Because in this case we start from the western boundary with a very simple function form of F(ρ,B), we cannot expect our solution would give the right detail near the eastern wall.

Fig. 3-15 shows the density and w-velocity profile on y = .76 (the central latitude of the subpolar gyre). One can see how isopycnals slope down eastward and that the w = 0 interface roughly corresponds to ρ = 1.02825 density surface. However, the u-velocity is large on this w = 0 interface due to the barotropicity of the subpolar gyre. How and where the thermocline solution matches to the thermohaline circulation is not clear.

For the present case ρ = const. along the ZWCL, so there is no interaction between the two gyres.

The corresponding potential vorticity section through the center of the basin, Fig. 3-16, shows the same low potential vorticity plateau in the middle of the subtropical basin. There is a high potential vortivity layer in the subpolar basin. Comparing our model with the picture from data in the North Pacific (Keffer, Rhines and Holland, 1984), there is similarity between them. The high potential vorticity layer in the subpolar basin might represent the sharp halocline in the North Pacific Ocean.OUr present example does not show a low potential vorticity plateau below the surface layer. This is due to the very simple functional form used for our two-gyre basin. One cannot expect to simulate every details of the double gyre structure with such a simple functional form.
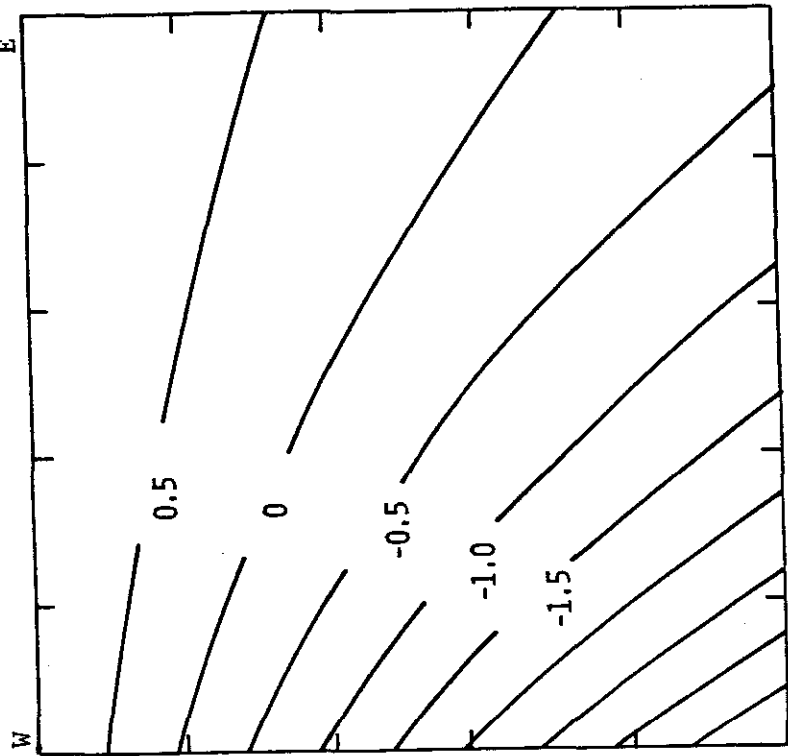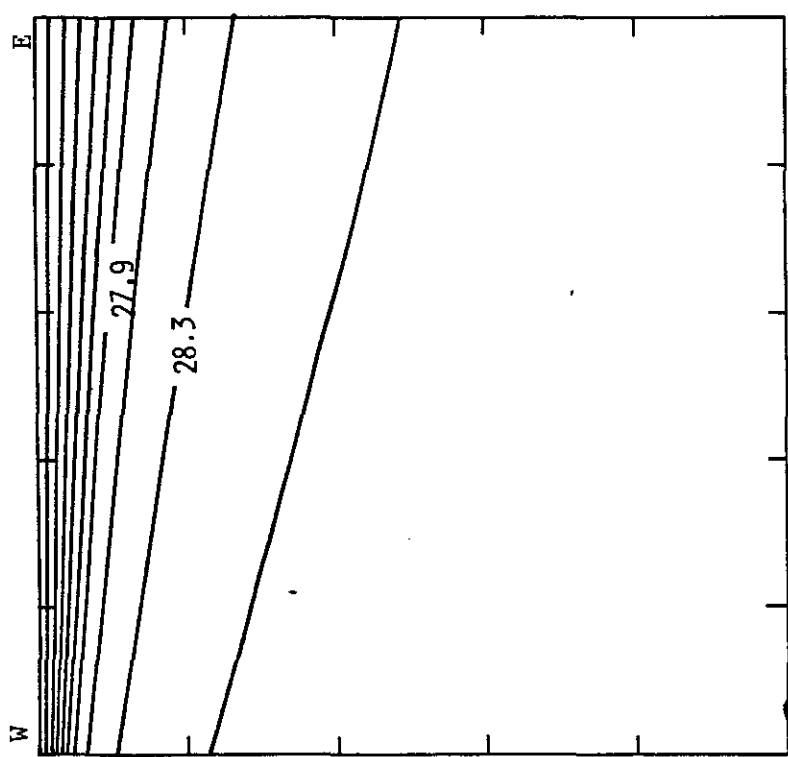
Fig. 3-15. Longitudinal section at y=0.76 (the central latitude of the subpolar gyre).
a) Density profile (sigma theta); b) w-velocity profile (in units of cm/sec).

142-a

POTENTIAL VORTICITY ON X=.5 SECTION   1984.

TWO-GYRE MODEL. WQAA

Depth(m)   CONTOURED FROM -5.400E1   TO -0.600E1   AT INTERVALS OF 0.600 E1
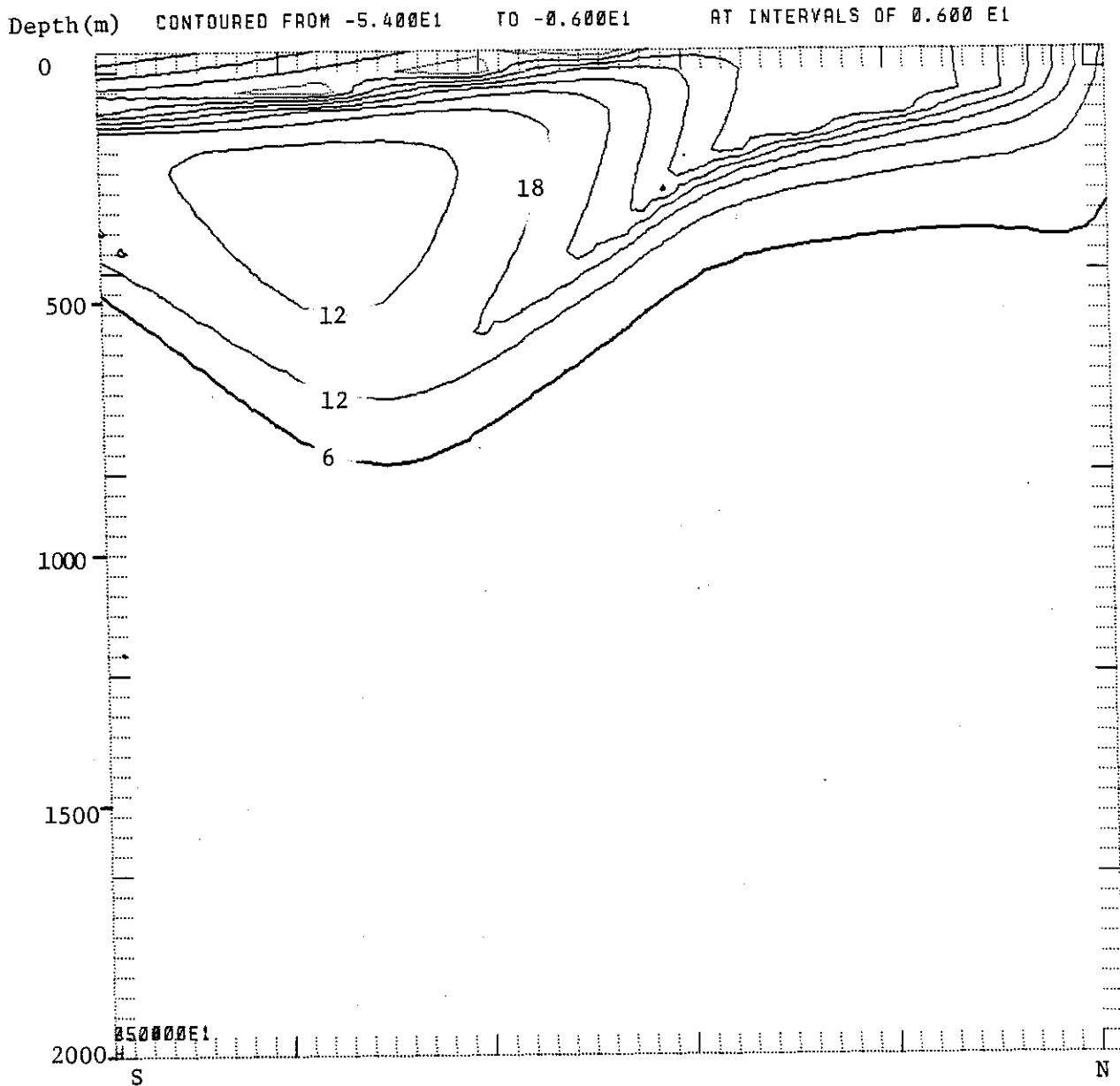

Fig. 3-16. Potential vorticity contours (in units of 10^{-13}/cm/sec) along
a meridional section through the center of a two-gyre basin. The
prominent feature includes the potential vorticity pleateau in the
subtropical basin and the high potential vortivity layer in the
upper part of the subpolar basin.

142-b

In a second case, ρ_s is a function of both x and y. Starting from the western boundary, the distribution of p_s can be easierly calculated along the ρ_s = constant lines. Fig. 3-17.a) shows the surface density distribution. Fig. 3-17(b,c) shows the density profiles on sections y = .76 and along the eastern wall (x = 1). One can see how the isopycnals outcrop within the subpolar gyre. Our model gives a structure very similar to the observations in the North Atlantic Ocean (Fig. 3-18).

Fig. 3-19 show the B-contours and depth of the ρ = 1.0274 surface. The present case does not have much water mass exchange across the ZWCL, so these two gyres are still fairly independent. There is a anticyclonic gyre in the subtropical basin, as described above. Within the subpolar gyre, water comes out of the western boundary current and turns northward, following a cyclonic path until it hits the outcropping line. This figure gives a complete physical realization of the abstract ideal concerning the unventilated thermocline and the potential vorticity field discussed in Section 6. Looking at this figure, one can see the role of the western boundary current in setting up the entire deep circulation. As pointed in Section 6, in a subpolar gyre, water particles move even before the corresponding layer outcrops.

Combining these figures with Fig. 3-6 yields a unified picture, Fig. 3-20, describing how water particles move within a two-gyre basin. In the subpolar gyre, the Ekman suction picks up water from below the mixed layer and the Ekman transport moves these water particles southward across the ZWCL into the subtropical gyre. In this process, air-sea interaction modifies the water properties. In the subtropical gyre the convergent Ekman flux pushes water down into the interior ocean. After entering the anticyclonic gyre there,
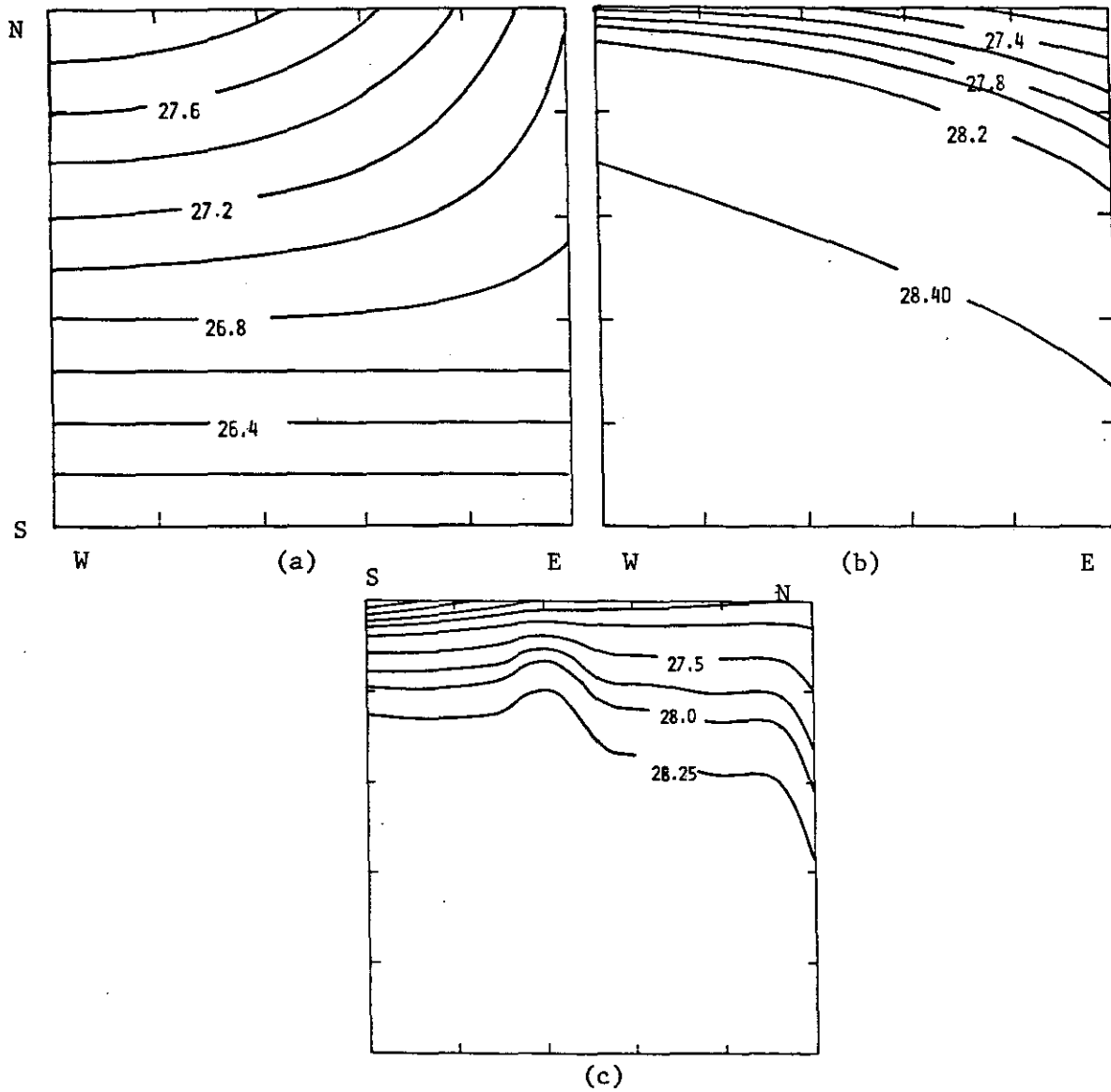
Fig. 3-17. Subtropical/subpolar gyre with surface density depended
on x and y: a) surface density profile; b) density profile at
y=0.76 section; c) density profile at x=1.0 section.
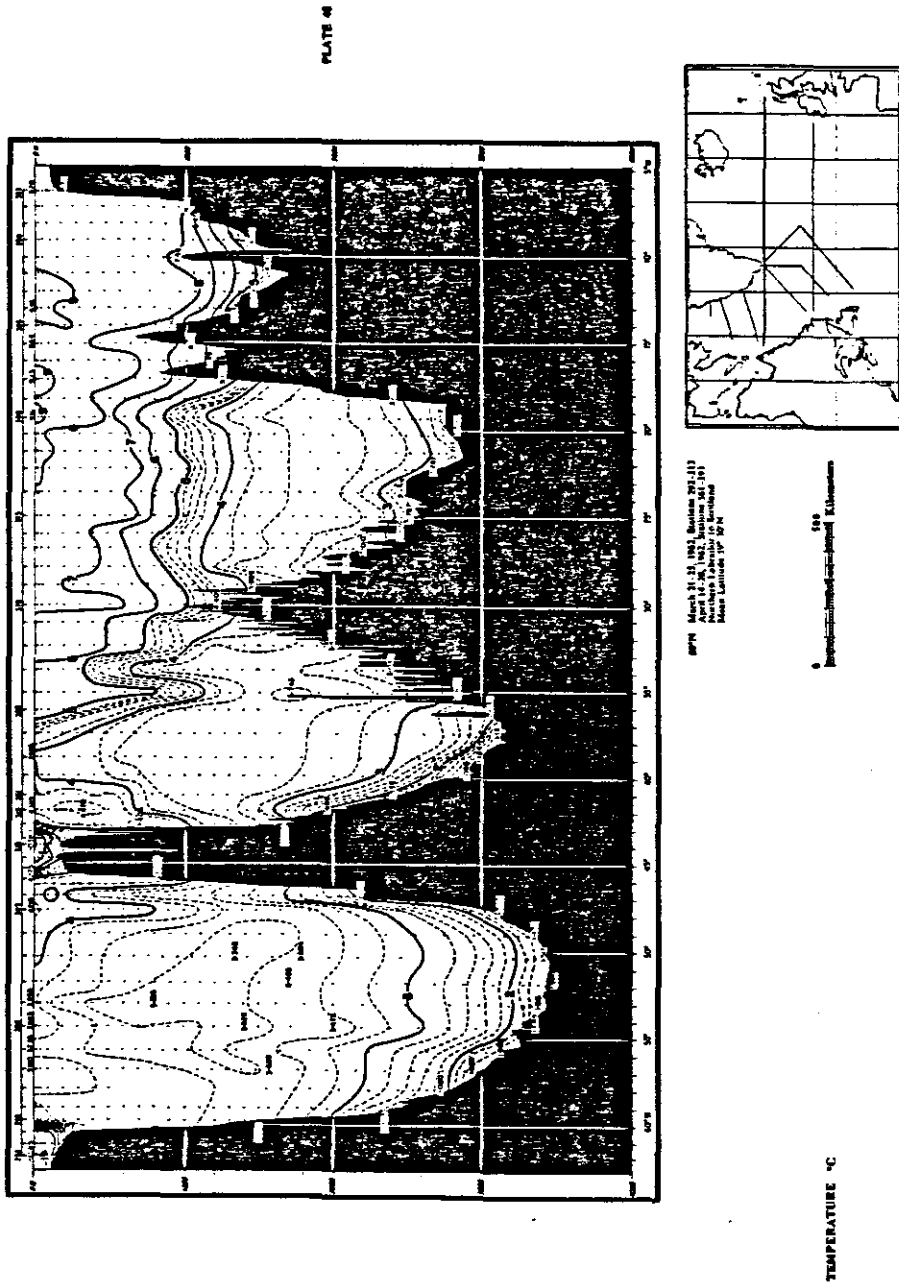
Fig. 3-18. Temperature profile at 60^0N of the North Atlantic Ocean (Worthington and Wright).
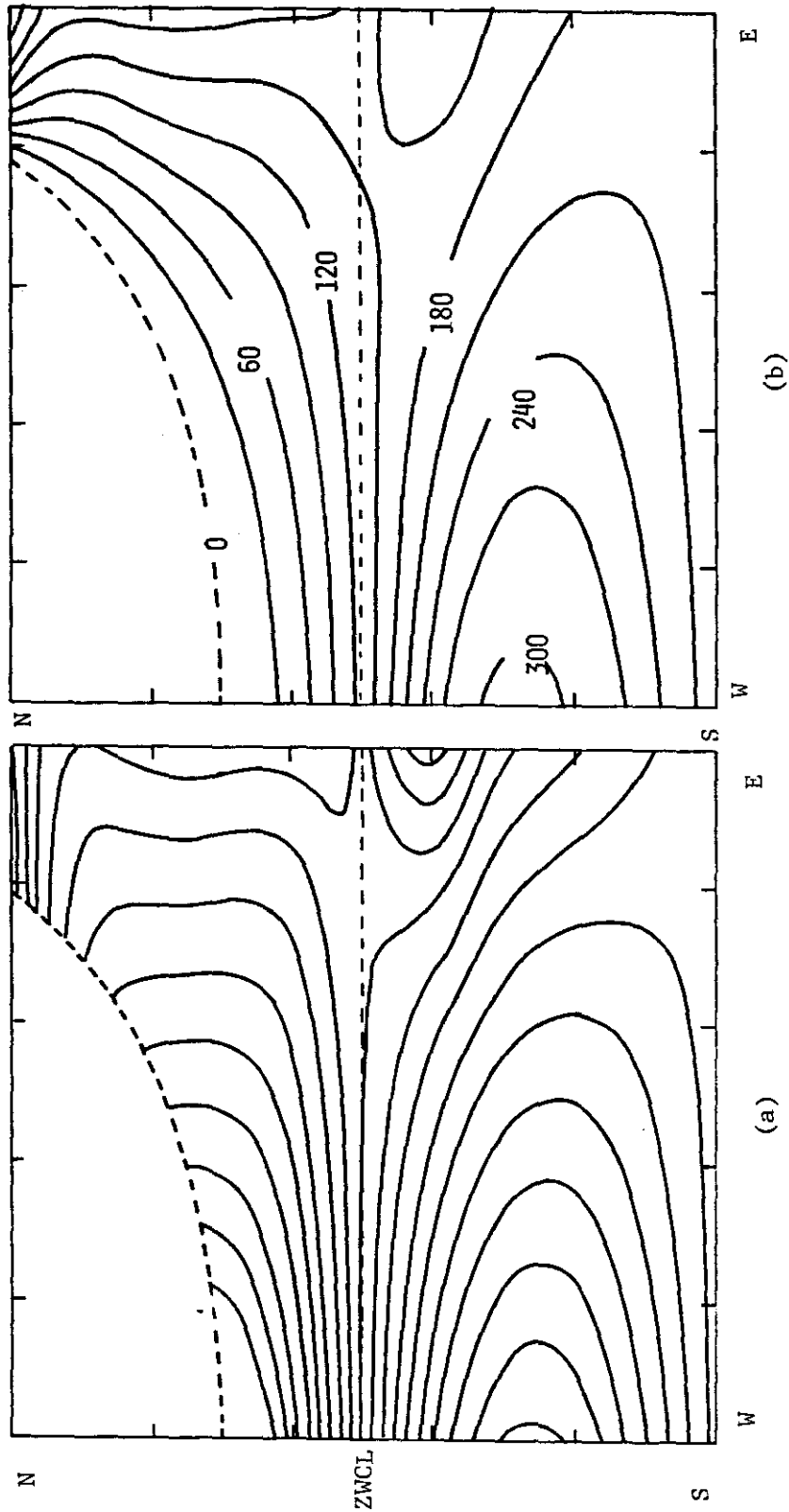
Fig. 3-19. Flow pattern on density surface $\sigma_\theta = 27.4$ (broken line is the outcropping line). a) Bernoulli function contours; b) depth of this density surface, in units of meter.
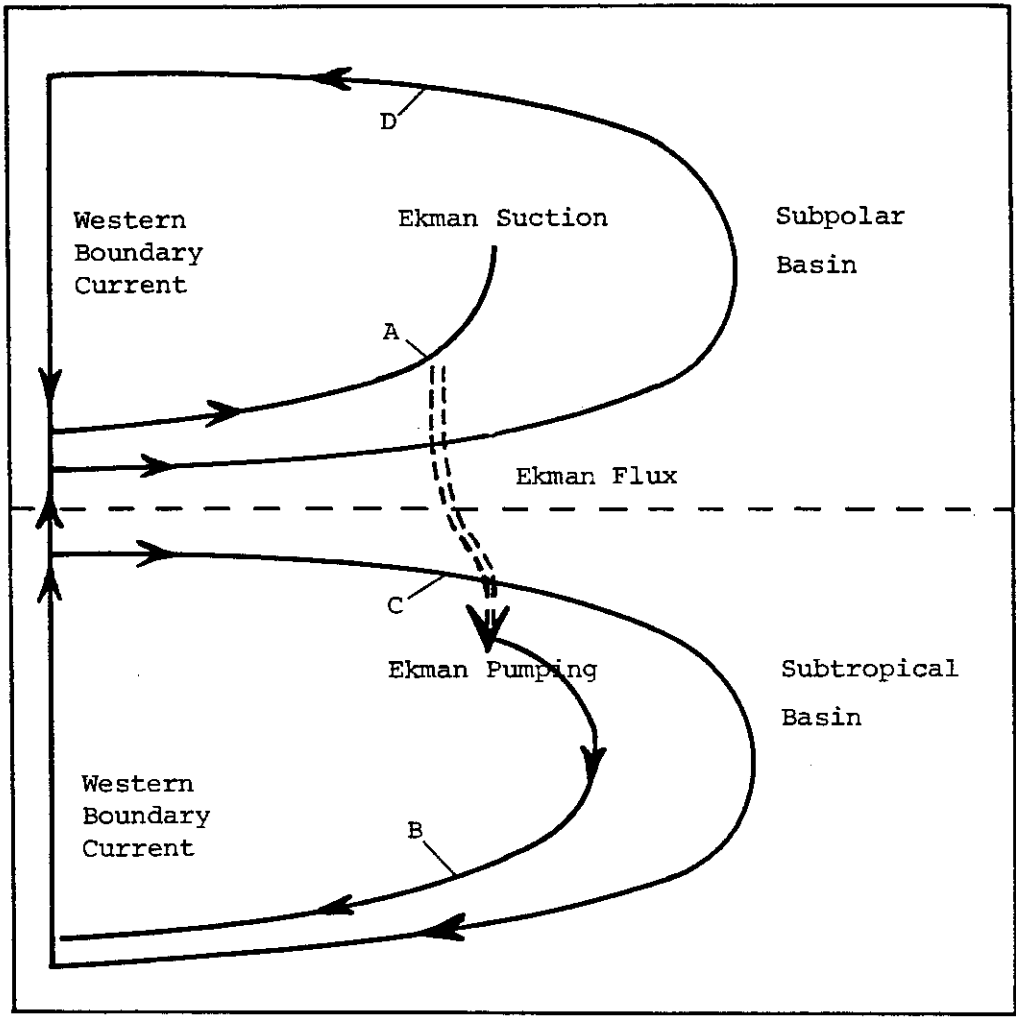
Fig. 3-20. Water mass transport pattern within a subtropical/
subpolar basin.

A, B are streamlines of the directly ventilated
thermocline.
C, D are streamlines of the non-directly ventilated
thermocline.

143-d

water particles move toward the western boundary, where they are transported northward. Along the western boundary (and part of the northern outcropping zone) air-sea interaction modifies the water properties again. Part of the western boundary current comes back to the subtropical gyre and becomes water in the recirculation layers (mode water). Some part of this goes into the subpolar basin (required by the mass balance), mixing with the southward-moving western boundary current of the subpolar gyre, and joins the cyclonic circulation. The upper part of the water mass in this cyclonic circulation will be picked up by the Ekman suction. The whole cycle is repeated again and again.

Of course, the above dynamical picture is an idealized case. In the real ocean the diffusion, eddy activity and deep water formation affect the total picture.

In a sense, the present model describes similar circulation patterns for both the subtropical and subpolar gyres. At least within our GFD model for a two-gyre basin the circulation in subpolar gyre seems a reverse for the subtropical gyre. In the subtropical gyre water is pumped down from the mixed layer and transported along downward anticyclonic paths; while water in the subpolar gyre is transported along upward cyclonic paths and sucked up by the mixed layer. At the same time, we notice the remarkable difference between these two gyres, namely the bowl-shaped thermocline in the subtropical gyre and the dome-shaped thermocline in the subpolar gyre.

Fig. 3-21 shows a case with a slightly different surface density pattern, but here there is water mass exchange across the ZWCL as shown in Fig. 3-21a). Some water particles leave the western boundary current of the subpolar gyre, flow southward and join the subtropical gyre circulation.
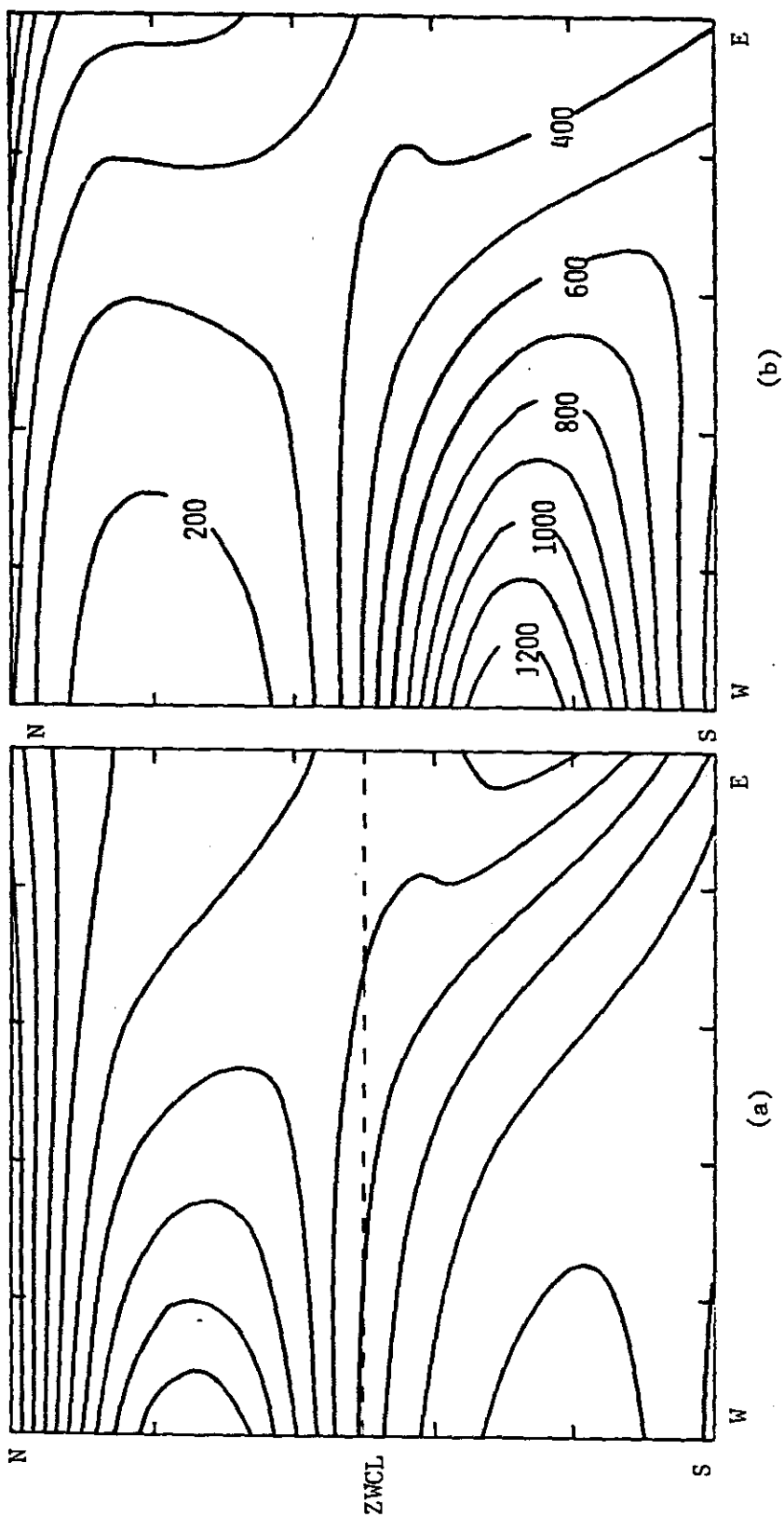
Fig. 3-21. Flow pattern on density surface $\sigma_\theta = 28.2$;

a) Bernoulli function contours; b) depth of this density surface, in units of meter.

We were not able to build a complete picture of a first baroclinic mode of water mass exchange across the ZWCL. Possibly the interfacial friction is essential for the existence of these baroclinic modes. Generally, layer models with density discontinuities at interfaces imply a kind of friction that makes the baroclinic mode possible. Further study is needed to find a solution for this problem.

8. Conclusions

For a long time, two theories about the thermocline and water mass formation have competed. Sverdrup et al's classic book, "The Oceans" presents both of them. The first theory explains the thermocline as the result of a diffusion process caused by the cold abyssal water upwelling through the main thermocline. The second theory describes the thermocline as the result of surface ventilation of an essentially ideal fluid. There is general agreement that diffusion is important in the thermal balance of the ocean. However, the ideal fluid approach can also give a very simple and clear picture for the oceans. Indeed, the analytical similarity solutions for the ideal fluid approach are basically the same as the similarity solutions for a diffusive model. Thus, the real question is how far the ideal fluid thermocline model can go in explaining the observed thermocline structure. Welander's solution was the first attempt; that solution, however, does not satisfy the important Ekman pumping condition.

The present model, with appropriate choice of F, produces three-dimensional thermocline and current structures in a continuously stratified wind-driven ocean which are quite realistic. (The deep velocities and inflows into the eastern boundary region were not dynamically specified and may not be realistic.) First, our solutions satisfy two essential upper boundary conditions and a homogeneous density condition in the abyssal layer. This is a big improvement compared with Welander's solution. As a result, our model can produce not only realistic basin-wide density structure, but also a reasonable three-dimensional velocity field. For example, we produce ß-spirals

which are very similar to observations in the oceans. In a sense, our model presents a simple way of generating a three-dimensional wind-driven circulation in a continuously stratified ocean which can be very useful for the general study of the oceans.

Second, our model advances the ideal fluid thermocline theory to a higher level. By appropriate choice of potential vorticity functional forms, we have demonstrated that this model can reproduce the main feature of the thermocline, such as the seasonal thermocline, the mode water region, the main thermocline, and the homogeneous abyssal water. Furthermore, our model can reconstruct the potential vorticity field, for example the low potential vorticity plateau, fairly successfully. At the same time, the present model also gives another possible explanation for the origin of the potential vorticity plateau -- it may be produced by the outflow from the western boundary layer.

Two major problems in this model are treating the boundary conditions and finding the potential vorticity functional forms.

Presently, neither the western nor the eastern boundary conditions can be satisfied by an ideal fluid thermocline model with continuous stratification. Our model only applies to the interior domain away from both the western and the eastern boundaries. In applying this model to the real oceans, we propose the existence of western and eastern boundary currents that can build up the corresponding potential vorticity field and return the mass flux at the right latitude and depths. Consequently, the validity of our solution depends on whether there are such boundary currents and how one can really construct them.

Although we do not include these boundary currents in our model, their dynamical roles in this model are very important. As seen from the thermal structure on the western wall, the isopycnals slope down southward. Therefore, to have a mass balance of the entire basin, there should be upwelling and cooling within the western boundary region to set the water properties required by the input condition on the western boundary for the ideal fluid thermocline problem. Here the vertical diffusion is dynamically essential. In this sense, water particles within the upper ventilated layer are subjected to strong diffusion in the western boundary current region for each cycle around the gyre.

The eastern boundary current plays a role similar to the western boundary current. Because the zonal flow velocity near the eastern wall is much less than near the western wall, the dynamical role of the eastern boundary current in determining the entire gyre structure is less important than the western boundary current.

The lower boundary condition for the ideal fluid thermocline also remains an open question. No solution for a continuously stratified ocean has been found that satisfies $w = 0$ on the bottom. Our model treats the lower boundary condition by using solutions in which ρ becomes asymptotically constant and horizontal velocity becomes relatively small in the abyssal region. In principle, by using more complicated functional forms and carefully choosing parameters, one might be able to satisfy the lower boundary condition more convincingly. Since we are yet not sure whether the ideal fluid thermocline theory can apply to the deep ocean, we choose to terminate our solution somewhere below the $w = 0$ interface. Our present knowledge about the deep

circulation is rather poor, and hence we propose that some kind of diffusive thermocline (or thermohaline) solution can be matched with our solution near this interface.

Imposing the functional form of $F(\rho, B)$ is a rather ad-hoc way of solving the thermocline problem. Actually, the interior potential vorticity field can not be determined without knowing the entire gyre structure, especially the western/eastern boundary currents and the outcropping zone near the northwest corner where the strong air-sea interaction and diffusion modify the water mass property. According to the model, we need the sea-surface density, the Ekman pumping velocity, and the sea-surface pressure on part of the boundary. By specifying $p_s(0, y)$ or $p_s(1, y)$, one imposes information about the property of water that moves into (or out of) the domain from the western/eastern boundary. However, the corresponding thermocline structure problem is still highly underdetermined. By specifying F, we pick one solution from an infinite number of solutions. In this sense, the ideal fluid thermocline problem can be only an incomplete idealization of the observed thermocline structure. The real structure in a basin is also determined by the upwelling/downwelling and the diffusive process in the western/eastern boundaries and the abyssal circulation. The input from the western/eastern boundary currents determines the interior potential vorticity distribution and the gyre structure.

In this model, we define a ventilation ratio $V_r = \beta L_y / f$, as the ratio of the ventilated thermocline depth to the entire thermocline depth. The fact that $V_r \sim 0.3 - 0.5$ for the subtropical gyres in both the North Atlantic Ocean and the North Pacific Ocean implies that there are big unventilated water pools in both of these oceans below the directly wind-driven ventilated layer.

In addition, we have clarified the existence of mass flux across the ZWCL. For a general case, there will be water mass exchange across the ZWCL, uniting the two gyres into a single body. Only if on the northern and southern boundaries the ZWCLs are constant density lines, will there be no water mass exchange (within the limitation of the ideal fluid thermocline theory, as presented above); hence the subtropical gyre can be studied as a single gyre. Note that even in such a special case there can be cross-gyre interactions, such as the Ekman flux and the western boundary or interior boundary currents. For general cases, information is needed wherever fluid moves into (or out of) the domain through the lateral boundaries.

In summary, the examples shown in this chapter demonstrate the power of the model. Although, this model gives some realistic feature, there are major deficiencies:

1) The potential vorticity field is specified in an ad-hoc way.

2) The model does not satisfy the eastern boundary condition.

3) The lower boundary condition is treated in an asymptotical way which needs further careful examination.

4) The mixed layer is not included in the model.

5) There is neither friction nor time dependence.

Further study on these topics seems very interesting and important.

Addendum to Part II

Mathematical Background

Abstract

Using the standard mathematical theory for classifying partial differential equation systems, various forms of the thermocline equation systems are analyzed. The ideal fluid thermocline equation is a nonlinear non-strict hyperbolic system. This system has one single real characteristic and one triple real characteristic. The single characteristic is bidirectional (reversible). No well-posed boundary value problem has been proved. A proper way to deal with a reasonable boundary value problem is proposed.

1. Introduction

For a long time people have been trying to find a correct formulation of a boundary value problem for the thermocline structure. Welander (1971a) suggested that a general formulation of the boundary conditions for the ideal fluid thermocline equations should be:

$$\rho = \rho_s, \quad w = w_e \qquad \text{at } z = 0$$

$$w = 0 \qquad \text{at } z = -H \tag{1.1}$$

Recently Luyten, Pedlosky and Stommel (1983), based on physical intuitions, have suggested a slightly different way:

$$\text{specify } \rho = \rho_s \text{ only where } w_e < 0 \tag{1.2}$$

Killworth (1983) argues that this means the equation system should be a hyperbolic system. In this Addendum we try to examine this problem from the standard theoretical point of view of partial differential equations. Our notations are based on the standard form in Courant's "Partial Differential Equations".

In fluid dynamics there are many problems involving first-order partial differential equation systems with 3 to 6 equations. These high-order partial differential equation systems have many strange properties, compared with the more straightforward classical results for second-order partial differential equations.

For second order partial differential equations, there is a standard way of classification, described in Courant and Hilbert (1962). From the original system, one derives the characteristic form of a second order partial

differential equation in two independent variables. If there is no real solution to the characteristic form, it is an elliptic differential equation. If there is one real double solution to the characteristic form, it is a parabolic differential equation. If there are two distinct real solutions, it is a hyperbolic differential equation. Because equations of different types have quite different properties, the classification of an equation is the first step in studying the corresponding boundary value problems for that equation.

The properties of a second-order hyperbolic differential equation, such as characteristics, domain of influence, domain of dependence and the Cauchy problems (or the initial value problem) are well known. Generally, a hyperbolic equation has more than one characteristic. Some information (in some cases, physically conserved quantities) is carried along with these characteristics. There may be discontinuities across these characteristics. Characteristics are unidirectional. In the corresponding physical (or mathematical) system, there is a kind of dissipation (or entropy) which makes the systems (and the directions of these characteristics) irreversible.

However, the classification of higher order partial differential equation systems is much more complicated. The corresponding characteristic forms are generally high order algebraic equations in the partial derivatives of the characteristic surfaces. If all roots are complex, we have an elliptic equation system. If all roots are real and distinct, we have a so-called complete hyperbolic equation system. A high-order complete hyperbolic equation system has basically the same properties as the classical second-order hyperbolic equation. However, there are many strange types of equation systems

which fall in between these two types. For example, some equation systems have all characteristics real, but some of these characteristics are multiple roots. This kind of system is called a non-strict hyperbolic system.

The ideal fluid thermocline equation belongs to the non-strict hyperbolic system because this system has a single characteristic and a real triple characteristic. The mathematical properties for this equation system are still largely unknown. The analysis in this chapter suggests that the single characteristic of this equation is reversible. A corresponding way to formulate a boundary value problem is proposed. There are two interesting points: 1) One can specify ρ_s even in the upwelling region and find the corresponding solution; 2) Density data is needed wherever water particles move into (or out of) the domain under study.

A general discussion of several other formulations of the thermocline problem also reveals interesting points concerning with the classification of equation systems and the existence of generalized solutions.

2. Basic Equations

For simplicity we use the ß-plane approximation. The spherical geometry modifies only the equations slightly. For a steady thermocline problem with only the vertical diffusion taken into consideration, the basic equations are:

$$u_x + v_y + w_z = 0$$

$$u\rho_x + v\rho_y + w\rho_z = K\rho_{zz}$$

$$uu_x + vu_y + wu_z + p_x = fv \qquad\qquad (2.1)$$

$$uv_x + vv_y + wv_z + p_y = -fu$$

$$uw_x + vw_y + ww_z + p_z = -\rho g$$

where

$$p = (p_{total} + \rho_0 gz)/\rho_0$$

$$\rho = (\rho_{total} - \rho_0)/\rho_0 \qquad\qquad (2.2)$$

ρ_0 is the reference density

$f = f_0 + \beta y$ is the Coriolis parameter

We introduce the non-dimensional variables by the following relations:

$$(x,y) = L(x',y'), \qquad z = Dz'$$

$$(u,v) = U(u',v'), \qquad w = \delta Uw'$$

$$p = f_0 ULp' \qquad\qquad (2.3)$$

$$\rho = f_0 LU/gD \cdot \rho'$$

$$f = f_0 f'$$

where

$$\delta = D/L \qquad \text{is the aspect ratio} \qquad\qquad (2.4)$$

The equation system then can be written, after dropping primes, as:

$$u_x + v_y + w_z = 0$$

$$u\rho_x + v\rho_y + w\rho_z = \lambda\rho_{zz}$$

$$\varepsilon(uu_x + vu_y + wu_z) + p_x = fv \qquad (2.5)$$

$$\varepsilon(uv_x + vv_y + wv_z) + p_y = -fu$$

$$\delta^2\varepsilon(uw_x + vw_y + ww_z) + p_z = -\rho$$

where

$$\varepsilon = U/fL \ll 1$$

$$\lambda = KL/D^2U \ll 1 \qquad (2.6)$$

$$\delta = D/L \ll 1$$

are small parameters.

3. The Ideal Fluid Thermocline

Now put $\lambda = 0$ into (2.5), but at present keep the advection terms. However, to distinguish terms resulting from each of the nonlinear convection terms we introduce the following factors

$$\varepsilon_1, \varepsilon_2, \varepsilon_3 \text{ which will take the values 0 or } \varepsilon, \qquad (3.1)$$

and rewrite (2.5) as

$$u_x + v_y + w_z = 0$$

$$u\rho_x + v\rho_y + w\rho_z = 0$$

$$\varepsilon_1(uu_x + vu_y + wu_z) + p_x = fv \qquad (3.2)$$

$$\varepsilon_2(uv_x + vv_y + wv_z) + p_y = -fu$$

$$\delta^2\varepsilon_3(uw_x + vw_y + ww_z) + p_z = -\rho$$

Using the matrix notation, equations (3.2) can be written as a single matrix equation

$$AF_x + BF_y + CF_z = G \qquad (3.3)$$

where

$$A = \begin{pmatrix} 1 & 0 & 0 & 0 & 0 \\ 0 & 0 & 0 & 0 & u \\ \varepsilon_1 u & 0 & 0 & 1 & 0 \\ 0 & \varepsilon_2 u & 0 & 0 & 0 \\ 0 & 0 & \varepsilon_3 \delta^2 u & 0 & 0 \end{pmatrix}, \qquad F = \begin{pmatrix} u \\ v \\ w \\ p \\ \rho \end{pmatrix},$$

$$B = \begin{pmatrix} 0 & 1 & 0 & 0 & 0 \\ 0 & 0 & 0 & 0 & v \\ \varepsilon_1 v & 0 & 0 & 0 & 0 \\ 0 & \varepsilon_2 v & 0 & 1 & 0 \\ 0 & 0 & \varepsilon_3 \delta^2 v & 0 & 0 \end{pmatrix}, \qquad G = \begin{pmatrix} 0 \\ 0 \\ fv \\ -fu \\ -\rho \end{pmatrix}, \qquad (3.4)$$

$$C = \begin{pmatrix} 0 & 0 & 1 & 0 & 0 \\ 0 & 0 & 0 & 0 & w \\ \varepsilon_1 w & 0 & 0 & 0 & 0 \\ 0 & \varepsilon_2 w & 0 & 0 & 0 \\ 0 & 0 & \varepsilon_3 \delta^2 w & 1 & 0 \end{pmatrix}.$$

The characteristic manifolds of this matrix equation are defined by the following equation

$$|A\Phi_x + B\Phi_y + C\Phi_z| = 0 \qquad (3.5)$$

or

$$\begin{vmatrix} \Phi_x & \Phi_y & \Phi_z & 0 & 0 \\ 0 & 0 & 0 & 0 & \Delta \\ \varepsilon_1 \Delta & 0 & 0 & \Phi_x & 0 \\ 0 & \varepsilon_2 \Delta & 0 & \Phi_y & 0 \\ 0 & 0 & \delta^2 \varepsilon_3 \Delta & \Phi_z & 0 \end{vmatrix} = 0 \qquad (3.6)$$

where

$$\Delta = u\Phi_x + v\Phi_y + w\Phi_z \tag{3.7}$$

With simple algebra, equation (3.6) becomes

$$\Delta^3[\varepsilon_3\delta^2(\varepsilon_2\Phi_x^2+\varepsilon_1\Phi_y^2)+\varepsilon_1\varepsilon_2\Phi_z^2] = 0 \tag{3.8}$$

which determines the characteristic manifolds $\Phi(x,y,z) = 0$ of the original equation system (3.2).

As discussed in the introduction, the characteristic manifolds of an equation system are useful for classifying the equation system. A manifold in three-dimensional space can be either a two-parameter surface or a one-parameter curve. If a characteristic is real and single, one can find a quantity that is conserved along this line, and across this line there may be discontinuities in the solution. If the characteristic manifolds are complex, the original equation system generally has properties similar to the classical elliptic differential equation.

1) Assuming $\varepsilon_3 = 0$, we have the hydrostatic approximation, but keep the nonlinear convection terms $\varepsilon_1 = \varepsilon_2 = \varepsilon \neq 0$. Thus the characteristic equation becomes

$$\varepsilon^2\Phi_z^2\Delta^3 = 0 \tag{3.9}$$

The second factor $\Delta^3 = (u\Phi_x+v\Phi_y+w\Phi_z)^3 = 0$ means that a streamline is a triple characteristic line. Along a streamline the density ρ, potential vorticity, and Bernoulli function are conserved. The fact that a streamline is a triple characteristic seems unrelevant to the fact that there are three conserved quantities along a streamline. As will be shown below, a streamline is a single characteristic for the ideal fluid thermocline equation; nevertheless, there are the same conserved quantities along a

158

streamline. The first factor $\Phi_z^2 = 0$ means that the z-axis is a double characteristic. The proper formulation of a well-posed boundary value problem is not clear for this nonlinear non-strict hyperbolic system.

For the traditional ideal fluid thermocline, the nonlinear convection terms are neglected. Thus $\varepsilon_1 = \varepsilon_2 = 0$, and we have a degenerate system. To find the corresponding characteristic manifolds, we have to eliminate an extra equation and get a non-degenerate system. We will discuss this matter below.

2) If we keep $\varepsilon_3 = \varepsilon \neq 0$, then the characteristic equation becomes

$$\varepsilon^2 \Delta^3 [\delta^2(\Phi_x^2 + \Phi_y^2) + \Phi_z^2] = 0 \tag{3.10}$$

The first factor $\Delta^3 = 0$ has the same meaning as before, but now we have a new factor:

$$\delta^2(\Phi_x^2 + \Phi_y^2) + \Phi_z^2 = 0 \tag{3.11}$$

which has no real characteristic solution; thus it is a complex characteristic manifold making the corresponding equation system a hyperbolic-elliptic composite type system. There are many examples of hyperbolic-elliptic composite type systems in fluid dynamics, but the corresponding mathematical theory is a relatively new research area for mathematicians. Some Russian mathematicians are active in this field now (Dzhuraev and Baimenov, 1980; Nurubloev, 1981; Sergienko, 1982), but there is no theory yet available for the well-posedness of the boundary value problem for this hyperbolic-elliptic composite type system.

3) Case with $\varepsilon_1 = \varepsilon_2 = \varepsilon_3 = \varepsilon = 0$, the classical ideal fluid thermocline. As discussed above, equation system (3.2) becomes a degenerate system in this case. To get a non-degenerate system, we can use the hydrostatic relation to eliminate the pressure. Then the original equation

system can be rewritten as

$$u_x + v_y + w_z = 0$$

$$u\rho_x + v\rho_y + w\rho_z = 0$$

$$fv_z \qquad + \rho_x = 0 \qquad\qquad (3.12)$$

$$fu_z \qquad - \rho_y = 0$$

which can be put in a matrix form again

$$AF_x + BF_y + CF_z = 0 \qquad\qquad (3.13)$$

where

$$A = \begin{pmatrix} 1 & 0 & 0 & 0 \\ 0 & 0 & 0 & u \\ 0 & 0 & 0 & 1 \\ 0 & 0 & 0 & 0 \end{pmatrix}, \quad B = \begin{pmatrix} 0 & 1 & 0 & 0 \\ 0 & 0 & 0 & v \\ 0 & 0 & 0 & 0 \\ 0 & 0 & 0 & -1 \end{pmatrix}, \quad C = \begin{pmatrix} 0 & 0 & 1 & 0 \\ 0 & 0 & 0 & w \\ 0 & f & 0 & 0 \\ f & 0 & 0 & 0 \end{pmatrix}, \quad F = \begin{pmatrix} u \\ v \\ w \\ \rho \end{pmatrix} \qquad (3.14)$$

Using the same procedure as above, the characteristic equation of equation (3.13) is

$$| A\Phi_x + B\Phi_y + C\Phi_z | = 0 \qquad\qquad (3.15)$$

or

$$f^2\Phi_z^3(u\Phi_x + v\Phi_y + w\Phi_z) = 0 \qquad\qquad (3.16)$$

From (3.16) factor $u\Phi_x + v\Phi_y + w\Phi_z = 0$ means that a streamline $dx/u = dy/v = dz/w = dt$ is a characteristic and $\Phi_z^3 = 0$ means the z-axis is a triple characteristic. The equation system for the ideal fluid thermocline is a non-strict hyperbolic system. (General references on non-strict hyperbolic systems, see Carasso and Stone, 1975; Bear, 1972.) Due to its nonlinearity and the special boundary conditions for a whole basin, the formulation of a well-posed problem is not yet clear. However, the discussion of a linearized model equation system in Appendix A suggests useful information.

160

Suppose we have a box far away from any solid boundary, and u, v, w do not change signs within this box. One appropriate boundary value problem for equation system (3.12) is then

BVP - A :

$$\rho = \rho_1(x,y) \qquad \text{on } z = 1$$

$$\rho = \rho_2(x,z) \qquad \text{on } y = 0$$

$$\rho = \rho_3(y,z) \qquad \text{on } x = 0 \qquad\qquad (3.17)$$

$$p_0 = p_0(x,y), \; w = w(x,y) \quad \text{on } z = 1$$

where we assume that u,v > 0 and w < 0 for the whole box (or for general cases, u, v, w do neither change sign nor become zero; this assumption should be checked after the whole solution has been found). By marching downward from z = 1 to z = 0 step by step, the whole solution can be easily found. This equation system has almost the same properties as the model equation system in Appendix A. This boundary value problem is well posed. It is not clear whether we can pose the second boundary value problem BVP-B as in Appendix A.

Actually, the physical meaning of this boundary value problem is not very clear. First, no traditional oceanographic measurement can give accurate sea surface pressure distribution within a few cruises. Second, this formulation is valid only if u, v, w do not change sign within the entire box. Therefore, it does not apply to an entire basin because u must change sign in a closed basin. In such cases we do not know where to input the lateral density data before we know the whole solution. Furthermore, it does not apply to the case where a ZWCL is inside the upper surface of the box. This case involves different signs for both v and w, so that it is difficult to use this approach. Thus BVP-A has only a mathematical meaning. A practical way of solving the ideal fluid thermocline problem has been discussed in Chapter III.

161

By introducing a function $M(x,y,z)$ (Welander, 1959)

$$\rho = -M_{zz}$$

$$u = -M_{zy}/f, \qquad v = M_{zx}/f \qquad\qquad (3.18)$$

$$w = M_x \beta/f^2$$

a single equation follows

$$-M_{zy}M_{zzx}+M_{zx}M_{zzy}+\beta/f \bullet M_x M_{zzz} = 0 \qquad\qquad (3.19)$$

As Killworth points out, (3.19) is unchanged under the following transformation

$$x \rightarrow -x \qquad\qquad (3.20)$$

Notice that the western boundary becomes an eastern boundary. Thus both the eastern and western boundaries have a similar role in a boundary value problem for the ideal fluid thermocline.

Another interesting property of this equation is that the characteristic ρ = const. has no preferable direction. One can go backward along a streamline. For most ordinary complete hyperbolic equations, there can be some strong discontinuities and dissipation in the solution; generally the characteristics are not reversible. The ideal fluid thermocline has, however, no dissipation at all. Therefore, density data can be given at either end of a streamline.

We can explain this strange property in two ways:

Firstly, one can pose a boundary value problem similar to BVP-A;

BVP-A':

$$\rho = \rho_1(x,y) \qquad\qquad \text{on } z = 0$$

$$\rho = \rho_2(x,z) \qquad\qquad \text{on } y = 1$$

$$\rho = \rho_3(y,z) \qquad\qquad \text{on } x = 1 \qquad\qquad (3.21)$$

$$p = p_0(x,y), \ w = w(x,y) \qquad \text{on } z = 0$$

where we assume that $u,v > 0$, $w < 0$ for the whole box. By marching upward from $z = 0$ to $z = 1$, the entire solution is easy to find.

If one knows all the necessary data somehow, both approaches, BVP-A and BVP-A', are equivalent mathematically.

Secondly, (3.19) is unchanged under the following transformation

$$x \rightarrow -x', \quad y \rightarrow -y', \quad z \rightarrow -z', \quad \beta \rightarrow -\beta \tag{3.22}$$

Now $u' = -u$, $v' = -v$, $w' = -w$ and the streamline in the new coordinates is

$$dx'/u' = dy'/v' = dz'/w' = dt' \tag{3.23}$$

For $dt' < 0$, the corresponding water particle moves backward along the streamline compared with the original case. This transformation (3.22) puts the eastern/western boundaries, the northern/southern boundaries and the upper/lower boundaries for the ideal fluid thermocline equation in more equivalent positions.

In trying to formulate the appropriate boundary value problem for a whole basin, the following arguments are important:

a) A streamlines is a single characteristic for the equation system. Along a streamline the density, potential vorticity, and the Bernoulli function are constant. The fact that a single characteristic carries three conserved quantities seems quite different from the classic situation for hyperbolic systems. This might be special property for non-strict hyperbolic system. Across a streamline there may be weak discontinuities in the solution (some derivatives, such as the gradients of velocity, density or potential vorticity, may have jumps). The most important thing is that we must specify the density ρ wherever the fluid moves into (or out of) the domain.

b) The western boundary condition. We must specify the density where the fluid joins the interior ocean, so that the ideal fluid thermocline problem cannot be solved without knowing the structure of the western boundary

163

current. In this sense, the so-called ideal fluid thermocline cannot be studied in isolation. Attempts have been made to solve this problem since its formulation by Welander, but his model, though simple and interesting, does not apply to the entire basin. The equation system must contain friction terms to satisfy the appropriate boundary conditions for a whole basin.

The eastern boundary condition has the same kind of role as the western boundary condition.

c) The upper and bottom conditions. It is not surprising to find out that we need three boundary conditions on the upper surface to start the integration. According to the previous argument, we have to specify ρ where $w_e < 0$, even if $w_e > 0$, we can specify ρ on the surface and trace back along a streamline. The boundary value problem BVP-A seems difficult to apply to the real ocean. Specifying $w = 0$ on the bottom may release one boundary condition on the sea surface; however, it seems difficult to find a solution which satisfies $w = 0$ on the bottom. If one specifies ρ on the bottom in order to release another sea surface boundary condition, w would not be zero on the bottom. Thus the best procedure may be not specifying the lower boundary condition.

d) Other lateral boundary conditions. Suppose the northern and southern boundaries are the ZWCLs. According to Sverdrup dynamics, the vertical integrated north-south mass flux across these boundaries is zero for the interior ocean. This does not mean, however, there is no baroclinic mode. In fact, we find baroclinic modes across the northern ZWCL in the two-layer model (See Chapters I and II). In such cases, we must specify the density where fluid moves into (or out of) our domain. The same difficulty arises: we don't know where to specify boundary conditions before we solve the whole problem.

164

4. The Thermocline Problem with Vertical Diffusion

Assuming that $\varepsilon_1 = \varepsilon_2 = \varepsilon_3 = \varepsilon = 0$, we can use the hydrostatic relation to eliminate the pressure. By introducing a new function $h = \rho_z$, we can convert the basic equation system (2.5) into a first order partial differential equation system

$$U_x + V_y + W_z = 0$$

$$U\rho_x + V\rho_y + W\rho_z - Kh_z = 0$$

$$\rho_z = h \qquad\qquad (4.1)$$

$$fv_z + \rho_x = 0$$

$$fu_z - \rho_y = 0$$

This system can be written as a single matrix equation

$$AF_x + BF_y + CF_z = G \qquad\qquad (4.2)$$

After simple manipulations, the characteristic equation is found to be

$$Kf^2\Phi_z^5 = 0 \qquad\qquad (4.3)$$

Thus a streamline is no longer a characteristic and there is no conserved quality along a streamline. Now $\Phi_z^5 = 0$ is a fivefold root. No well-posed boundary value problem has been discussed for this equation system.

5. The Existence of the Solution for a Steady Thermocline
with Diffusion

The existence of the solution for a steady thermocline model with both vertical and horizontal diffusions taken into account has recently been proved. Using the functional analysis in the Sobolev spaces W_2^2 and W_2^1, Kordzadze (1979) proves the theorem on the existence of a generalized solution u, v, p, $\rho \in W_2^2$ and $w \in W_2^1$.

Consider an ocean basin Ω of constant depth H with lateral surface σ and boundary S. The basic equation system for the thermocline can be written as

$$\mu\Delta u + \upsilon u_{zz} + fv = p_x/\rho_0 + \text{div}(uu)$$

$$\mu\Delta v + \upsilon v_{zz} - fu = p_y/\rho_0 + \text{div}(vu)$$

$$0 = -p_z - \rho g \qquad\qquad (5.1)$$

$$\text{div}(u) = 0$$

$$\mu_1\Delta\rho + \upsilon_1\rho_{zz} = \text{div}(u\rho)$$

$$u = (u, v, w)$$

with the boundary conditions

$$u_z = f_1(x,y), \quad v_z = f_2(x,y), \quad \rho_z = f_3(x,y), \quad w = 0 \quad \text{at } z = 0$$

$$\rho_z = 0, \qquad u = v = w = 0 \qquad\qquad \text{at } z = -H \qquad (5.2)$$

$$u = v = 0, \quad \rho = f_4(z,s) \qquad\qquad \text{on } \sigma$$

where f_1, f_2, f_3, f_4 are given functions with continuous first derivatives.

THEOREM (Kordzadze): There is at least one solution for the equation system (5.1) with boundary conditions (5.2).

Here, by "solution", we mean a generalized solution in the Sobolev spaces $u, v, p, \rho \in W_2^2$ and $w \in W_2^1$. (By definition, W_2^1 is a Hilbert space defined by the norm $\| F \|_{W_2^1} = |\text{grad}^2 F|^{1/2}$, W_2^2 is a Hilbert space defined by a norm $\| F \|_{W_2^2} = (\| F \|_{L_2} + |\text{grad}^2 F|)^{1/2})$. (See Richtmyer (1978).) By definition, a function in W_2^1 space is a function whose first derivatives are square-integrable and a convergent functional series in W_2^1 space is convergent according to the norm $|\text{grad}^2 F|^{1/2}$. A function in W_2^2 space is a function which is square-integrable and has square-integrable first derivatives. A convergent

functional series in W_2^2 space has convergent zero-order and first order derivatives (in square-integration sense).

Physically, Kordzadze's theorem guarantees that for given upper-surface wind stress (f_1 and f_2), heat flux (f_3) and density on the lateral surface (f_4), there is at least one generalized solution that has square-integrable first derivatives. (For oceanographic application, specifying a no-heat flux lateral boundary condition seems more realistic than specifying density on the lateral surface). The difference between W_2^1 and W_2^2 is the way in which functional series converge. Roughly, if one used a first-order finite element method to solve (5.1) numerically, the solution would belong to W_2^2 space.

It would be interesting to find a similar theorem for the ideal fluid thermocline equation. However, no proper way of formulating a boundary value problem has been discovered.

The above theorem guarantees the existence of the generalized solution, but the uniqueness of the solution is far more complicated. Actually, there may be more than one solution for the same given boundary conditions. In the case of the ideal fluid thermocline with no diffusion or with weak diffusion, there are examples of multiple solutions.

6. Conclusions

Though nonlinearity and other mathematical properties prevent us from attaining strict proof, the above analysis strongly suggests the following:

The ideal fluid thermocline cannot be solved in isolation. The corresponding partial differential equation system is a nonlinear, non-strict

167

hyperbolic system with streamlines as its characteristics and the z-axis as a triple characteristic. Along every streamline the density, the potential vorticity, and the Bernoulli function are conserved. To solve the thermocline problem density data are required wherever water moves into (or out of) the domain of interest.

On the western (or eastern) boundary, density has to be specified where water comes into (or goes out of) the interior ocean.

On the northern/southern boundaries density data are required wherever water moves into (or out of) the domain under study. Even if the northern/southern boundaries are the ZWCL, there can be some baroclinic modes of water mass exchange across these boundaries; thus the density data are required for solving the ideal fluid thermocline problem for the interior ocean.

In other words, the ideal fluid thermocline problem cannot be solved without knowing the western/eastern boundary current structures and the entire basin circulation.

Appendix A. A Linearized Model Equation for the Ideal
Fluid Thermocline

It is fairly easy to examine the local behavior of the ideal fluid thermocline equations. Putting $u = a$, $v = b$, $w = c$ into the second equation of (3.12) and assuming f is a constant, we obtain an analogous equation system which is considerably simpler:

$$u_x + v_y + w_z = 0 \qquad\qquad\qquad (A-1)$$

$$a\rho_x + b\rho_y + c\rho_z = 0 \qquad\qquad\qquad (A-2)$$

$$fv_z + \rho_x = 0 \qquad\qquad\qquad (A-3)$$

$$fu_z - \rho_y = 0 \qquad\qquad\qquad (A-4)$$

The corresponding characteristic equation is

$$(a\Phi_x + b\Phi_y + c\Phi_z)\Phi_z^3 = 0 \qquad\qquad\qquad (A-5)$$

The first factor means that the straight line $dx/a = dy/b = dz/c$ is a characteristic. Actually, it is easy to see that equation (A-2) is a statement that ρ is conserved along lines $dx/a = dy/b = dz/c$.

Consider the appropriate boundary value problem for this model equation system. Within a box in a subtropical gyre $a > 0$, $b > 0$ and $c < 0$. For a cubic volume [$0 \leqslant x \leqslant 1$, $0 \leqslant y \leqslant 1$, $0 \leqslant z \leqslant 1$], the following boundary value problems are well posed:

A) BVP-A:

1) $\rho = \rho_1(x,y)$ on $z = 1$.

    $\rho = \rho_2(x,z)$ on $y = 0$

    $\rho = \rho_3(y,z)$ on $x = 0$ (A-6)

2) u, v can be specified either on $z = 0$ or $z = 1$, but we can not specify u on both $z = 0$ and $z = 1$ (can nor specify v on $z = 0$, 1).

3) w can be specified either on $z = 0$ or $z = 1$.

The solution is very simple:

i) Using ρ = const. along $dx/a = dy/b = dz/c$ and the boundary conditions for ρ, the distribution of ρ in the whole volume is obtained.

ii) From (A-3) and (A-4)

$$v = v_0 - \int_{z_1}^{z} \rho_x/f \, dz \qquad \text{(A-7)}$$

$$u = u_0 + \int_{z_2}^{z} \rho_y/f \, dz \qquad \text{(A-8)}$$

where $v_0 = v_0(x,y,z_1)$, $u_0 = u_0(x,y,z_2)$ and z_1, z_2 are the places where we specify v, u.

iii) From (A-1)

$$w = w_0 - \int_{z_3}^{z}(u_x + v_y)dz \qquad \text{(A-9)}$$

where $z_3 = 0$ or 1, $w_0 = w(x,y,z_3)$.

Obviously, this boundary value problem is well posed. It is important to notice that we do not have to specify more data on lateral surfaces $x = 0, 1$; $y = 0, 1$; the solution (u, v, w) gives the corresponding value on these surfaces.

B) BVP-B:

1) $\rho = \rho_1(x,y)$ on $z = 1$

   $\rho = \rho_2(x,z)$ on $y = 0$ (A-10)

   $\rho = \rho_3(y,z)$ on $x = 0$

2) $v = v_1(x,y)$ on $z = 1$ (A-11)

3) $w = w_0(x,y)$ on $z = 0$

   $w = w_1(x,y)$ on $z = 1$ (A-12)

4) $u = u_{10}(y)$ on $x = 0, z = 1$ (A-13)

Using the characteristic $dx/a = dy/b = dz/c$ and the boundary conditions for ρ,

we find out $\rho = \rho(x,y,z)$. From equations (A-8) and (A-9)

$$w = w_1 + (u_{1x} + v_{1y})(1-z) \tag{A-14}$$

Now boundary condition (A-12) gives

$$u_{1x} = w_0 - w_1 - v_{1y} \tag{A-15}$$

which can be calculated from data. Afterward, u_1 is obtained from

$$u_1 = u_{10}(0,y,0) + \int_0^x u_{1x} \, dx \tag{A-16}$$

and u, v can be calculated from

$$u = u_1 - \int_z^1 \rho_y / f \, dz \tag{A-17}$$

$$v = v_1 + \int_z^1 \rho_x / f \, dz \tag{A-18}$$

This boundary value problem is well posed.

Lemma A. Both BVP-A and BVP-B are well posed.

Proof:

The existence of the solutions has been proved by actually constructing solutions in integration forms.

The stability of the solutions is guaranteed if the input density data is smooth enough, i.e., if $\int_0^1 |\rho_x| \, dz < \infty$ and $\int_0^1 |\rho_y| \, dz < \infty$.

Because (A-1,2,3,4) is a linear system, to prove the uniqueness of the solutions, one must prove that if input data is all zero, there is only a null solution. Now $\rho \equiv 0$, therefore u and v are independent of z. Differentiating (A-1) with z

$$w_{zz} = 0 \quad \text{or} \quad w = a + bz$$

For BVP-A, w_z is constant. However, $u \equiv v \equiv 0$ on $z = 0$ (or $z = 1$). Hence $w_z \equiv 0$, since $w = 0$ on $z = 0$ (or $z = 1$), thus $w \equiv 0$.

For BVP-B, $w = 0$ on $z = 0$, 1, and therefore a and b are both zero. Hence $w \equiv u \equiv v \equiv 0$.

<div align="right">Q.E.D.</div>

For this equation system, there also can be discontinuities. For example, ρ can have a discontinuity in its first-order derivatives. According to the theory of characteristics, the characteristics can be the interface between solutions which have quite different analytical structures. When we cross a characteristic manifold, there may be jump in the solution.

This model equation shows the reversibility of its characteristic clearly. If density data is given on $x = 1$, $y = 1$, $z = 0$ surfaces, the interior density field can be found by conservation law along the characteristic, the same as before.

For the calculation of the velocity field, one can specify $v = v_0(x,y)$ on $z = 0$ and $u = u_{00}(y)$ on $x = 0$, $z = 0$. The corresponding solution is calculated by integrating upward.

References:

Bears, R., 1972. Hyperbolic equations and systems with multiple
   characteristics, <u>Arch. Rat. Mech. Anal.</u>, 48, 123-152.

Carasso, A. and A.P. Stone (ed.), 1975. Improperly posed boundary value
   problems. (Research Notes in Mathematics Ser.: No.1), 157 p. Pit. Pub, MA.

Cox, M.D. and K. Bryan, 1983. A numerical model of the ventilated thermocline
   (preprint).

Courant, R. and D. Hilbert, 1962. Methods of mathematical physics, Vol II.
   Partial Differential Equations, John Wiley and Sons, New York.

Dzhuraev, T.D. and B. Baimenov, 1980. On the theory of boundary value problems
   for equations of mixed-composed type. <u>Izv. Akad. Nauk. UzSSR Ser.</u>
   <u>Fiz.-Mat. Nauk</u>, No. 3, 23-27, 98.

Holland, W.R., T. Keffer and P.B. Rhines, 1983. The dynamics of the oceanic
   general circulation: the potential vorticity field (preprint).

Ierley, G.R. and W.R. YOung, 1983. Can the western boundary layer affect the
   potential vorticity distribution in the Sverdrup interior of a wind gyre.
   <u>J. P. O.</u>, 13, 1753-1763.

Ivers, W.D., 1975. The Deep Circulation in the Northern North Atlantic, with
   Especial Reference to the Labrador Sea. Ph.D thesis, Uni. of Calif., San
   Diego.

Kordzadze, A.A., 1979. On the solvability of a three-dimensional steady-state
   quasilinear problem of a baroclinic ocean. <u>Doklady Akademi Nauk SSSR</u>. 244,
   No. 1, 52-56.

Kamenkovich, V.M. and G.M. Reznik, 1972. A Contribution to the Theory of
   Stationary Wind-driven Currents in a Two-Layer Liquid. <u>Izvestiya,</u>
   <u>Atmospheric and Oceanic Physica</u>, Vol 8, No. 4, 419-434.

Killworth, P., 1983. Some thoughts on the thermocline equations. Ocean modelling, No.48, 1-5 (unpublished manuscript).

Lazier, J.R.N., 1982. Seasonal Variability of Temperature and Salinity in the Labrador Current. J. Mar. Res. 40(Supp.), 341-356.

Leetmaa, A. and A.F. Bunker, 1978. Updated Charts of the Mean Annual Wind Stress, Convergence in the Ekman Layers, and Sverdrup Transports in the North Atlantic. J. Mar. Res., 36, No. 2, 311-322.

Luyten, J.R., J. Pedlosky and H. Stommel, 1983. The ventilated thermocline. J. P. O., 13, 292-309.

McCartney, M.S., 1982. The subtropical recirculation of mode waters, J. Mar. Res., vol 40(supp.), 427-464.

McCartney, M.S. and L.D. Talley, 1982. The subpolar mode water of the North Atlantic Ocean, J. P. O., 12, 1169-1188.

McCartney, M.S. and L.D. Talley, 1984. Warm-to-cold water conversion in the Northern North Atlantic Ocean. (preprint)

McIntyre, A. and Others, 1976. Glacial North Atlantic 18,000 years ago; A climap reconstruction. Geological Society of America Memoir 145, 43-75.

Newell, R.E., 1974. Changes in the poleward energy flux by the atmosphere and ocean as a possible cause for ice ages. Quaternary Research, 4, 117-127.

Newell, R.E., S. Gould-Stewart and J.C. Chung, 1981. A possible interpretation of paleoclimatic reconstructions for 18,000 B.P. for the region 60°N to 60°S, 60°W to 60°E. Paleoecology of Africa and the surrounding islands. Vol. 13 (Coetzee et al ed.), 1-19.

Nurubloev, M., 1981. A problem for a system of composite type in a three-dimensional bounded domain. Izv. Akad. Nauk. Tadzhik. SSR Otdl. Fiz.-Mat. Khim. i Geol. Nauk, No. 1, 79, 72-74.

Parsons, A.T., 1969. A Two-Layer Model of Gulf Stream Separation.

J. F. M. 39, part 3, 511-528.

Pedlosky, J. and W.R. Young, 1983. Ventilation, potential vorticity

homogenization and the structure of the ocean circulation, J. P. O., 13,

2020-2037.

Pedlosky, J., 1983a. Thermocline theories. Lecture notes (to be published).

Pedlosky, J., 1983b. Eastern boundary ventilation and the structure of the

thermocline. J. P. O., 13, 2038-2044.

Pedlosky, J., 1984. Cross-gyre ventilation of the subtropical gyre: an

internal mode in the ventilated thermocline (preprint).

Rhines, P.B. and W.R. Young, 1982. Homogenization of potential vorticity in

planetary gyres, J. F. M., 122, 347-367.

Rhines, P.B. and W.R. Young, 1982, A theory of the wind-driven circulation,

part I, J. Mar. Res., 40(supp.), 559-596.

Rhines, P.B., 1983. Gyration, Ocean Modelling, NO. 49, 1-4. (unpublished

manuscript).

Richtmyer, R.D., 1978. Principles of advanced mathematical physics, Vol. 1,

Spring-Verlag, New York.

Schott, F. and H. Stommel, 1978. Beta spiral and absolute velocity in different

oceans. Deep-Sea Res., 25, 961-1010.

Sergienko, L.S., 1982. On a degenerate system of composite type.

Differentsia'nye Uravneniya, 18, No. 2, 349-351, 366.

Stommel, H., 1948. The Westward Intensification of Wind-driven Ocean Currents.

Trans. Am. Geophys. Unin., 29, 202-206

Talley, L.D. and M.S. McCartney, 1982. Distribution and circulation of

Labrador Sea water, J. P. O., 12, 1188-1205.

Welander, P., 1959. An advective model of the ocean thermocline. _Tellus_, 11, 309-318.

Welander, P., 1966. A two-layer frictional model of wind-driven motion in a rectangular oceanic basin. _Tellus_, XVIII, 54-62.

Welander, P., 1971a. Some exact solution to the equations describing an ideal fluid thermocline. _J. Mar. Res._, 29, 60-68.

Welander, P., 1971b. The thermocline problem. _Phil. Tran. Roy. Soc. Lon._ A., 270, 415-421.

Veronis, G., 1973. Model of World Ocean Circulation: I. Wind-driven,two-layer. _J. Mar. Res._, 31, 228-288

Veronis, G., 1980. Dynamics of large-scale ocean circulation. Evolution of Physical Oceanography (Warren and Wunsch ed.), The MIT Press, Cam., MA.

Worthington, L.V., 1976. On the North Atlantic circulation. The Johns Hopkins Oceanographic Studies 6: 110 pp.